APPLICATION OF POST-STACK SEISMIC INVERSION FOR THE CHARACTERIZATION OF POROUS RESERVOIR SAND, GAMBAT BLOCK, CENTRAL INDUS BASIN, PAKISTAN

MUHAMMAD RASHID

(01-262232-017)

BAHRIA UNIVERSITY, ISLAMABAD

APPLICATION OF POST-STACK SEISMIC INVERSION FOR THE CHARACTERIZATION OF POROUS RESERVOIR SAND, GAMBAT BLOCK, CENTRAL INDUS BASIN, PAKISTAN



MUHAMMAD RASHID
(01-262232-017)

A thesis submitted in fulfilment of the requirements for the award of the degree of Masters of Geophysics

Department of Earth and Environmental Sciences

BAHRIA UNIVERSITY, ISLAMABAD

AUGUST, 2026

APPROVAL FOR EXAMINATION

Scholar's Name: Muhammad Rashid **Registration No**. 61995

Program of Study: MS Geophysics

Thesis Title: Application of post stack seismic inversion of the characterization of porous reservoir sand, Gambat block, central Indus basin, Pakistan

It is to certify that the above scholar's thesis has been completed to my satisfaction and to my belief, its standard is appropriate for submission for examination. I have also found the thesis in a format recognized by the BU for the MS thesis.

NOTE: The Plagiarism report is attached at the end of thesis.

Principal Supervisor's Signature: _____

Date: 17 August 2026

Name: Dr Fahad Mehmood

AUTHOR'S DECLARATION

I, Muhammad Rashid hereby state that my MS/MPhil thesis titled "Application of post stack seismic inversion for the characterization of porous reservoir sand, Gambat block central Indus basin Pakistan" is my own work and has not been submitted previously by me for taking any degree from this university Bahria University or anywhere else in the country/world.

At any time if my statement is found to be incorrect even after my Graduate the university has the right to withdraw/cancel my MS/MPhil degree.

Name of student: Muhammad Rashid
Date: August 27, 2026

PLAGIARISM UNDERTAKING

I, solemnly declare that research work presented in the thesis titled "Application of post stack seismic inversion for the characterization of porous reservoir sand, Gambat block central Indus basin Pakistan" is solely my research work with no significant contribution from any other person. Small contribution / help wherever taken has been duly acknowledged and that complete thesis has been written by me.

I understand the zero-tolerance policy of the HEC and Bahria University towards plagiarism. Therefore, I as an Author of the above titled thesis declare that no portion of my thesis has been plagiarized and any material used as reference is properly referred/ cited.

I undertake that if I am found guilty of any formal plagiarism in the above titled thesis even after award of MS/MPhil degree, the university reserves the right to withdraw / revoke my MS/MPhil degree and that HEC and the University has the right to publish my name on the HEC / University website on which names of students are placed who submitted plagiarized thesis.

Scholar / Author's Sign: _____

Name of student: Muhammad Rashid

ACKNOWLEDGEMENTS

To begin with, we express our gratitude to the Almighty Allah (SWT) for guiding us through difficult times and enabling us to complete this report. We also pay our respects to the Holy Prophet (Peace be upon him) for helping us recognize our Creator. Without Allah's blessings, we could not have completed this report.

We also extend our thanks to our parents who have been a constant source of support and guidance throughout our academic journey. At this level of understanding, comprehending a wide range of knowledge would not have been possible without proper guidance and support.

During the course of our assignment, we received guidance and assistance from a number of respected individuals, to whom we are greatly indebted. We express our appreciation to our thesis supervisor, Dr. Fahad Mahmood, for his unwavering support and guidance. We are also thankful to Dr. Umair Ullah Jamil, Head of Department at Bahria University Islamabad Campus, for providing us with all the necessary resources for our thesis.

ABSTRACT

The Lower Goru C-sand of the Gambat Block, Central Indus Basin, is a proven gas reservoir whose quality varies sharply over short distances. Lateral facies change, diagenetic porosity heterogeneity and fault compartmentalization produce amplitude responses that conventional interpretation cannot resolve unambiguously, and only three wells penetrate the productive interval. This study characterizes the porous reservoir sand by combining four methods: petrophysical evaluation of Tajjal-1, Tajjal-2 and Tajjal-3 in GVERSE Petrophysics; structural and stratigraphic interpretation of a 3D seismic volume in IHS Kingdom; post-stack seismic inversion; and AVO analysis with supporting rock physics, both carried out in CGG Hampson-Russell.

Petrophysical evaluation identifies the reservoir intervals as clean quartzose sandstone with low shale volume, developed effective porosity, elevated deep resistivity and reduced water saturation. Neutron-density crossover within the clean sands, corroborated by the density-neutron and M-N cross plots, indicates gas rather than brine. Seismic interpretation traces the Upper Goru marker, the Lower Goru marker and the C, B and A sand intervals across three inlines and three crosslines. The horizons are laterally persistent in both structural directions and gently deformed, cut by a single fault near Tajjal-3, and the gridded picks were converted to depth using velocities from the wells.

Model-based inversion weas applied to the same volume. At Tajjal-1 the sparse-spike result reaches a correlation of 0.9888 with a residual error of 0.1968, and the model-based result 0.9986 with an error of 0.0829. Both resolve the porous sands as laterally coherent low-impedance zones at the same positions, and the horizon maps of the top C and top B intervals show corresponding fairway patterns, which indicates that the mapped distributions do not depend on the choice of algorithm. Gassmann fluid substitution and angle-gather modeling identify an AVO class 2 response, in which the reflection is weak at normal incidence and its magnitude increases with offset. The Vp-Vs, acoustic impedance against Poisson's ratio, and lambda-rho against mu-rho cross plots separate gas sands from brine sands and shales, and extended elastic impedance at a chi angle of 32° gives the clearest discrimination obtained in the study.

The low-impedance fairways mapped on the top B interval are the most prospective targets in the block. Because the reservoir is weak at near offsets and develops its amplitude only at far offsets, its AVO signature can be overlooked where a class 3 response is assumed.

TABLE OF CONTENT

Pages

APPROVAL FOR EXAMINATION iii
AUTHOR'S DECLARATION iv
PLAGIARISM UNDERTAKING v
ACKNOWLEDGEMENTS vi
ABSTRACT vii
TABLE OF CONTENT viii
LIST Of FIGURES xii
CHAPTER 1 1
INTRODUCTION 1
1.1 Introduction 1
1.2 Study Area 2
1.3 Research Objectives 4
1.4 Problem Statement 5
1.6 Thesis Outline 7
CHAPTER 2 8
LITERATURE REVIEW 8
2.1 Introduction 8
2.2 Regional Tectonic Setting of the Indus Basin 8
2.3 Geological Setting of the Gambat Block 10
2.4 Structural Framework of the Study Area 11
2.5 Stratigraphy of the Study Area 12
2.6 Petroleum System of the Study Area 14
2.6.1 Source Rocks 14
2.6.2 Reservoir Rocks 14
2.6.3 Seal Rocks 14
2.6.4 Traps and Migration 14
2.7 Reservoir Characterization: Concepts and Data Integration 15
2.8 Petrophysical Properties and Reservoir Evaluation 15
2.8.1 Porosity 15
2.8.2 Fluid Saturation 16
2.8.3 Lithology Determination 16
2.9 Acoustic Impedance and Post-Stack Seismic Inversion 17

2.10 Amplitude-Versus-Offset (AVO) Analysis 18
2.11 Previous Reservoir-Characterization Studies in the Indus Basin 19
2.12 Literature Review 20
CHAPTER 3 24
METHODOLOGY 24
3.1 Adopted Methodology 24
3.2 Dataset 25
3.2.1 Seismic Data 26
3.2.2 Well Data 26
3.3 Petrophysical Analysis 26
3.3.1 Quality Control of Log Curves 26
3.3.2 Volume of Shale 27
3.3.3 Porosity Estimation 27
3.3.4 Formation-Water Resistivity 28
3.3.5 Water and Hydrocarbon Saturation 28
3.3.6 Cross plots 29
3.3.7 Density-Neutron Cross plot 29
3.3.8 M-N Cross plot 29
3.4 Seismic Data Interpretation 29
3.4.1 Quality Control of Seismic Data 29
3.4.2 Loading of Seismic Data 30
3.4.3 Synthetic Seismogram and Well-to-Seismic Tie 30
3.4.4 Fault and Horizon Interpretation 30
3.4.5 Time and Depth Maps 31
3.5 Post-Stack Seismic Inversion 31
3.5.1 Loading of Data 31
3.5.2 Wavelet Extraction 32
3.5.3 Well-to-Seismic Tie 32
3.5.4 Low-Frequency Model 32
3.5.5 Model-Based Inversion Analysis 32
3.5.6 Interpretation of the Inverted Acoustic Impedance 33
3.6 Amplitude-Versus-Offset (AVO) Analysis 33
3.6.2 AVO Forward Modelling 34
3.6.3 AVO Attribute Extraction 34

3.6.4 AVO Interpretation 35
3.6.5 Rock Physics 35
3.6.6 Cross Plot for Vp versus Vs 35
3.6.7 Cross Plot for AI vs Poisson Ratio 36
3.6.8 Cross Plot for Lambda-Rho vs Mu-Rho 36
3.6.9 EEI Analysis 36
3.6.10 Cross Plot for Lambda-Rho vs EEI at Chi 32 36
3.7 Integration of Results 36
CHAPTER 4 38
RESULTS AND INTERPRETATION 38
4.1 Introduction 38
4.2 Petrophysical Analysis 39
4.2.1. Cross Plots 42
4.2.1.1 Density-Neutron Cross Plot 42
4.2.1.2 M-N Cross Plot 43
4.3 Seismic Data Interpretation 44
4.3.1 Synthetic Seismogram of Tajjal-01 45
4.3.2 Interpreted Seismic Sections 46
4.3.3 Time Maps 52
4.3.4 Depth Maps 56
4.4 Seismic Inversion 60
4.4.1 Wavelet Extraction 61
4.4.2 Low-Frequency Model 62
4.4.3 Flow Chart for the Model-Based Inversion Technique 63
4.4.4 Inversion Analysis Results of Model-Based Inversion 64
4.4.5 The Inverted Impedance of Model-Based Inversion 65
4.4.6 Horizon Map of the Top C and B Intervals Resolved by Three Post-Stack Inversion Techniques 66
4.5 AVO Modelling and Rock Physics 67
4.5.1 Workflow for Gassmann Substitution, AVO Modelling and Rock Physics Analysis 67
4.5.2 Synthetic Seismogram of Tajjal-01 68
4.5.3 Base Map with Seismic Line Displaying Synthetic Seismogram 69

4.5.4 The Sand Intervals of Lower Goru Formation B Interval Under Study and the Seismic Event 70
4.5.5 Fluid Substitution 71
4.5.6 AVO Classes on the Basis of AVO Response 72
4.5.7 AVO Classes (Rutherford and Williams) 73
4.5.8 Fluid Substitution and AVO Analysis 74
4.5.9 AVO Class 2 Intercept and Gradient Response 75
4.6 Rock Physics 76
4.6.1 Cross Plot for Vp versus Vs 76
4.6.2 Cross Plot for AI versus Poisson's Ratio 77
4.6.3 Cross Plot for Lambda-Rho versus Mu-Rho 78
4.6.4 Chi 32 Angle Best Separates Both the 02 Fluids as well as the 02 Lithologies 79
4.6.5 Cross Plot for Lambda-Rho versus EEI at Chi 32 80
CONCLUSIONS 82
REFERENCES 83

LIST Of FIGURES

Pages

Figure 1. 1 Location Map of Gambat Field....4
Figure 2. 1 Generalized Tectonic Settings map of Lower Indus....9
Figure 2. 2 Generalized stratigraphy of the Lower Indus Basin. 13
Figure 3. 1Methodology....25
Figure 4. 1 Base Map 45
Figure 4. 2 Synthetic Seismogram of Tajjal 01....46
Figure 4. 3 Inline 1327 47
Figure 4. 4 Inline 1413 48
Figure 4. 5 Inline 1455 49
Figure 4. 6 Crossline 420 50
Figure 4. 7 Crossline 440 51
Figure 4. 8 Crossline 515 52
Figure 4. 9 Lower Guru Time Map....53
Figure 4. 10 C Interval Sand Time Map....54
Figure 4. 11 B Interval Sand Time Map....55
Figure 4. 12 A Interval Time Map 56
Figure 4. 13 Lower Guru Depth Map....57
Figure 4. 14 C Interval Sand Depth Map 58
Figure 4. 15 B Interval Sand Depth Map 59
Figure 4. 16 A Interval Sand Depth Map....60
Figure 4. 17 Tajjal 01 Result....40
Figure 4. 18 Tajjal 02 Result....41
Figure 4. 19 Tajjal 03 Result....42
Figure 4. 20 Density Neutron Cross plot....43
Figure 4. 21 M N Cross plot....44
Figure 4. 22 Post stack inversion method for seismic impedance estimation....61
Figure 4. 23 Extracted seismic statistical wavelet for seismic inversion analysis 62
Figure 4. 24 Showing Low frequency model used for seismic model-based inversion algorithm 63
Figure 4. 25 Flow chart for the model-based inversion technique....64
Figure 4. 26 Inversion analysis results of model-based inversion with inverted impedance (red), log impedance (blue), low impedance model (black)....65

Figure 4. 27 The inverted impedance of model-based inversion algorithm.....65
Figure 4. 28 Horizon map of the top C interval resolved by three post stack inversion techniques.....66
Figure 4. 29 Horizon map of the top B interval resolved by three post stack inversion techniques.....67
Figure 4. 30 Synthetic Seismogram of Tajjal-01 69
Figure 4. 31 Synthetic Seismogram of Tajjal-01 (continued).....69
Figure 4. 32 Base map with Seismic line displaying synthetic seismogram.....70
Figure 4. 33 The sand intervals of Lower Goru Formation B interval under study and the seismic event 71
Figure 4. 34 Fluid substitution 72
Figure 4. 35 AVO classes on the basis of AVO response (Ostrander, 1984) 73
Figure 4. 36AVO classes (Rutherford and Williams, 1989) 74
Figure 4. 37 Fluid substitution and AVO analysis 75
Figure 4. 38 AVO class 2 intercept and gradient response 76
Figure 4. 39 Cross plot for Vp vs Vs.....77
Figure 4. 40 Cross plot for AI vs Poisson ratio 78
Figure 4. 41 Cross plot for Lambda Rho vs Mu Rho 79
Figure 4. 42 EEI Analysis 80
Figure 4. 43 Cross plot for Lambda Rho vs EEI at chi 32 81

CHAPTER 1

INTRODUCTION

1.1 Introduction

In subsurface hydrocarbon there is geophysical and petrophysical are working together on and off and telling a different part of hydrocarbon bearing formation. In this process there is also geological method is present. Petrophysical analysis turns wireline-log responses into quantitative reservoir properties like as porosity & fluid saturation. Seismic data interpretation shows the structural and stratigraphical results in which reservoir is mapped. Advance seismic techniques such as Post stack seismic inversion to convert the band limited reflectivity and acoustic impedance which are directly related to the lithology, porosity & fluid. To detect and separate the gas & fluid effect from lithology AVO analysis is used which gives the angle behavior of seismic reflection data.

The Gambat block of the central Indus basin, Pakistan is a reservoir. The kind of reservoir we need. hosed in the Hosted in the shallow-marine to deltaic sands of the Lower Goru Formation and sealed by laterally persistent shales, the Lower Goru B-sand reservoir shows rapid facies transitions and systematic lateral porosity changes that defeat conventional amplitude-based interpretation (Afzal et al., 2005). The structural geometry, normal fault-bounded horst-and-graben blocks on the flank of the Khairpur High, controls both the hydrocarbon migration pathways and the distribution of the reservoir sands, so accurate seismic structural interpretation is a prerequisite for any meaningful characterization (Ahmad et al., 2004). And because only a few wells penetrate the productive interval, the full range of lateral property variation can be resolved only by extending well-derived petrophysical information into the inter-well volume with spatially continuous seismic techniques.

Post-stack seismic inversion is now the standard way to turn reflectivity data into an absolute rock property that relates to reservoir quality. Recovering acoustic impedance, the product of compressional velocity and bulk density, lets the inversion separate porous, potentially gas-charged sandstones, which have low impedance, from tight sands and encasing shales of higher impedance (Toqeer et al., 2021). AVO analysis adds to this by examining how reflection amplitude changes with source-receiver offset, or equivalently with angle of incidence. Porous gas-bearing sands usually have a low Poisson's ratio relative to the surrounding brine-saturated shales, so they show a characteristic increase in reflection

magnitude with offset that works as a direct hydrocarbon indicator (Ostrander, 1984; Yasin et al., 2020). AVO attribute analysis and impedance inversion show two equally supporting lines of geophysical evidence that describe the quality and presence of the reservoir sand.

To apply this workflow to the Gambat Block it require a need for the characterization of Lower Guru and B Sand at Tajjal wells The Petrophysical analysis, sequence stratigraphic and model-based inversion has been covered in last few studies on the Lower Goru sand of the Lower Indus Basin (Afzal et al., 2005; Munir et al., 2011; Toqeer et al., 2021), but a focused study has not been performed at Tajjal well that link the petrophysical reservoir assessment to the post-stack inversion and AVO analysis. This study uses four different methodologies for research purposes. Seismic data interpretation for structural and stratigraphic trap geometry, Petrophysics for the qualitative analysis of Tajjal11, Tajjal-2 and Tajjal-3 well, post-stack seismic inversion for the mapping of lateral distribution of acoustic impedance and sand reservoir porosity. And AVO analysis to identify the gas bearing zone.

1.2 Study Area

Gambat block lies in Khiarpur District, Sind province of Pakistan. At the thar desert Gambat block structurally lies on the southeastern side of the Khairpur High within the Central Indus Basin Indus Basin is divided into two sub basins Upper Indus basin & lower Indus Basin divided by Sargodha High Lower Indus basin is also divided into two sub basin Central (Middle) Indus basin and lower Indus Basin. (Zaigham & Mallick, 2000). The broader Indus Basin is bounded to the east by the Indian Craton, to the north by the Kohat-Potwar Plateau, and to the west by the Sulaiman and Kirthar fold-and-thrust belts (Kadri, 1995). The primary data of the Tajjal-1, Tajjal-2, Tajjal-3 well penetrate the Lower Goru and B-sand in the Gambat block and the gives the wireline log sets and 3-D control the petrophysical analysis, seismic interpretation, post-stack inversion and AVO modeling.

The tectonic history of the study area goes back to the Mesozoic era during the separation of the Indian Plate from Gondwana land 120 Ma, and the separation of the Seychelles and Madagascar block and also associated Deccan volcanism during Late Cretaceous (Kazmi & Jan, 1997). The convergence of the Eurasian plates and Indian plate closes the Tethys Ocean and formed the Himalayan region. The late Eocene to Oligocene was the phase of the trap geometries and the period of principle secondary migration and reservoir charge (Ahmad et al., 2004).

The petroleum play of the Central Indus Basin succession starts with the Sember formation of Early Cretaceous ae, the primary hydrocarbon source rock of the Central Indu Basin are the organic-rich shelf-marine shales. (Kazmi & Jan, 1997). Above the Sember

formation is the Lower Goru formation which is the main reservoir in the study area. The Lower formation is divided into alternating sand & shale intervals. The B-sand interval is the primary target in study area with shallow marine to deltaic deposits.

B-interval-sand porosities usually run 12 to 16 percent, reaching higher values at favorable spots, while shale content and impedance rise systematically toward the west (Alam, 2002). Intra-formational Lower Goru shales and the overlying Upper Goru Formation provide the lateral and vertical seals (Munir et al., 2011).

The Gambat gas field was discovered in the late 1990s and has produced gas from the Lower Goru C-sand reservoir since then. The Tajjal wells used in this study penetrate that productive interval and supply the log measurements, formation-evaluation data, and depth-time control needed for the integrated geophysical characterization of the porous reservoir sand described in the chapters that follow.

- Latitude: Min: 26.916701, Max: 27.124399
- Longitude: Min 68.750600, Max: 69.083298

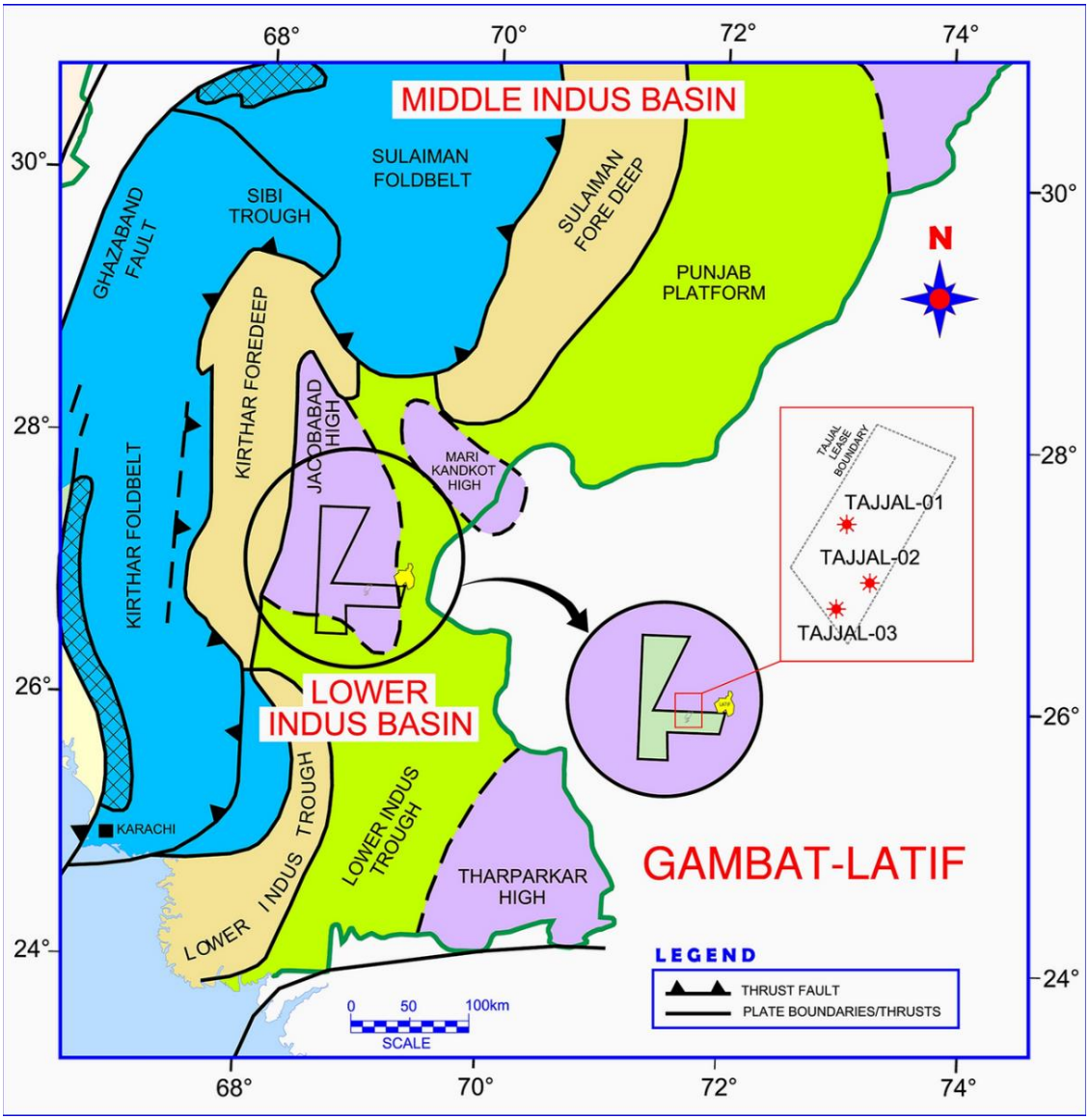


Figure 1. 1 Location Map of Gambat Field (Muhammad Toqeer, 2011)

1.3 Research Objectives

This research aims to characterize the porous reservoir sand of the Lower Goru B-sand interval in the Gambat Block by integrating petrophysical analysis, seismic interpretation, post-stack seismic inversion, and AVO analysis. The specific objectives are:

1. To carry out petrophysical analysis at the Tajjal-1, Tajjal-2, and Tajjal-3 wells, quantifying shale volume, effective porosity, and fluid saturation, and so to identify and evaluate the porous reservoir sand within the Lower Goru B-sand interval.
2. To interpret the subsurface structural and stratigraphic configuration of the study area from 3D seismic data, defining the geometry of the reservoir-bearing horizons and the hydrocarbon-trapping mechanism.

3. To apply post-stack seismic inversion to the 3D seismic volume, deriving an acoustic-impedance model and mapping the lateral distribution and quality of the lower goru formation B-sand interval away from well control.
4. To carry out AVO analysis, independently characterizing the fluid content of the lower goru formation B-sand and corroborating the presence of porous, gas-bearing sand within the interpreted closure.

1.4 Problem Statement

Several studies have investigated the Lower Goru Formation and B-sand reservoir in the Gambat and Central Indus Basin. Afzal et al. (2005) used seismic and well-log data to establish the sequence-stratigraphic framework of the Lower Goru B-sand in the Gambat area. Ahmad et al. (2004) demonstrated the application of sequence stratigraphy for predicting reservoir distribution in the Lower Goru fairway, while Munir et al. (2011) investigated the sequence stratigraphy of the Sember Formation and Lower Goru Member. More recent studies, including Toqeer et al. (2021), demonstrated that model-based post-stack seismic inversion can distinguish porous reservoir sands from tight and shaly lithologies in the Lower Goru Formation.

Despite these studies, the reservoir characterization of the Lower Goru B-sand at the Tajjal wells remains incomplete. Previous work has established the geological and stratigraphic framework and demonstrated the potential of seismic inversion for Lower Goru reservoir characterization, but the available studies do not provide a focused integration of petrophysical evaluation, 3D seismic interpretation, post-stack seismic inversion, and AVO analysis for the Tajjal-1, Tajjal-2, and Tajjal-3 wells.

The main unresolved problem is therefore the reliable characterization of the porous reservoir sand between the limited well locations. Well-log data provide detailed information about shale volume, porosity, and fluid saturation but are restricted to the well locations, whereas conventional seismic amplitude interpretation is affected by variations in lithology, porosity, fluid content, tuning, and structural effects. Consequently, amplitude anomalies alone cannot reliably distinguish porous gas-bearing sand from other low-impedance lithologies.

This study addresses this gap by integrating petrophysical analysis of the Tajjal wells with structural and stratigraphic interpretation of 3D seismic data, post-stack seismic inversion for acoustic-impedance-based mapping of the porous reservoir sand, and AVO analysis for independent assessment of fluid effects. The integrated approach is intended to

improve the characterization of the distribution, quality, and fluid content of the Lower Goru C-sand reservoir in the Gambat Block.

1.5 Significance of the Study

For a better identification and development of the Gambat Block, this study contributes to three key aspects: petrophysical, structural, and geophysical characterization. All three aspects are important for identifying and evaluating the porous reservoir sand (Afzal et al., 2005; Toqeer et al., 2021).

Petrophysical interpretation of the three wells, Tajjal-1, Tajjal-2, and Tajjal-3, provides information about the reservoir characteristics and quality. Wireline log data are used to estimate volume of shale, porosity, and water saturation. These results, together with inter-well correlation, establish the reservoir properties at the well locations and help identify potential hydrocarbon-bearing intervals within the Lower Goru B-sand. The petrophysical results provide the well-based constraints required for seismic interpretation, inversion, and AVO analysis (Yasin et al., 2020; Toqeer et al., 2021).

A complete 3D structural and stratigraphic interpretation of the Gambat Block provides the distribution of faults and reservoir-related horizons. Structural interpretation supports reservoir mapping by defining the trapping geometry and the spatial configuration of the reservoir. Time-structure and depth-structure maps of the Lower Goru and B-sand intervals are generated to understand the geometry of the reservoir and to provide structural control for seismic inversion. These maps can also assist in identifying fault-related compartments and potential areas for future development drilling (Ahmad et al., 2004; Afzal et al., 2005).

The two advanced seismic techniques, post-stack seismic inversion and AVO analysis, provide complementary information for reservoir characterization. Post-stack inversion estimates acoustic impedance, which can help delineate lithological and reservoir-property variations beyond the well locations. However, acoustic impedance alone may not uniquely distinguish porous gas-bearing sand from other low-impedance lithologies. AVO analysis complements inversion by examining the variation of seismic reflection amplitude with offset or incidence angle and can provide additional evidence for fluid effects in the reservoir (Toqeer et al., 2021; Yasin et al., 2020).

Post-stack inversion transforms the seismic data into an acoustic-impedance volume, which can be used to investigate the lateral distribution and quality of the reservoir sand away from well control. AVO analysis provides additional information about the fluid-related seismic response of the reservoir and helps assess whether the interpreted porous sand

may be gas-bearing. Therefore, the integration of petrophysical analysis, seismic interpretation, post-stack inversion, and AVO analysis provide a more reliable basis for characterizing the distribution, quality, and fluid content of the Lower Goru C-sand reservoir in the Gambat Block (Toqeer et al., 2021; Yasin et al., 2020).

1.6 Thesis Outline

This thesis is organized into five chapters, each corresponding to a principal stage of the research.

Chapter 1 sets the introductory context: the background to porous reservoir-sand characterization in clastic settings, the geological and petroleum significance of the Gambat Block, the research objectives and questions, the problem statement, and the significance of the study.

Chapter 2 reviews the literature relevant to the study. It covers the regional tectonic and stratigraphic setting of the Central Indus Basin and the Gambat Block; the petroleum system of the study area; petrophysical property evaluation from wireline logs; the theory and application of seismic interpretation, acoustic-impedance inversion, and AVO analysis; and previous reservoir-characterization studies of the Lower Goru Formation in the Indus Basin.

Chapter 3 gives a detail description of the data set and complete methodology used in this study. Chapter 3 gives the details of the 3D seismic cube of the Gambat block and the log data obtained from Tajjal-1, Tajjal-2 and Tajjal-3 wells, the sequential workflow which is adopted in this study which include; GVERSE petrophysics software for Petrophysical data interpretation, HIS kingdom software for structural and stratigraphic interpretation, CGG Hampson-Russell for post-stack seismic inversion and AVO modeling. Along with this chapter also explain Well to seismic tie, data conditioning and wavelet extraction.

Chapter 4 describe and explain the research results in detail. In this chapter results of petrophysical analysis, Seismic data interpretation, Post stack model-based inversion and AVO modeling response analysis of the Lower Guro and C-sand in the Gambat Block and Tajjal well are presented. All these results were studied together to characterize the distribution, quality, and fluid content of the reservoir sand of the field.

Chapter 5 describes the conclusion of the study.

CHAPTER 2
LITERATURE REVIEW

2.1 Introduction

This chapter aim to review and understand the geophysical, geological and petrophysical information for the reservoir characterization of the porous sand.in Gambat Block, Central Indus basin. It helps to understand the regional tectonic, stratigraphic setting and petroleum system of the Indus basin. This chapter will also help to explain the theory behind the basic methods used in this research, petrophysical interpretation form wireline log data, seismic data interpretation for structural and stratigraphic interpretation, post-stack inversion for acoustic impedance and AVO (amplitude-verses-offset) for the determination of fluid. At end this review compare current research with previous research of Lower Guro formation in central Indus Basin.

2.2 Regional Tectonic Setting of the Indus Basin

One of the most studied sedimentary basins of South Asia is the Indus Basin that covers an area of 500,000 km² across Pakistan, northwestern India, and the adjacent continental shelf of the Arabian Sea. The formation of Indus basin was due to collision of two continental plates Indian and Eurasian plate, the collision of Indian and Eurasian plate begins in Early Eocene, 50-55 ma and still Indian plate in subducting in Eurasian plate at a speed of 4-5 cm per year. (Kazmi & Jan, 1997). The Himalayan Orogenic belt is the result of the continuous collision of the Indian and Eurasian plate. During the same period a foreland basin was formed to the south and southwest, where a large sequence of sediments accumulated from the erosion of mountains. These sediments formed a thick layer of rock over time period and now it plays an important part in the geological structure of the Indus Basin.

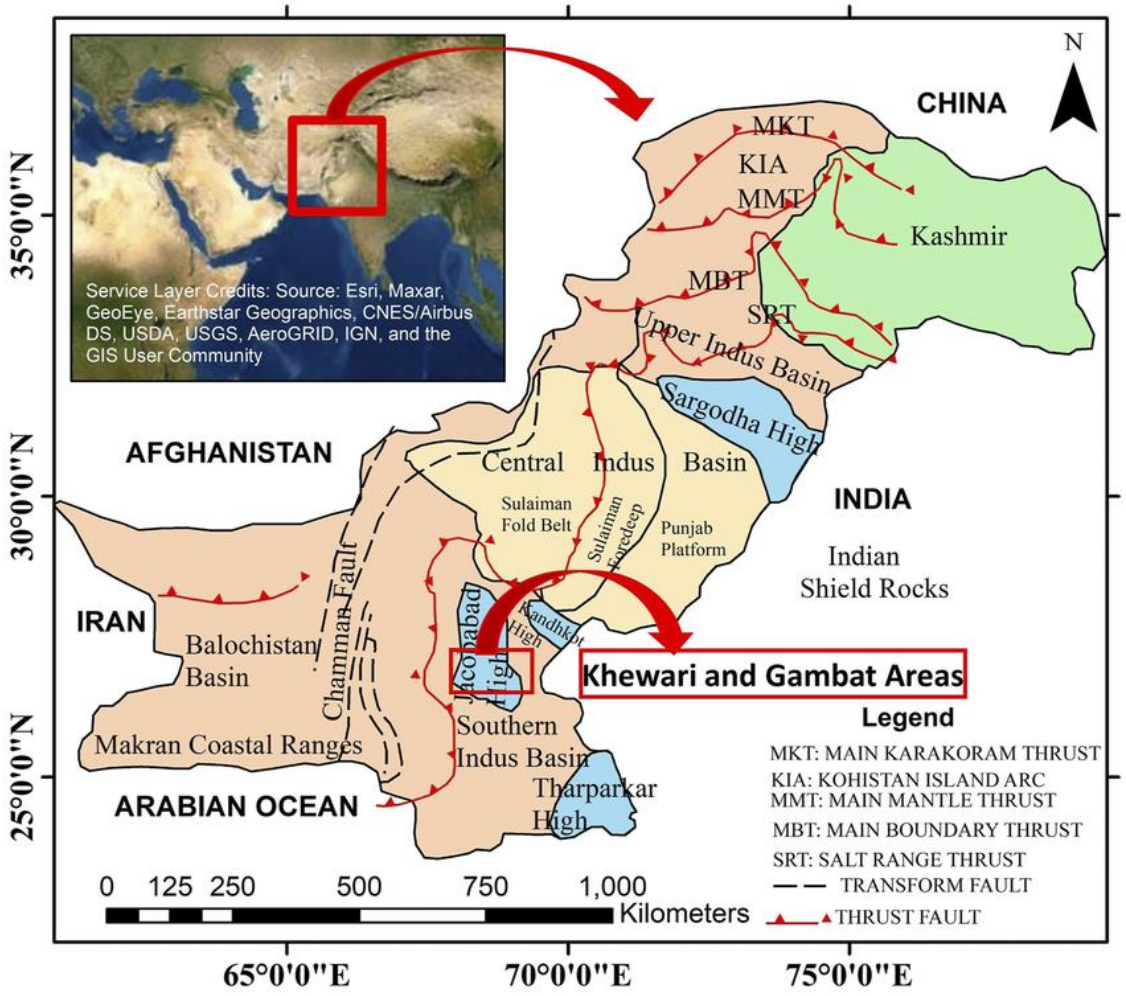


Figure 2. 1 Generalized Tectonic Settings map of Pakistan (Kadri, 1995)

Indus Basin is divided into three sub basins Upper Indus basin, Central Indus basin and lower Indus Basin due to different structural style, stratigraphic development and petroleum system. Upper Indus Basin is subdivided into two basins, Potwar Basin and Kohat Basin divide by Indus River. The Upper and Central Indus Basin are divided by Sargodha high and Central Indus Basin consist of the central platform and adjacent cratonic are in Sindh Provence, Gambat Block also lie in Central Indus Basin, the lower Indus Basin cover the southern platform to the Arabian sea. (Kadri, 1995). Each sub-basin represents a different stage in the geological history of the region and a different intensity of geodynamic processes.

The tectonic formation of the Indus Basin is generally divided into three major phases. The initial stage was the rifting phase in Jurassic and Early Cretaceous ag e, where the Indian plate was rifted from Gondwana Land and the opening of the Tethys Ocean, created half-grabens and normal fault geometry. The second phase was the thermal-sag phase in Late Cretaceous and Early Paleogene, a passive continental margin was formed due to

gradually subduction of land, resulting in broad and shallow marine environments, these environments were ideal for the formation of the source and reservoir rock, which are now the main source rock in the study area. The third phase of the Indus Basin formation was the Foreland Basin phase for the Eocene to the present. This was the phase when Indian Plate collied with Eurasian Plate and the form Himalayan Thrust Sheet which created the compressional structures and inversion structure in the Earth. The extensional and compressional structure form the many types of trap geometry and present structure. (Kazmi & Jan, 1997). The basic components of the Gambat Block Petroleum System, such as source rocks, reservoir rocks, and seal rocks, were formed in early geological stages, and the trap geometry were formed later as a result of the extensional and compressional phase

The western boundary of the Indus Basin is bounded by the Sulaiman and Kirthar fold-and-thrust belts, which are the tectonically active zone in Pakistan area. A large number of fold and thrust belts are present in this area. The previous study and research in this area shows the shape and structure of the thrust sheets, and the detachment levels within the soft and weak Cretaceous shales where rocks can slide over each other. (Kadri, 1995). This regional geological framework provides the fundamental basis for understanding the structural geometry of the Gambat Block and interpreting the trapping mechanism of oil and gas in the Lower Goru Reservoirs.

2.3 Geological Setting of the Gambat Block

The Gambat Block is located in the Central Structural Domain of the Indus Basin. This region is a relatively stable cratonic region, the crystalline basement rock of the Indian Shield lies under the Precambrian. Above these rocks are thin layers of Paleozoic age while above are the thicker layers of Mesozoic to Cenozoic age (Kadri, 1995). The stratigraphic record has been better preserved in Gambat Block because it has subsided less than the surrounding fold-and-thrust belts. The topography of the basement and the fault trends have significant impact on the geological structure of the area and these are the main factors that controls the shape, geometry and determine where and how structural traps will form in the area.

Gambat Block is located. on the southeastern side of the Khairpur High, extending from northeast to southwest, which is considered a major hydrocarbon province in the Central and Lower Indus Basin. The reservoir rock that is producing gas in Gambat Field is Lower Goru Formation of Cretaceous age, gas held by a mix of structural closure and up-dip stratigraphic pinch-out beneath the regional Upper Goru shale seal (Afzal et al., 2005). Gambat Block structure also helps in studying the neighbor field such as Swana, Miano and

Kadanwari field because he geological structure of the Gambit Block is a representative example of the Central Platform Petroleum System as a whole.

Geologically Gambat Block is quite complex because of the influence of three main factors lateral facies variability of Lower Goru Formation, heterogeneity of the porosity and structural classification by normal faults. At well scale it hard to understand because all these factors make are large variation in reservoir quality, Therefore, petrophysical analysis is used with post-stack seismic inversion and AVO analysis, to get an accurate and clear information on the porous reservoir sand (Toqeer et al., 2021).

2.4 Structural Framework of the Study Area

Two different period involve in the present geological structure of the Gambat Block, first during the rifting due to moving apart of Indian plate from Gondwana land in Mesozoic Era and later compression caused geological changes, that effected pre-existing faults and structures. As a result, the movement of these faults changed and they played a significant role in the formation of the present geological structure, faults, and hydrocarbon traps (Kadri, 1995). The flexural folding due to the reactivated fault segments overlying rock layers together form such closures.

Gambat block lies in an extensional regime and the structural trend of the faults are normal fault trending northwest to southeast and cutting the Cretaceous strata. At first there is only one single fault but at the depth of Lower Goru and upper Goru these faults convert into multiple faults and make it more complex to determine the hydrocarbon bearing zone. Intraformational faults that cut through the reservoir interval can act as a barrier, affecting the lateral flow of oil, gas, or water. This results in the reservoir being divided into distinct compartments, a process called compartmentalization. This division makes accurate reservoir mapping and volumetric estimation of oil and gas reserves more difficult, as each compartment may behave differently from the others. The determination of seismic amplitude alone is not possible weather a particular fault is acting as a seal or forming a partial baffle that only reduce the flow of fluid, post-stack inversion and AVO modeling is used to determine this accurately and to understand the true character and fault (Afzal et al., 2005).

Structural Interpretation of the Gambat Block uses 3D Seismic Reflection maps combined with Well-Top data from Exploration and Appraisal Wells, this method gives an accurate and better image of structure, depth, and distribution of subsurface rock layers and faults, enabling the accurate identification. In time-to-depth conversion of seismic data some uncertainty is introduced due to the velocity model, in field this uncertainty is high due to

facies compaction, therefore an error may occur while time to depth conversion if velocity model is not accurate and it may affect the true depth estimation, composition and location of the reservoir. It is necessary to convert time to depth accurately for mapping of subsurface rock and preparation of low frequency model used in post-stack inversion (Toqeer et al., 2021).

2.5 Stratigraphy of the Study Area

The exploration well in Gambat Block indicate the stratigraphy of the study area, the stratigraphic column ranges from the hard crystalline basement of the Precambrian period to the alluvium of the quaternary period. The stratigraphic framework is developed by combining information from three main sources, bio stratigraphic zonation, lithostratigraphic correlation between wells, and regional seismic stratigraphic interpretation (Kadri, 1995). The most studied rocks in this study are Cretaceous rock for reservoir characterization.

Lowest Cretaceous rock layer of Sembar formation plays an important role in petroleum system. Deposited in cool & calm and anoxic environment condition, it is dark-grey to black organic-rich shales and siltstones with minor fine-grained sandstones (Kazmi & Jan, 1997). Log data results indicate high gamma-ray, low resistivity and high bulk density. As moving upward Sembar formation changes into Lower Goru Formation, which indicates that over the time deep water environment change into shallow marine, where source rock ends and reservoir rock begin.

The primary reservoir interval for hydrocarbon is Lower Goru Formation, the Lower Goru Formation is divided into sand dominated interval the sand shale interval act as seals and baffles in between the formation. B-Sand formation was deposited in fluvio- deltaic and shallow-marine environment, is the primary gas-bearing zone in Tajjal well, good net-to gross ratio and porosity (Munir et al., 2011). The internal structure of the B-sand shows the general characteristics of deltaic system where lateral facies change in rock Channel-fill sand, distributary Mouth-Bar Sand and Interdistributary Silts and Clay. This heterogeneity is the main reason for the differences in reservoir quality in different places in the Gambat block, therefore the main goal of post-stack inversion and AVO modeling is to identify this heterogeneity and map it properly.

The Upper Goru Formation lies above the Lower Goru Formation formed in Cretaceous period, mostly marine shales, marls and argillaceous limestones deposited during transgression. The shale layers of the Upper Goru Formation are soft and mechanically ductile, lateral extend of hundreds of kilometers and have very low permeability for this reason these rock layer formation play an important role as regional seal and prevent

hydrocarbon to escape (Munir et al., 2011). Above the Upper Goro Formation are Paleogene rocks consist of carbonate rock, an important stratigraphic indicator for the regional correlation of the different layer.

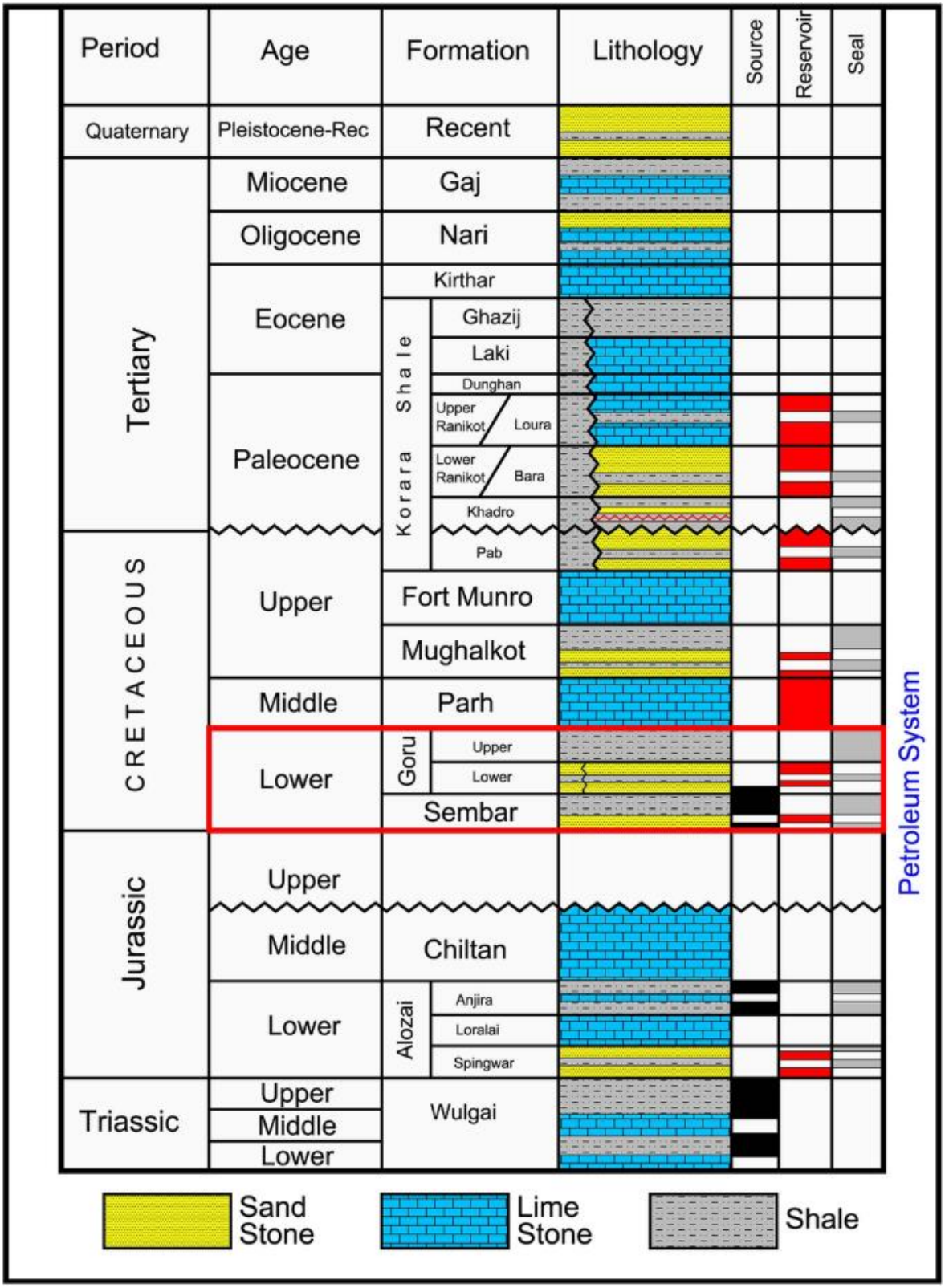


Figure 2. 2 Generalized stratigraphy of the Lower Indus Basin (modified after Kadri, 1995).

2.6 Petroleum System of the Study Area

2.6.1 Source Rocks

The primary source rock in Central Indus Basin is Sembar formation, it is the rock that produce hydrocarbon. Organic geochemical analysis was carried out by cutting and core sample for the determination of characteristic from various exploration well in study area. The amount of Total Organic Carbon (TOC) typically ranges from 1.0% to 4.0% by weight, higher organic matter has accumulated TOC can be higher (Kazmi & Jan, 1997). The kerogen in this rock is mostly a mixture of Type II and Type III, for this reason, this kerogen has the potential to produce both oil and gas, although in some areas the potential for gas production is greater. Since Type III is dominant in the Sambar Formation, the Gambat field is primarily a gas-producing area. Thermal maturity indicators show that in most of the part of central platform Sembar formation has entered gas window. peak gas generation and expulsion broadly during main phase of Himalayan thrust loading the burial

2.6.2 Reservoir Rocks

The Lower Goru Formation is the principal reservoir formation in the Gambat Block and consists of multiple sandstone intervals, including A, B, C and D sands. Reservoir quality varies between and within these sand units because of depositional facies, shale content, compaction and diagenesis. Variations in porosity and lithology influence the acoustic impedance and seismic response of the reservoir. In this study, the B-sand is the primary reservoir target, and its petrophysical properties are evaluated at the Tajjal wells and extended laterally using seismic inversion and AVO analysis.

2.6.3 Seal Rocks

The regional seal integrity of the Upper Goru shales in the Gambat area is confirmed by the significant gas columns in the producing wells, which show the seal has held throughout the post-charge history (Munir et al., 2011). The shale's strength and ductility make brittle failure and fracture-related seal bypass under current in-situ stress unlikely across most of the field, though fault-related seal breach has to be judged segment by segment. Within the Lower Goru, intra-formational shales between the sand members act as hydraulic barriers limiting vertical communication between the stacked reservoirs; their thickness and lateral continuity set the degree of vertical compartmentalization and directly affect the pressure regime of individual sand members during production.

2.6.4 Traps and Migration

The trap at the Gambat Block is the combination of structural closure around the crest of the reservoir horizons and up-dip stratigraphic pinch-out of the Lower Goru sands, sealed

by the overlying and intra-formational shales. The closure is sensitive to depth-conversion uncertainty in the seismic velocity model, so accurate structural interpretation is essential to defining trap limits and spill points (Afzal et al., 2005). Primary migration from the Sembar source to the Lower Goru reservoir went by a mix of vertical migration along permeable fault zones and lateral migration within permeable sandstone carrier beds. The short migration distances favored efficient charging, and the geochemical signature of the produced gas matches generation from the thermally mature Sembar source, which supports the proposed pathway.

2.7 Reservoir Characterization: Concepts and Data Integration

The purpose of reservoir characterization is qualitative and accurate estimation of the reservoir's Geometry, Rock properties and hydrocarbon presence. This process reduces uncertainty, what is the quality and how much effective it will be (Tiab & Donaldson, 2015). In this research the main challenge is that the subsurface acquired data is spatially spares and indirect. Well log data information about petrophysical properties of formations are in very high in resolution but limited to the well and seismic data provide information about the entire area but resolution of seismic data not good as well log data. To remove this gap post-stack inversion and AVO analysis methods are used to obtain accurate information, and estimate the reservoir properties

Reservoir characterization in the Gambat Block requires consideration of the unique complexities of the Lower Grove C-Sand, which are; Lateral Facies Change, Porosity variability due to diagenesis and Structural compartmentalization due to faults, to understand these issues some methos have been used in this study; Petrophysical analysis, Seismic data interpretation, post-stack seismic inversion and AVO Analysis. Together all these methods provide a comprehensive, coherent, and constant assessment of porous reservoir sand. (Toqeer et al., 2021).

2.8 Petrophysical Properties and Reservoir Evaluation

2.8.1 Porosity

Numbers of pore spaces present in total volume of rock is called porosity, it is the most important parameter in reservoir characterization as hydrocarbon accumulate in rock formation if it has good porosity, isolated pores which are not connected to each other while effective porosity refer to the pores which are inter connected (Tiab & Donaldson, 2015). (Tiab & Donaldson, 2015). In the clay-rich intervals of the Lower Goru Formation, the difference between total and effective porosity is especially important, because clay-

associated microporosity can add to the total porosity a log tool reads without contributing meaningfully to hydrocarbon storage.

Log-based porosity in the Lower Goru Formation relies on bulk-density and neutron-porosity measurements, with sonic transit time giving a complementary, partly independent estimate. The density-porosity method gets porosity from the measured formation bulk density, the matrix grain density of the dominant mineralogy, and the pore-fluid density. Combined neutron-density analysis picks out gas-bearing intervals through the characteristic neutron-density separation, or gas crossover, caused by the low hydrogen index of gas relative to brine (Asquith & Krygowski, 2004). Clay content introduces systematic errors in log-derived porosity that have to be corrected with the gamma-ray-derived shale volume before the porosity is reliable for reservoir evaluation.

2.8.2 Fluid Saturation

Water saturation, the fraction of pore volume filled with formation water, sets the hydrocarbon saturation and so the hydrocarbon pore volume available for production. Resistivity logs play an important role in petrophysical analysis to determine the saturation of water established by Archie (1942), which show how formation resistivity factors; Porosity, Cementation exponent, Water saturation, Saturation exponent are related to each other. Archie explained that if we know the electrical resistance (Resistivity), porosity, and rock structure of the rock, we can estimate how much water is present in the reservoir. Lower Guro sand stone section contain clay mineral which conduct electricity, if it is ignored water saturation will be overestimated by the Archie equation, this is why reservoirs model that contain the electricity of clay give more accurate results such as; Indonesia Equation and Simandoux Equation (Poupon & Leveaux, 1971; Tiab & Donaldson, 2015).

2.8.3 Lithology Determination

Well logs are used to first determine which layers are good sandstone reservoirs and which are shales or hard cemented rocks. Only after this basic division is other reservoir properties, such as porosity, water saturation, and the presence of gas, accurately estimated. The gamma-ray log is the standard first-order lithology indicator, responding to the natural radioactivity of clay minerals, with high values marking clay-rich intervals and low values clean sandstones (Asquith & Krygowski, 2004). Multi-log cross plot analysis adds to the gamma-ray read by using the differing sensitivities of the tools; the neutron-density cross plot in particular flags gas-bearing sands and separates the main mineralogical assemblages. These log-derived lithology and fluid indicators are the well-scale ground truth the seismic inversion and AVO results are calibrated against.

2.9 Acoustic Impedance and Post-Stack Seismic Inversion

Acoustic impedance, the product of compressional-wave velocity and bulk density, is a fundamental elastic property that links seismic reflection amplitudes to subsurface rock and fluid properties. A reflection occurs at any interface where acoustic impedance changes, with the normal-incidence reflection coefficient proportional to the impedance contrast across it (Sheriff & Geldart, 1995). Conventional amplitude is therefore an interface property responding to the contrast between two layers, and its interpretation is muddied by tuning, wavelet interference, and the combined effect of lithology, porosity, and fluid. Seismic inversion gets past this by turning the reflection record from an interface reflectivity series into a layer acoustic-impedance property, moving the data from a band-limited derivative domain into an absolute property domain more directly related to petrophysical parameters (Yilmaz, 2001).

Post-stack seismic inversion works on the stacked, zero-offset volume and recovers a single acoustic-impedance value per layer. Several approaches exist, including recursive (trace-integration) inversion, sparse-spike inversion, and model-based inversion. Model-based inversion, used here, starts from an initial low-frequency impedance model and updates it iteratively until the synthetic seismogram from the model matches the observed seismic within a set convergence criterion (Hampson & Russell, 1991). It suits reservoir characterization because it builds in geological constraints from the well data and yields a stable, geologically plausible impedance volume. Pendrel (2001) reviewed the principal inversion methods and showed that model-based inversion, properly constrained by a reliable wavelet and low-frequency model, gives a robust estimate of the acoustic-impedance distribution for reservoir mapping.

Low Frequency impedance mode is used in post-stack inversion model, the main reason of using this model to provide low frequency information that is not available in bandwidth of the seismic wavelet, by interpolating and smoothing the impedance obtained from well logs with the interpreted horizons (Pendrel, 2001). The accuracy of the low-frequency model and the precision of the wavelet extraction are the main controls on inversion quality; errors in either carry into the inverted impedance. In clastic reservoirs such as the Lower Goru C-sand, the inverted impedance is an effective discriminator between reservoir and non-reservoir rock, because porous, gas-bearing sandstones have low impedance while tight sands and shales are higher (Mavko et al., 2009). The inverted impedance volume therefore maps the porous reservoir sand across the survey and substantially cuts the ambiguity of conventional amplitude interpretation.

Post-stack model-based inversion of the Lower Goru Formation has been shown in the Central Indus Basin by Toqeer et al. (2021), who characterized reservoir sands with porous, tight, and mixed facies and found that the inverted acoustic impedance distinguished the porous reservoir sand from the surrounding lithologies. Yasin et al. (2020) likewise derived petrophysical parameters from seismic inversion of Lower Goru data and showed the value of impedance in reservoir-quality prediction. These regional studies confirm that post-stack inversion works for the Lower Goru reservoir and set the precedent for applying it to the Tajjal wells of the Gambat Block here.

2.10 Amplitude-Versus-Offset (AVO) Analysis

AVO analysis uses the angle-dependent behavior of seismic reflections at an interface between two rock units of differing elastic properties to separate lithological from fluid-related contrasts. Where post-stack inversion works on the stacked zero-offset data and is sensitive mainly to acoustic impedance, AVO works on the pre-stack data and keeps the information in how reflection amplitude varies with source-receiver offset, or angle of incidence. Because that offset-dependent behavior is set by the contrast in both compressional and shear properties, and so by the Poisson's ratio contrast, AVO is sensitive to pore fluid in a way acoustic impedance alone is not (Castagna & Backus, 1993).

The theory behind AVO is the Zoeppritz (1919) equations, which describe how incident wave energy partitions into reflected and transmitted compressional and shear waves as a function of the angle of incidence and the elastic properties of the two layers. The full equations are exact but algebraically messy, and their non-linearity hides the physical controls on the amplitude variation. Practical AVO therefore uses linearized approximations. Ostrander (1984) first showed empirically that gas-bearing sands have an anomalous increase in reflection magnitude with offset, from their low Poisson's ratio relative to the surrounding brine-saturated shales, which established AVO as a practical gas-detection tool. Shuey (1985) then derived a widely used two-term approximation that splits the angle-dependent reflectivity into an intercept, corresponding to the normal-incidence reflection coefficient, and a gradient describing the rate of change of amplitude with offset.

The intercept and gradient attributes derived from the AVO approximation presented by Shuey (1985) are the basis for most AVO interpretations. The intercept represents the reflectivity at zero-offset and is closely related to the acoustic impedance contrast. This is why this study directly links AVO analysis to post-stack inversion. The gradient describes how the seismic amplitude changes at different offsets. This change helps in identifying the fluid in the reservoir, i.e. gas, oil or water. The intercept and gradient are then cross-plotted,

which divides the different reflection events into the AVO classes introduced by Rutherford and Williams (1989), which were later refined by Castagna and Swan (1997). With the help of these AVO Classes: High-Impedance Sand Near-Zero Impedance Sand Low-Impedance Gas Sand can be separated from each other based on their position in the Intercept–Gradient Cross plot. This gives a systematic frame for interpreting the AVO response of the Lower Goru C-sand and for picking out the anomalies tied to porous, gas-bearing reservoir sand.

For the Lower Goru reservoir, AVO supplies the independent fluid discrimination needed to resolve what impedance inversion leaves ambiguous, since a low-impedance response can come from a porous gas sand, a porous brine sand, or a lithological variation. Isolating the offset-dependent component of the reflectivity, AVO separates the gas-bearing sand from those alternatives and so corroborates the characterization from petrophysical analysis and inversion. Applying post-stack inversion and AVO together to gas-sand reservoirs of the Indus Basin has been shown to make reservoir and fluid prediction more reliable than either method alone (Yasin et al., 2020), which is the rationale for the integrated workflow used here.

2.11 Previous Reservoir-Characterization Studies in the Indus Basin

Reservoir-characterization work in the Indus Basin has grown a great deal since the early 1990s, alongside faster exploration and development and better data. Regional syntheses of the petroleum geology of Pakistan by Kadri (1995) and of the region's geology and tectonics by Kazmi and Jan (1997) set the framework for source-rock characterization, reservoir-quality prediction, and seal assessment across the Central and Lower Indus Basin. These Foundational Works describe the main components of the Indus Basin Petroleum System and the major geological controls that control the distribution of hydrocarbons (oil and gas). All these studies provide a regional context for interpreting and understanding the results of a field-specific study. In simple words: Previous research work has shown that: How oil and gas form and accumulate in the Indus Basin. What geologic factors (such as Source Rock, Reservoir Rock, Seal, Faults and Traps) cause hydrocarbons to occur in different locations. Keeping this basic information in front, the reservoir of Gambit block was interpreted in this study. In other words, these older studies provide a basic regional geological framework for this research, with the help of which the Gambit block results can be better understood and explained.

Sequence-stratigraphic and reservoir-characterization studies of the Lower Goru Formation have sharpened the picture of the depositional architecture and reservoir distribution of the C-sand fairway. Afzal et al. (2005) presented a seismic and well-log-based

sequence stratigraphy of the Lower Goru C-sand of the Gambat sub-basin, setting the depositional framework directly relevant to this study area. Ahmad et al. (2004) showed sequence stratigraphy working as a predictive tool in the Lower Goru fairway of the Central and Lower Indus platforms, and Munir et al. (2011) analyzed the sequence stratigraphy of the Sembar Formation and Lower Goru Member with specific implications for reservoir characterization. Together these define the stratigraphic architecture of the Lower Goru reservoir and provide the geological basis for interpreting the impedance and AVO responses obtained here.

The previous studies provide an important geological and geophysical framework for the Lower Goru reservoir succession, but the primary focus of the present study differs in targeting the B-sand interval. The A, B, C and D sands are considered as components of the Lower Goru reservoir succession, while the detailed petrophysical, inversion, AVO and rock-physics characterization is concentrated on the B-sand.

Quantitative seismic reservoir-characterization studies of the Lower Goru Formation have specifically shown the value of seismic inversion for reservoir and fluid prediction. Toqeer et al. (2021) applied model-based post-stack inversion to Lower Goru reservoir sands with porous, tight, and mixed facies in the Central Indus Basin, directly analogous to this study, and found that the inverted acoustic impedance separated the porous reservoir sand from the surrounding tight and shaly lithologies. Yasin et al. (2020) estimated petrophysical parameters from seismic inversion of Lower Goru data and confirmed that impedance-based methods work for reservoir-quality prediction. These studies establish post-stack inversion, integrated with petrophysical analysis and, where the data allow, AVO analysis, as an appropriate and proven method for characterizing the Lower Goru reservoir in the Indus Basin.

Despite this progress, no focused study integrating petrophysical analysis, seismic interpretation, post-stack inversion, and AVO analysis for the porous reservoir sand at the Tajjal wells of the Gambat Block appears in the open literature. This study fills that gap by applying the integrated workflow to the Lower Goru C-sand of the study area, contributing a field-specific reservoir characterization and reinforcing the precedent for applying impedance inversion and AVO analysis together in the Central Indus Basin.

2.12 Literature Review

This chapter has reviewed the geological, petrophysical and geophysical literature relevant to characterizing the Lower Goru reservoir succession in the Gambat Block, with particular emphasis on the B-sand as the primary target of the present study. The Lower Goru

contains A, B, C and D sand intervals, while the overlying Upper Goru Formation provides the principal regional seal. The regional tectonic and stratigraphic setting of the Central Indus Basin was laid out, showing that the structural and stratigraphic configuration of the study area reflects the interplay of Mesozoic extensional and later tectonic phases seen across the broader Indus Basin. The petroleum-system elements, the Sembar Formation source, the Lower Goru reservoir, the Upper Goru seal, and the combined structural and stratigraphic traps, were reviewed to set the geological rationale for the methodology used in the following chapters.

Previous studies have established a strong geological and geophysical basis for characterizing the Lower Goru Formation in the Central Indus Basin, but their approaches address different parts of the reservoir-characterization problem. The sequence-stratigraphic studies of Afzal et al. (2005), Ahmad et al. (2004), and Munir et al. (2011) provide important constraints on depositional architecture and reservoir distribution, but sequence stratigraphy alone cannot quantify the spatial variation of reservoir properties or distinguish fluid effects. Similarly, the post-stack inversion study of Toqeer et al. (2021) demonstrated that acoustic impedance can be calibrated with well-derived porosity and used to predict reservoir properties between wells. However, the authors also recognize that seismic-derived porosity is subject to uncertainty, meaning that impedance should not be treated as a unique measure of porosity or fluid content. This limitation is particularly important because low acoustic impedance may result from several factors, including porosity, lithology, or fluid saturation. Therefore, although inversion improves the interpretation beyond conventional seismic amplitude, it does not by itself provide a definitive fluid interpretation.

The literature therefore indicates that the main limitation is not the absence of individual characterization techniques, but the lack of integration between their different types of information. Petrophysical analysis provides detailed reservoir properties at the well locations, while seismic interpretation defines the structural framework and inversion extends impedance information laterally; however, each method contains inherent ambiguity when used independently. The existing studies demonstrate the usefulness of these individual approaches, but the literature reviewed in this thesis does not show a focused integration of petrophysical analysis, 3D structural interpretation, post-stack inversion, and AVO analysis specifically for the Tajjal wells of the Gambat Block. The critical implication is that reservoir characterization should not rely on a single seismic attribute: well-derived properties should constrain the seismic interpretation, inversion should be calibrated against those properties, and AVO should be used as complementary evidence for fluid effects rather than as a

standalone hydrocarbon indicator. This provides the basis for the integrated workflow adopted in the present study.

Well-log data are the primary quantitative source for reservoir characterization, giving continuous vertical profiles at centimeter-to-decimeter resolution through the drilled section. Indus Basin wells generally use a standard set of wireline logs, Natural Gamma Ray Log to determine lithology, Caliper for borehole diameter Log, Resistivity Logs for fluid saturation, Neutron & Bulk Density Log for porosity determination and Sonic Log for velocity determination Asquith & Krygowski, 2004). In this study Density and Sonic log are most important to obtain acoustic impedance which is the main target property of post-stack seismic inversion.

QC of well log data is important before the interpretation of well data, processing is performed in following steps; Environmental Correction, Depth Matching, Normalization and Flagging Anomalous Data (Tiab & Donaldson, 2015). Properly conditioning of ensure the reliability and consistency of the well log data, density and sonic log are used to generate synthetic seismogram to ensure that the seismic to well tie and low frequency model are also error free, because the unwanted artifacts or errors can corrupt the inversion.

Seismic Reflection Data provides a continuous information about the subsurface in hydrocarbon exploration and field development, seismic waves which are the contras of density and velocity travel through different layers in subsurface and reflect back to surface and generate an image of subsurface which shows geological structures and stratigraphic features such as arrangement and distribution of different rock layers, faults and anticlines. The modern 3D seismic data acquisition forms a dense grid using large number of sources and recovers to get a detail image of subsurface data. This image can be seen in detail down to a few dozen meters horizontally and about 10–30 meters vertically, allowing for accurate mapping of reservoirs, faults, and rock layers (Sheriff & Geldart, 1995). The important function of seismic data in reservoir characterization is; mapping reservoir geometry and hydrocarbon trap configuration, imaging facies boundaries & depositional system and predict reservoir properties quantitative analysis of seismic amplitude and acoustic impedance. In seismic data interpretation for reservoir characterization different geological horizons and faults are marked, synthetic seismogram is used match reelection events with original geological information (Yilmaz, 2001). Interpreted horizons and faults describe the actual structure and shape of the reservoir, which is necessary for seismic inversion, this is followed by time-to-depth conversion, which uses a velocity model developed from well

check shot data and interval velocity data to convert time domain data into depth domain which is used to estimate the volume of the reservoir and hydrocarbon reserves.

CHAPTER 3
METHODOLOGY

3.1 Adopted Methodology

This chapter describes the integrated workflow used to characterize the Lower Goru B-sand interval at the Tajjal wells in the Gambat Block of the Central Indus Basin, Pakistan. The Lower Goru reservoir succession comprises A, B, C and D sand intervals, while the overlying Upper Goru Formation acts as the principal regional seal. The study integrates four main techniques: petrophysical analysis, seismic data interpretation, post-stack seismic inversion, and AVO analysis with supporting rock physics. The primary data consist of wireline logs from Tajjal-1, Tajjal-2 and Tajjal-3 and a 3D seismic volume of the Gambat Block.

This research used combination of 4 geological and geophysical techniques; Seismic data interpretation, Petrophysical analysis. Post-stack inversion and AVO (Amplitude-Versus-Offset) analysis for reservoir characterization of the Gambat Block. The primary data used in this research: well logs from Tajjal-1, Tajjal-2 and Tajjal-3 with high resolution 3D seismic survey of the Gambat Block. The sequential workflow which is adopted in this study which include; GVERSE petrophysics software for Petrophysical data interpretation, HIS kingdom software for structural and stratigraphic interpretation, CGG Hampson-Russell for post-stack seismic inversion and AVO modeling. All stage results are interconnected with each other and each stage based on the information of previous stage.



Figure 3. 1Methodology

3.2 Dataset

Two main type of data sets were used in this study A high resolution 3D seismic reflection data and wireline log data from Tajjal-1, Tajjal-2 and Tajjal-3 well of the Gambat Block, Central Indus Basin, Pakistan. QC of the data performed before any qualitative analysis.

Well Data	Seismic Data
Tajjal 1 Tajjal 2 Tajjal 3	3D seismic data of area.

3.2.1 Seismic Data

This study used a high-resolution seismic pre-stack reflection data covering entire study area. It was provided in SEG-Y format and loaded directly into IHS Kingdom for structural interpretation. The survey was acquired with a nominal bin spacing of 12.5 by 25 meters and a record length long enough to image the primary reservoir intervals. Trace headers carrying inline and crossline coordinates, shot-point geometry, and two-way travel time were verified before loading. The dominant frequency and signal-to-noise characteristics were assessed during the well-to-seismic tie in Section 3.4.3. Because the AVO analysis needs the offset-dependent amplitude information in the pre-stack data, the corresponding pre stack gathers were also available and were used for the AVO workflow in Section 3.6.

3.2.2 Well Data

Wireline-log suites and vertical seismic profile (VSP) surveys were available for the three wells: Tajjal-1, Tajjal-2, and Tajjal-3. The log suites held, at minimum, gamma ray (GR), bulk density (RHOB), neutron porosity (NPHI), deep resistivity (RT), and sonic compressional slowness (DT), enough for the full petrophysical workflow and for computing the acoustic-impedance log needed for the seismic tie and inversion. Check shot and zero-offset VSP data from each well-built the depth-time relationships for the well-to-seismic tie. Log data came in LAS (Log ASCII Standard) format and were loaded into GVERSE Petrophysics for quality control and petrophysical evaluation.

3.3 Petrophysical Analysis

Petrophysical analysis was done in GVERSE Petrophysics for all three Tajjal wells, to estimate shale volume, effective porosity, formation-water resistivity, and fluid saturation across the reservoir intervals and so to identify the porous, hydrocarbon-bearing reservoir sand within the Lower Goru C-sand. The workflow ran: log quality control, shale-volume estimation, porosity estimation, formation-water resistivity, and water- and hydrocarbon-saturation calculation.

3.3.1 Quality Control of Log Curves

Before any computation, every log curve was checked for common acquisition artefacts. Depth difference between log curves was corrected (log-to-log correlation) different logs were compared for this purpose and the appropriate depth shift was applied with the help of caliper log. Caliper and Density correction curves were used to identify the effect of cycle skips and borehole washout on density and neutron log in the sonic log. Unusual reading was removed by using a median filter, environmental corrections, which

were performed according to standard industry guidelines (Ellis & Singer, 2007). The Quality-Controlled Log Suite produced after all this quality control and data conditioning became the basis for all subsequent computations and analyses.

3.3.2 Volume of Shale

Gamma Ray Log help to estimate Volume of Shale, as Gamma Ray Log is sensitive to radioactive bearing clay minerals which are mostly found in clastic strata, from linear relationship gamma-ray index was calculated:

$$IGR = (GRlog - GRmin) / (GRmax - GRmin) \quad (3.1)$$

The GRlog value is directly recorded from gamma-ray at given depth, GRmin is the minimum gamma-ray that represent the clean sand patch and GRmax is the maximum gamma ray value that represent shale patch. The GRmin and GRmax values are directly picked from the histograms of the gamma ray response (Asquith & Krygowski, 2004). Non-linear correction following Larionov (1969) was applied because Gamma-Ray Index (IGR) sometimes overstates the amount of shale, especially in rocks containing radioactive feldspars or heavy minerals.

$$Vsh = 0.33 \times [\, 2^{\wedge} (2 \times IGR) - 1 \,] \quad (3.2)$$

3.3.3 Porosity Estimation

Neutron and Density Logs are used for the estimation of effective porosity; first density was calculated from bulk density log using standard relationship then neutron porosity and density porosity were combined to obtain effective porosity. (Schlumberger, 1989):

$$\varphi D = (\rho ma - \rho b) / (\rho ma - \rho fl) \quad (3.3)$$

In this equation ρma refers to the rock matrix which was assumed to be 2.65g/cm³ for quartz sandstone, ρb refers to bulk density that is directly measured from the density log. ρfI refers to density of the fluid pores which was assumed to be 1.0 g/cm for formation water. Neutron-porosity values were read directly from the tool-corrected neutron curve calibrated to a sandstone matrix. A combined neutron-density porosity was then derived to reduce gas-effect and lithology biases:

$$\varphi ND = \sqrt{\,[\, (\varphi N^2 + \varphi D^2) / 2]} \quad (3.4)$$

Gas lowers the density-log response and the neutron count rate at the same time, which produces the characteristic gas-crossover on the neutron-density overlay. This was used qualitatively to flag gas-bearing zones, while the combined neutron-density porosity gave a more reliable estimate than either log alone there. The shale-corrected effective porosity was then obtained by removing the shale-bound porosity contribution:

$$\varphi e = \varphi ND - (Vsh \times \varphi sh) \qquad (3.5)$$

where φsh is the neutron-density porosity measured within the adjacent shale reference intervals (Rider & Kennedy, 2011).

3.3.4 Formation-Water Resistivity

Formation-water resistivity is a critical input to the Archie saturation equation. With no laboratory-measured water sample, it was estimated from the spontaneous-potential (SP) log using the static SP relationship (Doll, 1948):

$$SSP = -K \times \log (Rmfe / Rwe) \qquad (3.6)$$

where SSP is the static spontaneous potential in millivolts recorded opposite clean, water-bearing sands, K is the electrochemical coefficient given by $K = 65 + 0.24 \times T$ with T the formation temperature in degrees Fahrenheit, Rmfe is the mud-filtrate-equivalent resistivity corrected for temperature, and Rwe is the equivalent formation-water resistivity. The equivalent resistivity was then converted to true formation-water resistivity using standard temperature-correction charts for the reservoir temperature. As a check, a Pickett plot, a log-log cross plot of true resistivity against neutron-density porosity, was built for clean, water-bearing intervals (Pickett, 1966). At one hundred percent water saturation, the Archie equation reduces to:

$$\log (Rt) = \log (a \times Rw) - m \times \log(\varphi ND) \qquad (3.7)$$

so, the water line in the Pickett plot has a slope of negative m and an intercept of log (a × Rw), which gives the formation-water resistivity, the cementation exponent m, and the tortuosity factor a together. The two methods gave formation-water resistivity values in close agreement, and the Pickett-plot estimate was adopted as the final value.

3.3.5 Water and Hydrocarbon Saturation

Water saturation was calculated using the standard form of the Archie equation (Archie, 1942):

$$Sw = [(a \times Rw) / (\varphi e^{m} \times Rt)] ^ (1/n) \qquad (3.8)$$

where Rt is the true formation resistivity from the deep-reading resistivity log, φe is the effective porosity, a is the tortuosity factor, m is the cementation exponent, and n is the saturation exponent. The values a = 1.0, m = 2.0, and n = 2.0, appropriate for well-cemented clean sandstone reservoirs, were used as initial estimates and then refined from the Pickett-plot analysis above (Asquith & Krygowski, 2004). In shaly-sand intervals with shale volume between 0.10 and 0.30, a shale-corrected saturation model, the Indonesia equation of Poupon and Leveaux (1971), was applied to account for the extra conductivity from the clay minerals. Hydrocarbon saturation was taken as the complement of water saturation:

$$SHC = 1 - Sw \qquad (3.9)$$

3.3.6 Cross plots

Cross plots were used as part of the petrophysical workflow to evaluate the lithological composition and reservoir characteristics of the Lower Goru C-sand at the Tajjal wells. The cross plots integrate responses from different wireline logs and provide an additional check on the lithology and porosity interpretation derived from conventional log analysis.

3.3.7 Density-Neutron Cross plot

The density-neutron cross plot was used to evaluate lithology, porosity, and possible gas effects in the reservoir interval. Bulk density (RHOB) was plotted against neutron porosity (NPHI), and the distribution of data points was compared with standard sandstone, limestone, and dolomite trends. For the Lower Goru C-sand, particular attention was given to the position of the data relative to the sandstone trend and to neutron-density separation associated with hydrocarbon effects.

3.3.8 M-N Cross plot

The M-N cross plot was used to further evaluate matrix lithology using density, neutron, and sonic-log responses. The calculated M and N parameters reduce the influence of porosity and allow the data to be compared with characteristic lithological fields. This provides an independent lithological check on the density-neutron interpretation and supports the identification of the dominant sandstone matrix within the Lower Goru reservoir.

3.4 Seismic Data Interpretation

Structural and stratigraphic interpretation of the 3D seismic volume was carried out in IHS Kingdom, to map the geometry of the reservoir-bearing formations and the principal fault systems controlling the closure, and to generate time and depth structure maps for the inversion workflow. The interpretation ran through five steps: seismic data quality control, data loading, synthetic-seismogram generation, fault and horizon interpretation, and time-to-depth conversion.

3.4.1 Quality Control of Seismic Data

Initial quality control of the 3D seismic volume was done before loading into Kingdom. The SEG-Y file was interrogated to verify the byte locations for the inline, crossline, X, and Y coordinates, so every trace was positioned correctly. To process the amplitude spectrum and frequency content of the seismic data a statistical wave let was generated from window of the seismic data, to achieve the required resolution the frequency

of the seismic data was sufficient. Fold maps and amplitude-gradient maps were inspected for acquisition-footprint artefacts. The polarity was confirmed as zero-phase, SEG normal, in which a positive reflection coefficient corresponds to a positive peak, as the model-based inversion algorithm requires. No significant data-quality issues that would block quantitative analysis were found.

3.4.2 Loading of Seismic Data

The quality-controlled 3D seismic volume was loaded into the Kingdom project through the SEG-Y import utility. Inline and crossline numbering, areal extent, bin dimensions, and datum elevation were registered and checked against the survey-acquisition report. Well locations were projected into the seismic grid using the dataset's coordinate system, and deviation surveys tied deviated well trajectories to the correct traces. The GVERSE petrophysical outputs, shale volume, effective porosity, water saturation, and the acoustic-impedance logs from the density and sonic data, were also imported into Kingdom so the log curves could be shown alongside the seismic traces at each well. This allowed the reflection events to be calibrated to geology directly during horizon picking.

3.4.3 Synthetic Seismogram and Well-to-Seismic Tie

A synthetic seismogram was generated for each of the three Tajjal wells to fix the depth-to-time relationship and calibrate the tie between the well stratigraphy and the seismic reflections. The acoustic-impedance log, the product of bulk density and compressional velocity, was computed from the density (RHOB) and sonic (DT) logs in GVERSE and exported to Kingdom. Reflection coefficients were then computed from the impedance contrasts at each lithological boundary:

$$RC = (Zp2 - Zp1) / (Zp2 + Zp1) \qquad (3.10)$$

where Zp1 and Zp2 are the acoustic impedances of the upper and lower layers at each interface (Yilmaz, 2001). An extracted wavelet, obtained by statistically cross-correlating the measured seismic traces at the well location with the reflectivity series, was convolved with the reflection-coefficient series to produce the synthetic seismogram:

$$s(t) = w(t) * r(t) + n(t) \qquad (3.11)$$

where s(t) is the synthetic trace, w(t) is the extracted wavelet, r(t) is the reflectivity series, the asterisk denotes convolution, and n(t) is noise. The Depth-to-Time Conversion was iteratively improved, until the generated Synthetic Seismogram achieved a Cross-Correlation Coefficient of at least 0.85 with the closest real seismic trace. The resulting time-depth relationships were used throughout the interpretation and inversion.

3.4.4 Fault and Horizon Interpretation

Structural interpretation was done on the 3D seismic volume using arbitrary lines, time slices, and variance (similarity) attribute volumes generated within Kingdom. Fault planes were first picked on variance time slices, which highlight the lateral waveform discontinuities at fault zones. Fault sticks were digitized on a regular grid of inlines and crosslines through the fault zones and assembled into fault surfaces. The primary reservoir reflection events, identified and calibrated through the synthetic-seismogram analysis, were picked on a grid of inlines and crosslines and interpolated automatically with the guided auto-tracking algorithm. Manual editing was applied where signal quality was poor or the structure complex, to keep the interpretation geologically consistent. All horizon picks were validated against the well-top markers at the three Tajjal wells before acceptance.

3.4.5 Time and Depth Maps

Two-way travel-time structure maps were generated from the interpreted horizon surfaces for the top and base of the principal reservoir intervals. Depth conversion used an interval-velocity model built from the check shot data at the three wells. A layered velocity model was made by assigning interval velocities between the key reflectors, and the velocities were interpolated laterally across the survey with a kriging algorithm in Kingdom. The time maps were then converted to depth by applying the velocity model to the two-way travel-time values. The resulting depth maps were the structural framework for the seismic inversion and the subsequent characterization of the porous reservoir sand.

3.5 Post-Stack Seismic Inversion

Post-stack model-based seismic inversion was done in CGG Hampson-Russell to turn the 3D seismic amplitude volume into a volumetric acoustic-impedance model. The workflow had five steps: data loading, wavelet extraction, well-to-seismic tie, low-frequency model construction, and model-based inversion analysis. The inverted acoustic-impedance volume was the primary geophysical basis for mapping the distribution and quality of the porous reservoir sand away from well control.

3.5.1 Loading of Data

The seismic volume, the interpreted horizons and fault polygons, and the well data, including the full log suites and the depth-to-time curves from Kingdom, were loaded into the Hampson-Russell project. The acoustic-impedance logs from GVERSE were set as the target property for the inversion. All well trajectories and log data were confirmed correctly projected into the seismic-grid coordinate system before the inversion began. Wavelet extraction and inversion were restricted to the time window bracketing the reservoir interval, defined by the top and base horizons imported from Kingdom.

3.5.2 Wavelet Extraction

An accurate wavelet is a prerequisite for reliable model-based inversion, because the algorithm effectively deconvolves the wavelet from the seismic trace to recover the reflectivity. A statistical wavelet was first extracted from a window of the 3D volume around the reservoir interval using a least-squares technique that minimizes the difference between the synthetic and real traces at all three wells at once. The phase and frequency content of the extracted wavelet were carefully examined. This examination confirmed that the wavelet had a Near-Zero Phase feature, which was consistent with the seismic polarity detected by the previously performed seismic quality control. Then, Well-to-Seismic Tie Cross-Correlation Analysis was used to further refine the wavelet phase spectrum. Finally, a deterministic wavelet was selected, which was shaped in such a way that the best match was achieved between the synthetic seismograms and the real seismic data in all wells (Tajjal-1, Tajjal-2 and Tajjal-3) (Hampson & Russell, 1991).

3.5.3 Well-to-Seismic Tie

Well to seismic tie was performed in Hampson-Russell software where the reflectivity series obtained from acoustic impedance was convolved with extracted wavelet which result in synthetic seismogram, this actual seismic trace was compared with this synthetic seismogram at individual well to establish best match. To test the accuracy of the well to seismic tie a cross-correlation coefficient was calculated, the reason is to correct minor difference between them. (White & Simm, 2003). The final ties reached cross-correlation coefficients above 0.85 for all three wells, confirming the wavelet and time-depth relationships were adequate for model-based inversion.

3.5.4 Low-Frequency Model

Post-stack seismic data are band-limited and lack the low-frequency component, generally below six to eight hertz, of the acoustic impedance. A low-frequency model was therefore built to supply those missing frequencies, which control the bulk impedance trend of the inverted volume. It was made by interpolating the low-pass-filtered acoustic-impedance logs from the three Tajjal wells along the interpreted horizons with a kriging algorithm in Hampson-Russell. The interpolation was constrained to honour the reservoir's structural geometry from the Kingdom depth maps. The resulting 3D low-frequency volume was combined with the reflectivity-based component of the inversion to give a broadband impedance model, following Pendrel (2001).

3.5.5 Model-Based Inversion Analysis

Model-based inversion was run on the post-stack amplitude volume with the Hampson-Russell model-based algorithm (Hampson & Russell, 1991). It iteratively updates an initial acoustic-impedance model, derived from the low-frequency model, until the synthetic seismogram from the model matches the observed traces within a user-defined convergence criterion. The objective function minimized during inversion is:

$$J = \| d - Lm \|^2 + \lambda \| Wm \|^2 \qquad (3.12)$$

where d is the observed seismic data vector, L is the forward-modelling operator representing the convolution of the wavelet with the derivative of the impedance, m is the impedance model, W is a weighting matrix that stabilizes the solution, and λ is a regularization parameter controlling the trade-off between data fit and model smoothness. The inversion was run with hard constraints, upper and lower bounds on acoustic impedance from the well logs, to keep impedance values geologically reasonable. Convergence was tracked by inspecting the residual between the synthetic and observed seismic at each iteration. The result was checked by blind-well testing, repeating the inversion with one well left out at a time and comparing the inverted impedance at the omitted well with its measured impedance log. The resulting 3D acoustic-impedance volume was the primary input for characterizing the porous reservoir sand.

3.5.6 Interpretation of the Inverted Acoustic Impedance

The inverted acoustic-impedance volume gave a continuous, spatially interpolated picture of acoustic impedance across the 3D survey at seismic resolution. Being the product of density and compressional velocity, acoustic impedance responds to lithology, porosity, and pore-fluid content, which makes it a strong discriminator between reservoir and non-reservoir rock in clastic settings (Mavko et al., 2009). Low values correspond to porous, potentially gas-bearing sandstones; higher values mark tight sands and shales. Cross plots of the inverted acoustic impedance against the petrophysical derived effective porosity and shale volume at the wells fixed the quantitative relationship between impedance and reservoir quality. Impedance thresholds for net-reservoir conditions were then derived from that relationship and applied to the inverted volume to map the porous reservoir sand within the interpreted closure.

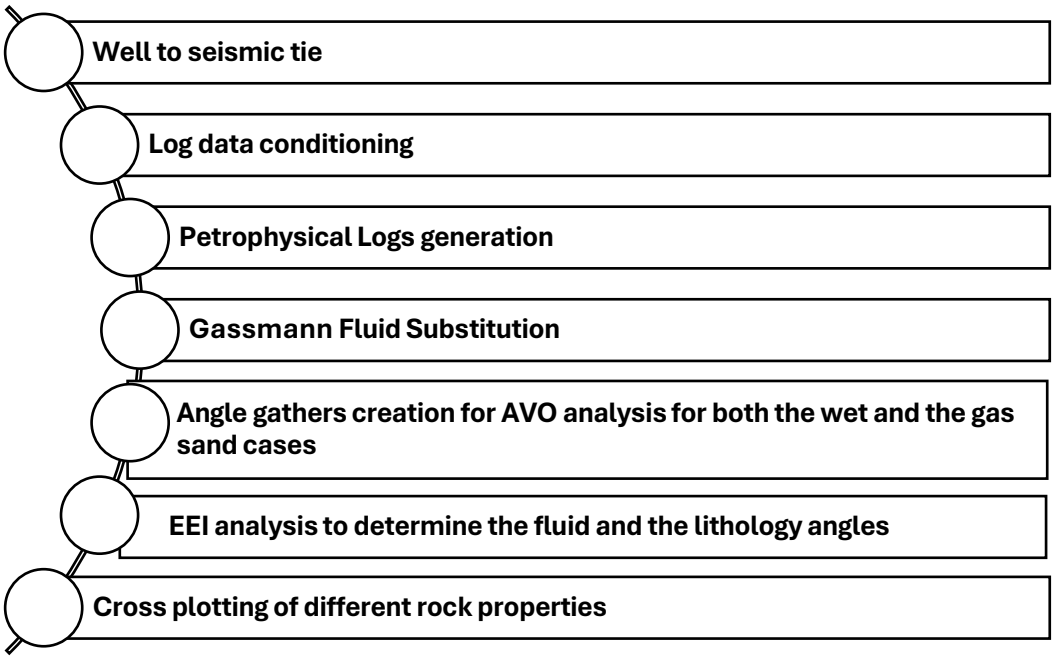
3.6 Amplitude-Versus-Offset (AVO) Analysis

AVO analysis was done in CGG Hampson-Russell to characterize the fluid content of the Lower Goru C-sand and to give an independent geophysical check on the porous, gas-bearing reservoir sand identified from the petrophysical analysis and the acoustic-impedance inversion. Where the post-stack inversion works on the stacked, zero-offset volume and is

sensitive mainly to acoustic impedance, the AVO analysis was done on the pre-stack data and used the variation of reflection amplitude with source-receiver offset, which carries the extra information on the shear properties and Poisson's ratio contrast that is diagnostic of pore fluid. The AVO workflow had four steps: conditioning the pre-stack gathers, AVO forward modelling at the wells, extracting the AVO attributes, and interpreting the AVO response.

3.6.2 AVO Forward Modelling

Synthetic AVO forward modelling was carried out at the wells to establish the expected AVO response of the Lower Goru C-sand under in-situ fluid conditions and to give a template for comparing the observed response. Using the compressional velocity, shear velocity where available, and density from the logs, synthetic angle gathers were generated by computing the offset-dependent reflection coefficients across the reservoir interfaces. Where a measured shear-velocity log was missing, shear velocity was estimated from compressional velocity and lithology using an established empirical relationship for water-saturated clastic (Castagna & Backus, 1993). The synthetic gathers confirmed the character of the AVO response expected for the porous gas sand and calibrated the interpretation of the observed pre-stack amplitudes.



Workflow chart of AVO and Rock physics

3.6.3 AVO Attribute Extraction

The angle-dependent reflectivity was analyzed using the two-term linear approximation of Shuey (1985), which expresses the reflection coefficient as a function of the angle of incidence:

$$R(\theta) \approx A + B \sin^2\theta \qquad (3.13)$$

where $R(\theta)$ is the reflection coefficient at angle of incidence θ, A is the intercept, corresponding to the normal-incidence reflection coefficient and closely related to the acoustic-impedance contrast, and B is the gradient, describing the rate of change of amplitude with offset and controlled by the contrast in Poisson's ratio across the interface. The intercept and gradient attributes were extracted from the conditioned angle gathers by fitting the linear relationship of Equation 3.13 to the observed amplitudes at each time sample. The resulting intercept and gradient volumes were the basis for the AVO interpretation.

3.6.4 AVO Interpretation

The AVO response of the Lower Goru C-sand was interpreted by cross-plotting the intercept against the gradient and looking at where the reservoir reflections fall in the intercept-gradient domain (Castagna & Swan, 1997). The porous gas-bearing sand was expected to show an anomalous AVO response, an increase in reflection magnitude with offset that sets it apart from the surrounding brine-saturated and shaly lithologies, matching the AVO class defined by Rutherford and Williams (1989) for the reservoir's impedance contrast. The intercept and gradient volumes were combined into AVO attribute displays that highlight the reservoir anomaly, and the resulting response was compared with the acoustic-impedance inversion and the petrophysical results at the wells. The AVO fluid indicator, the low-impedance response, and the log-derived hydrocarbon saturation agreeing gave the integrated, mutually reinforcing evidence for the presence and quality of the porous reservoir sand that is the principal outcome of the study.

3.6.5 Rock Physics

Rock physics analysis was performed using well-log-derived elastic properties to investigate the relationship between lithology, porosity, and pore-fluid effects in the Lower Goru C-sand. The analysis included V_p, V_s, acoustic impedance (AI), Poisson's ratio, Lambda-Rho ($\lambda\rho$), Mu-Rho ($\mu\rho$), and Extended Elastic Impedance (EEI). These parameters were crossplotted to identify trends and clusters associated with reservoir lithology and fluid effects and to provide well-based constraints for the seismic interpretation and AVO analysis.

3.6.6 Cross Plot for Vp versus Vs

The V_p versus V_s crossplot was generated to examine the elastic relationship between compressional and shear-wave velocities and to assess variations associated with lithology and pore-fluid conditions. The distribution of the well-log data was used as a reference for evaluating the elastic response of the Lower Goru reservoir intervals.

3.6.7 Cross Plot for AI vs Poisson Ratio

The acoustic impedance versus Poisson's ratio cross plot was used to evaluate the combined response of acoustic impedance and elastic deformation properties. AI is calculated from V_p and density, while Poisson's ratio is derived from V_p and V_s. Their relationship provides an additional basis for distinguishing reservoir and non-reservoir intervals and assessing fluid-related changes.

3.6.8 Cross Plot for Lambda-Rho vs Mu-Rho

The Lambda-Rho ($\lambda\rho$) versus Mu-Rho ($\mu\rho$) crossplot was used to separate variations related to pore-fluid sensitivity and rock rigidity. Lambda-Rho is more sensitive to changes in incompressibility and pore-fluid content, whereas Mu-Rho is more closely related to the rigidity of the rock matrix. The crossplot was therefore used to evaluate lithology and fluid-related trends within the Lower Goru C-sand.

3.6.9 EEI Analysis

Extended Elastic Impedance (EEI) analysis was performed to identify an elastic parameter that provides improved sensitivity to selected reservoir properties. Different chi (χ) angles were evaluated to determine the EEI response most suitable for the Lower Goru reservoir. EEI was used as a complementary rock-physics attribute rather than as a standalone indicator of reservoir fluids.

3.6.10 Cross Plot for Lambda-Rho vs EEI at Chi 32

The Lambda-Rho versus EEI cross plot at $\chi = 32°$ was generated to examine the combined sensitivity of these two elastic attributes. This cross plot was used to evaluate the separation of the interpreted reservoir and non-reservoir responses and to provide additional support for the fluid and lithology interpretation presented in Chapter 4.

3.7 Integration of Results

The four stages of the workflow were integrated into a coherent characterization of the porous reservoir sand of the Lower Goru C-sand in the Gambat Block. The key characteristics of petrophysical analysis at each well scale are: Volume of shale, Effective porosity and Fluid and Water Saturation for the identification of porous hydrocarbon bearing zones, density and sonic logs were obtained from petrophysical analysis which formed the

base of seismic-to-well tie and provide basic information for seismic inversion reliability. Through seismic interpretation we obtained Structural & stratigraphic framework and real geometry of the data in depth domain Seismic Amplitude is converted into Acoustic Impedance Volume with the help of post=stack seismic inversion, this acoustic impedance volume helped in distribution of the porous reservoir sand this acoustic impedance was calibrated with petrophysical properties to establish a relationship between impedance and porosity. AVO gave an independent fluid indicator conforming that low impedance porous sand was a gas bearing, all the results were combined in chapter 4. Distribution, Quality and fluid content of porous reservoir sand in the study area were determined with the all these results which formed the basis for the final conclusions and recommendation of this study.

CHAPTER 4
RESULTS AND INTERPRETATION

4.1 Introduction

This chapter reports the results and reads them for what they say about the reservoir character of the Lower Goru B sands in the Gambat Block. Four analyses feed it: the petrophysical evaluation of the three control wells, the structural and stratigraphic interpretation of the 3D seismic volume, the post-stack seismic inversion, and the AVO modelling with its rock physics. They appear in the order the work was done, since each stage builds on the last and how much you can trust the later, more quantitative results depend on how good the earlier ones are.

Petrophysical evaluation comes first. The petrophysical evaluation of Tajjal-01, Tajjal-02 and Tajjal-03 then measures what the wells actually hit. Volume of shale, effective porosity and water saturation are computed through the target intervals, and the density-neutron and M-N cross plots fix the matrix mineralogy and confirm the gas effect seen on the porosity logs. These numbers are the ground truth for judging the seismic-derived properties later on.

The base map fixes the survey geometry and where Tajjal-1, Tajjal-2 and Tajjal-3 sit within it. The synthetic seismogram at Tajjal-01 ties the depth-domain logs to the seismic volume, which lets the formation tops be carried onto the sections in two-way time. Six interpreted profiles, three inlines and three crosslines through the wells, trace the Upper Goru marker, the Lower Goru marker and the C, B and A sand intervals across the block. Gridding those picks gives the two-way time structure maps, and the well velocities convert them to the depth maps.

The petrophysical evaluation of Tajjal-01, Tajjal-02 and Tajjal-03 then measures what the wells actually hit. Volume of shale, effective porosity and water saturation are computed through the target intervals, and the density-neutron and M-N cross plots fix the matrix mineralogy and confirm the gas effect seen on the porosity logs. These numbers are the ground truth for judging the seismic-derived properties later on.

The third section covers the post-stack seismic inversion, which turns the reflectivity of the seismic volume into acoustic impedance. It runs through the statistical wavelet extraction, the low-frequency model built from the well logs, the model-based and sparse-spike algorithms and the correlation each reaches at the wells, and ends with the inverted impedance sections and the horizon maps of the top C and B intervals, where the porous sand fairways stand out as low-impedance zones.

The AVO modelling and rock physics close the chapter. Gassmann fluid substitution builds the brine and gas cases at Tajjal-01, angle gathers modelled from those cases fix the AVO class of the reservoir, and a set of cross plots tests which elastic attributes best pull the porous gas sands apart from the brine-bearing sands and the encasing shales: P-wave against S-wave velocity, acoustic impedance against Poisson's ratio, lambda-rho against mu-rho, and extended elastic impedance at the optimal chi angle. Between them the four analyses give a consistent description of the C and B sand intervals and show how far that description carries away from well control.

4.2 Petrophysical Analysis

The petrophysical evaluation of Tajjal-01 turns the full wireline suite into a quantitative description of the reservoir, the ground-truth the seismic and inversion interpretations are calibrated against. The composite display holds the gamma-ray, spontaneous potential and caliper curves for lithology, the deep, medium and shallow resistivity curves for fluid, the neutron and density porosity logs, the sonic curve, and the computed volume of shale, porosity and water saturation tracks. Within the reservoir the gamma-ray drops sharply, marking clean sandstone units well separated from the higher gamma-ray shales, and these clean sands line up with the developed porosity and reduced shale volume that make them reservoir-quality rock.

The clearest diagnostic is the crossover between the neutron and density porosity curves in the cleaner sands, the classic signature of gas-bearing porous sandstone, which says the reservoir at Tajjal-01 holds hydrocarbon rather than water. The elevated deep resistivity across the same intervals backs this up, as does the separation between the deep and shallow resistivity curves, the invasion behavior expected of a permeable, hydrocarbon-bearing formation. Computed water saturation drops in these zones, confirming significant hydrocarbon saturation, and the porosity track reads values consistent with an effective reservoir. So Tajjal-01 establishes the Lower Goru sands here as clean, porous and gas-bearing, and it sets the petrophysical benchmark that ties the low-impedance and neutron-density crossover responses to real reservoir quality, the physical basis for the inversion and fluid-substitution work that follows.

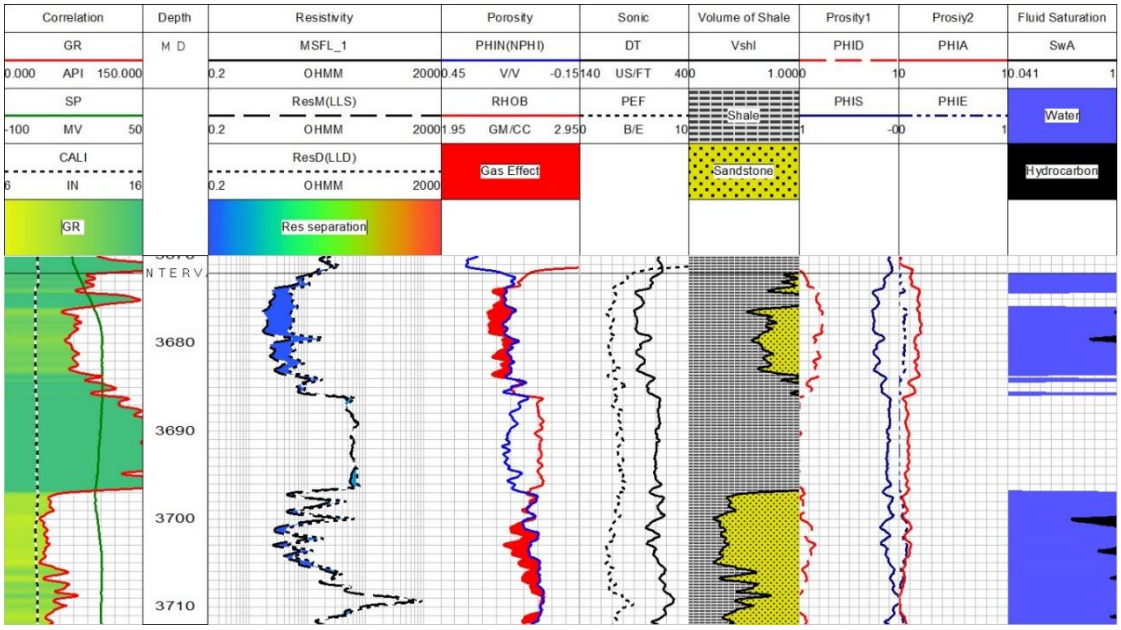


Figure 4. 1 Tajjal 01 Result Petrophysical evaluation of Tajjal-01 showing lithology, porosity, and fluid-saturation responses.

The Tajjal-02 result carries the reservoir evaluation into the central part of the survey and tests the character seen at Tajjal-01 at a second, independent control point. The log suite again separates clean sand from shale on the gamma-ray and shale-volume tracks, reads fluid content from the resistivity curves, and puts numbers on porosity from the neutron, density and sonic responses. The reservoir sands here show up as intervals of reduced gamma-ray and shale volume with developed porosity, which confirms the porous Lower Goru sands are present and mappable in the center of the block, in line with the lateral continuity inferred from the sections.

The porosity and resistivity curves across the sands point to effective reservoir rock, and any neutron-density crossover and resistivity rise within the interval carries the same hydrocarbon meaning as at Tajjal-01. Setting Tajjal-02 against Tajjal-01 shows how reservoir quality varies between the northern and central wells: where the two agree, the reservoir looks laterally persistent; where porosity or net sand differ, that difference is the heterogeneity the inversion is meant to map. A calibrated petrophysical description at the central control point strengthens the well-to-seismic link in the interior of the survey and adds an anchor for carrying reservoir properties away from well control.

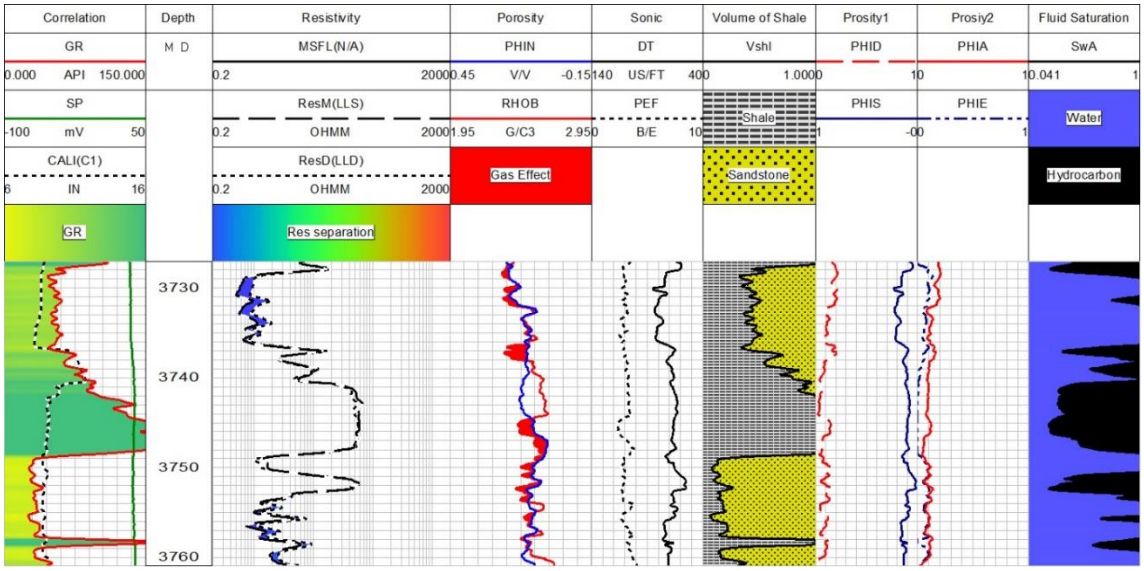


Figure 4. 2 Tajjal 02 Result Petrophysical evaluation of Tajjal-02 showing lithology, porosity, and fluid-saturation responses.

The Tajjal-03 evaluation closes out the well-based characterization with the sand development in the south-west, the third calibration point needed to pin down the lateral variability of the Lower Goru sands. As at the other wells, the gamma-ray and shale-volume tracks separate clean sand from shale, the resistivity curves drive the fluid interpretation, and the porosity logs measure the pore volume. The reservoir sands here show the porous Lower Goru intervals reaching into the southern part of the block, correlating with the equivalent units at Tajjal-1 and Tajjal-2 and matching the horizon continuity on the sections.

The porosity and resistivity character of the sands at Tajjal-03 lets reservoir quality in the south-west be set against the north and center, and how alike or different the three wells are giving a direct measure of heterogeneity across the survey. Where the sands stay clean and porous, the reservoir is laterally continuous; where their character shifts, that variation defines the property trends the inversion resolves between wells. With three calibrated wells across the block, the petrophysical analysis gives a spatially representative description of the reservoir, fixes the relationship between log-derived properties and seismic response, and feeds the cross plots, the fluid substitution modelling and the inversion that follow.

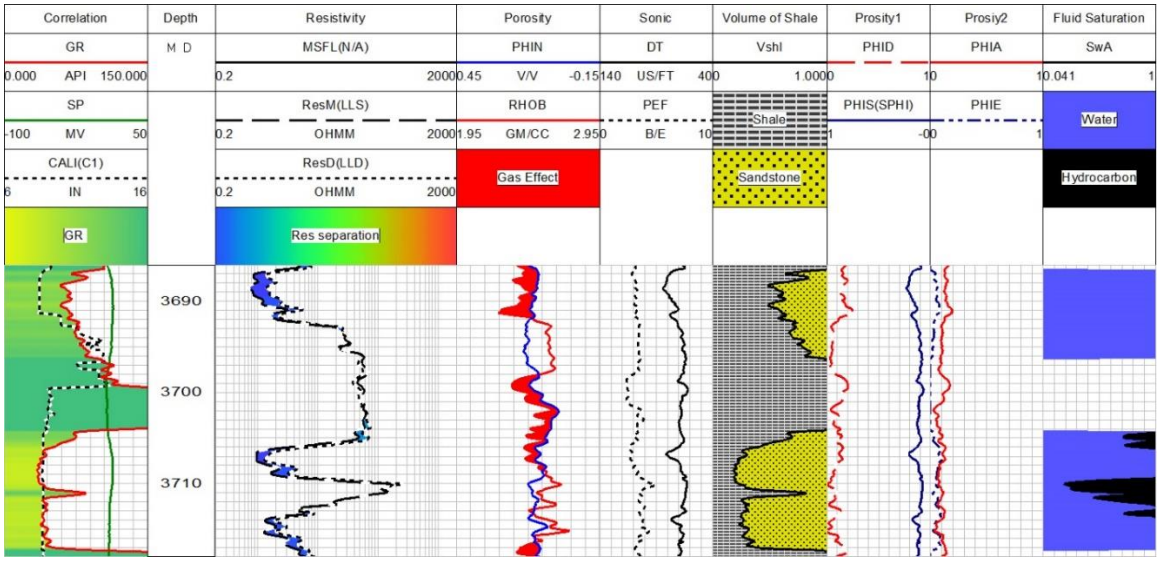


Figure 4. 3 Tajjal 03 Result Petrophysical evaluation of Tajjal-03 showing lithology, porosity, and fluid-saturation responses.

4.2.1. Cross Plots

4.2.1.1 Density-Neutron Cross Plot

The density-neutron cross plot pulls lithology and fluid apart in a domain sensitive to both matrix composition and pore fluid, a property-based view to set beside the depth-based petrophysical evaluation. The data points plot against the standard mineral lines for quartz sandstone, limestone and dolomite, color-coded by gamma-ray so the effect of shale content reads directly. The clean, low-gamma-ray sands plot toward the quartz sandstone trend, which confirms their siliciclastic makeup, while the higher gamma-ray points move off the sandstone line toward the shale region as clay content rises.

The feature that carries the fluid information is the shift of some sand points toward lower density and lower apparent neutron porosity, the classic gas-effect direction, which happens because gas in the pore space cuts both the bulk density and the hydrogen index the neutron log reads. This independently backs the hydrocarbon interpretation from the neutron-density crossover in the individual well evaluations and confirms the porous sands hold gas rather than water. Pulling the clean gas-bearing sands apart from the shales and any water-bearing intervals, the density-neutron cross plot gives the petrophysical basis for telling reservoir from non-reservoir on rock and fluid properties, and it links the log measurements to the elastic responses used in the inversion and AVO work.

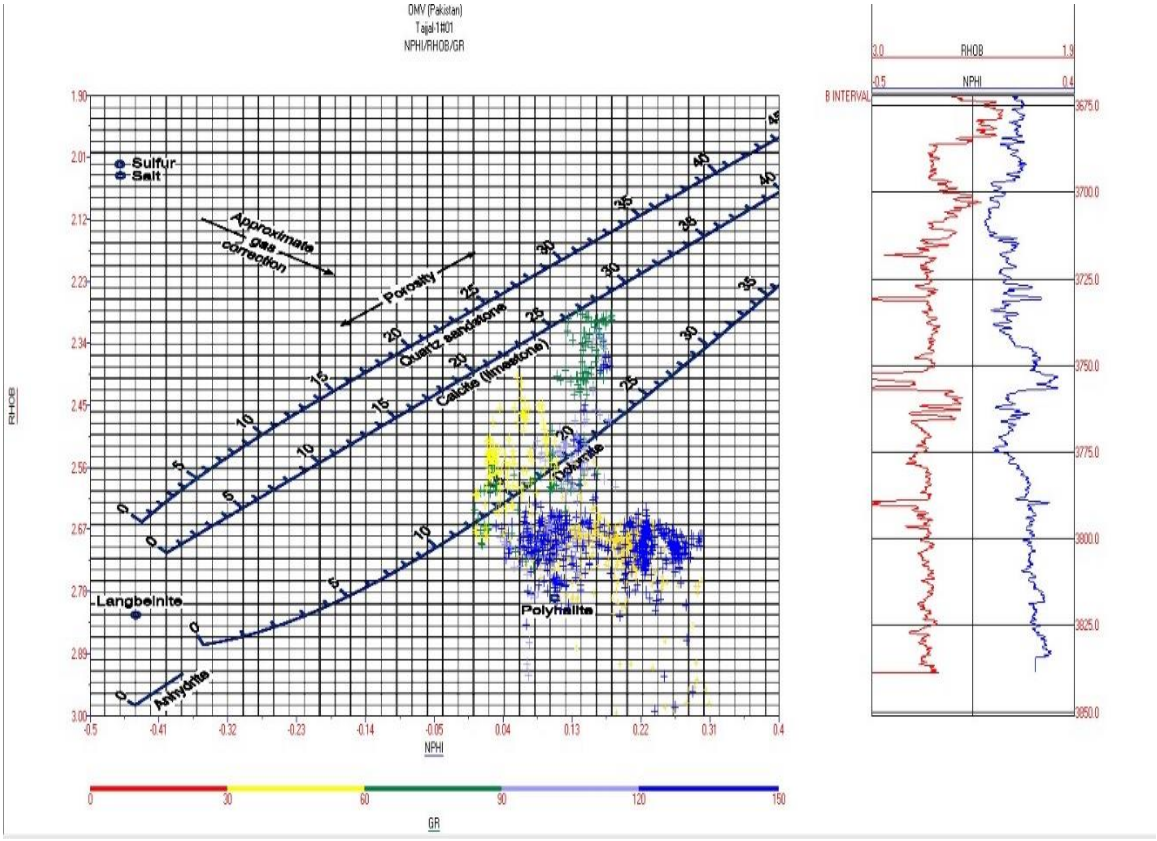


Figure 4. 4 Density Neutron Cross plot Density-neutron cross plot showing lithological and porosity relationships in the reservoir interval.

4.2.1.2 M-N Cross Plot

The M-N cross plot sharpens the mineralogy by folding the sonic, density and neutron responses into two lithology-sensitive parameters that are largely independent of porosity, which isolates the matrix character from the pore space. The data plot against the positions of the main rock-forming minerals, quartz sandstone, limestone, dolomite and the evaporite and clay end-members, so the mineralogical affinity of the reservoir and non-reservoir intervals reads straight off the point cloud. The reservoir sands cluster in the quartz sandstone region, confirming the siliciclastic mineralogy from the density-neutron analysis, while points trending toward the shale and carbonate fields mark the non-reservoir and cement-affected intervals.

The point distribution also picks up secondary porosity and gas, which push the data in characteristic directions and add evidence for porous, hydrocarbon-bearing sandstone in the succession. Confirming the reservoir units are mainly quartzose and separating them from the shaly and carbonate-affected intervals, the M-N cross plot takes the ambiguity out of the lithology and strengthens the case for the clean sands as the effective reservoir. With the density-neutron cross plot, it fixes the mineralogical and fluid picture: the target is porous

quartz sandstone charged with gas, the exact rock-and-fluid combination the low-impedance inversion response and the AVO modelling are built to detect.

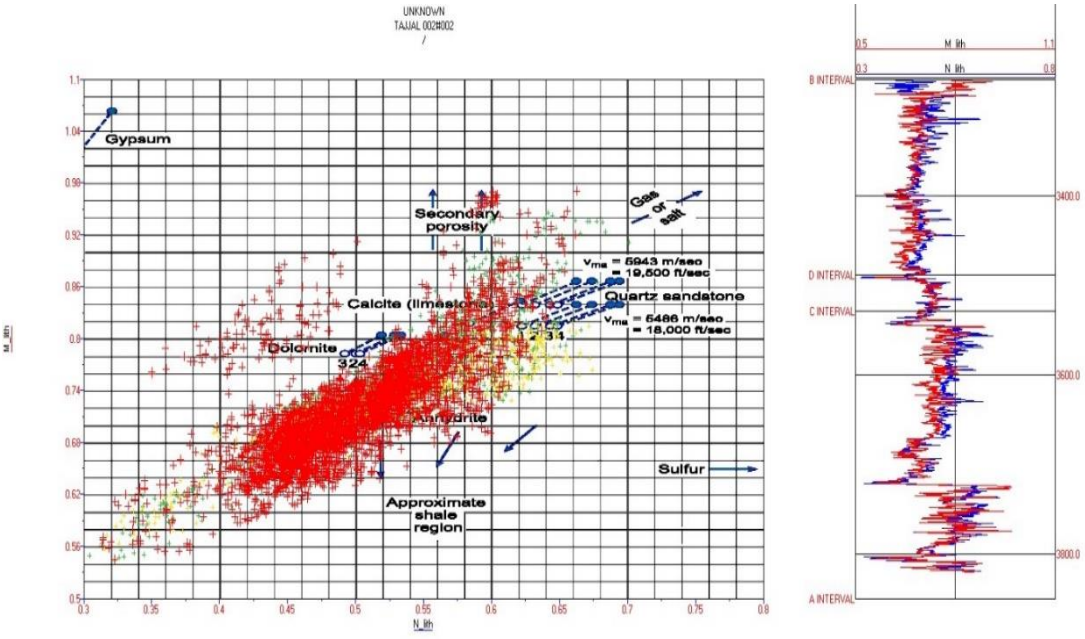


Figure 4. 5 M N Cross plot M-N cross plot showing the interpreted lithological characteristics of the reservoir interval.

4.3 Seismic Data Interpretation

The base map sets the spatial frame for everything that follows. The survey is a 3D grid tilted obliquely to geographic north, inline and crossline numbers climbing across the acquisition footprint, and the three control wells, Tajjal-1, Tajjal-2 and Tajjal-3, sit in the northern, central and south-western parts of the block. That spread is what letting the seismic character at each borehole be carried out laterally with reasonable confidence, rather than pushed out from a single point. Tajjal-1 is in the north at roughly inline 1455, crossline 525, Tajjal-2 lies in the central-eastern region, and Tajjal-3 to the south-west, so the wells bracket the structural and stratigraphic range of the Lower Goru interval this study is after.

The regular bin geometry and even well coverage make the dataset fit for quantitative work, horizon mapping, time-to-depth conversion and post-stack inversion, since no large untied gaps spoil the interpolation between wells. Where the wells sit also governs how the porous Lower Goru sand fairways correlate between boreholes and how far an inverted impedance anomaly can be trusted away from control. The synthetic ties, the interpreted sections, the time and depth maps and the inversion volumes all rest on this geometry.

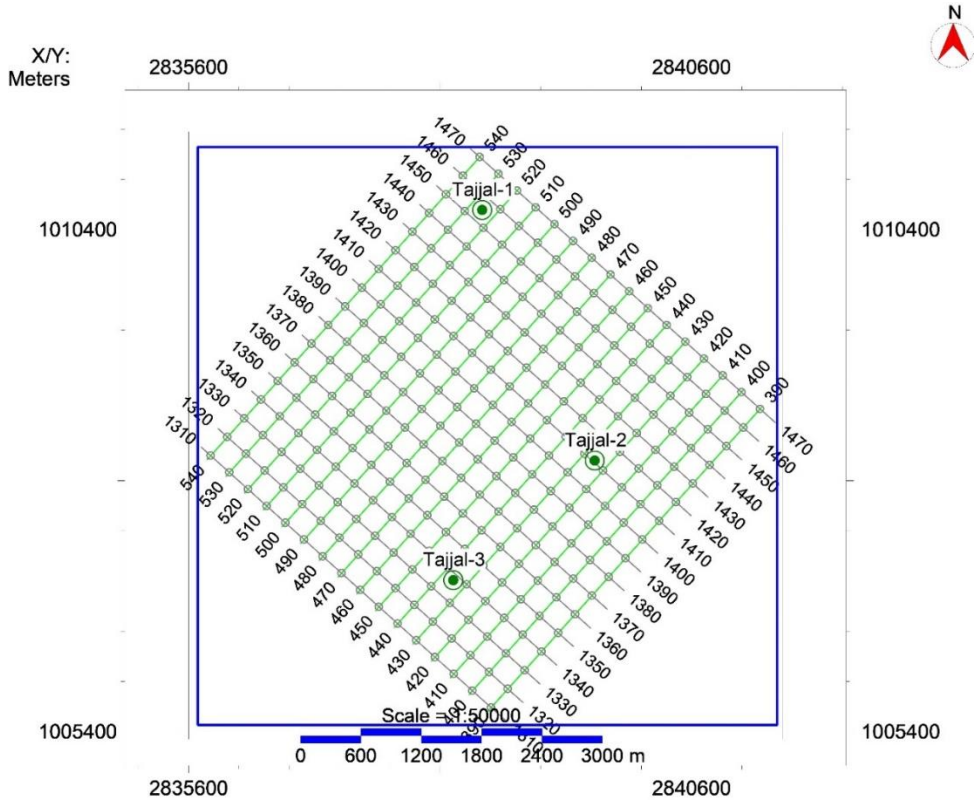


Figure 4. 6 Base map showing the seismic survey and locations of Tajjal-1, Tajjal-2, and Tajjal-3 wells.

4.3.1 Synthetic Seismogram of Tajjal-01

The Tajjal-01 synthetic seismogram links the depth-domain well measurements to the time-domain seismic volume, and the whole interpretation stands or falls on how well it ties. The display shows the sonic and density logs, the derived acoustic impedance and reflection coefficient series, the extracted wavelet, and the synthetic trace beside the composite seismic trace at the well. Through the zone of interest, the synthetic and the real seismic agree well, the main reflection events lining up in two-way time. So, the velocity and density functions were converted to time correctly, and the reflections come from real impedance contrasts rather than noise or processing artefacts.

The reflectivity series follows the vertical succession of impedance contrasts, and the strong events within the interval mark the boundaries between the shale-dominated background and the interbedded Lower Goru sands. Because the tie fixes the two-way time position of these markers, the Upper Goru, the shale interval and the C, B and A sand intervals can be projected onto the sections with confidence. Everything quantitative downstream depends on this tie. The wavelet estimated here is reused for horizon picking and, more importantly, for the inversion, so a bad tie would push error straight into the inverted impedance and into any conclusion about where the porous sands are. In short, the

Tajjal-01 synthetic calibrates the seismic to geology and validates the wavelet and time-depth relationship the inversion relies on.

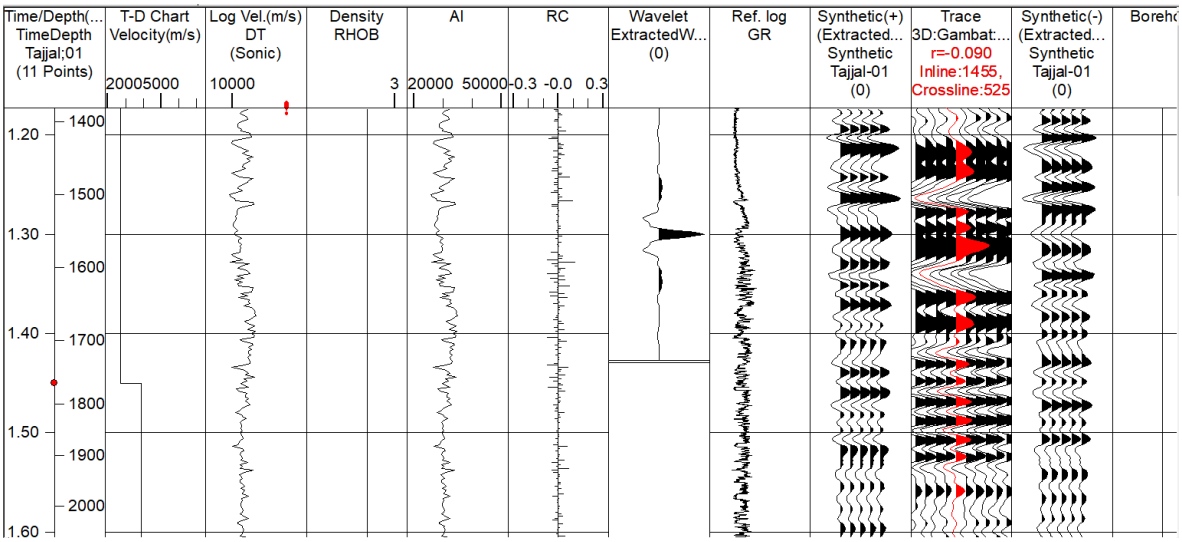


Figure 4. 7 Synthetic seismogram showing the well-to-seismic correlation at Tajjal-01.

4.3.2 Interpreted Seismic Sections

Inline 1327 runs near Tajjal-3 and shows the interpreted Upper Goru, Lower Goru marker, and the C and B sand intervals as continuous, laterally traceable reflections. The reflectors hold across most of the profile, which points to a stable depositional setting and the layer-cake stratigraphy typical of the passive-margin shelf sequence of the Lower Goru in the Central Indus Basin. The geometry is gentle and coherent, and between the Lower Goru marker and the deeper sand events the interval alternates high- and low-amplitude reflections, the signature of interbedded sands and shales. A mapped fault on this line cuts the otherwise continuous reflectors and may control reservoir compartmentalization and the migration and trapping of hydrocarbons.

The well tops tie to specific seismic loops, which confirms the target sands hold a consistent stratigraphic position and can be followed away from Tajjal-3. Zones where the reflection weakens or the waveform changes are worth a look, since such variations can mark lateral changes in lithology or porosity within the sands. Inline 1327 sets the structural and stratigraphic template for the southern part of the survey and shows the reservoir horizons are laterally persistent enough to map across the full volume, with the fault as the one discontinuity to weigh when judging reservoir continuity.

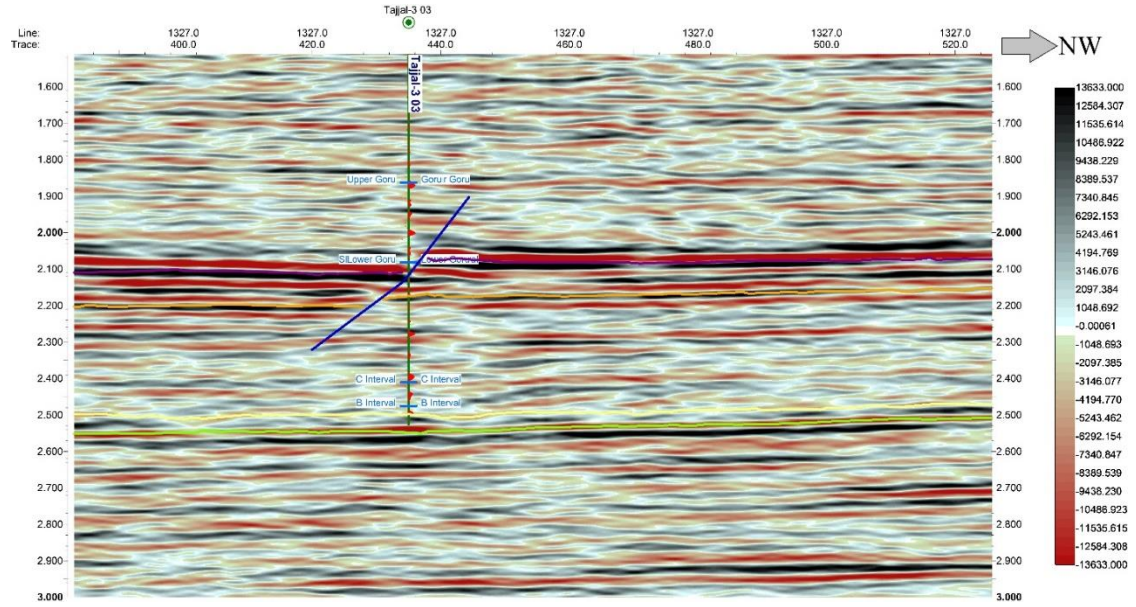


Figure 4.8 Seismic inline 1327 showing the interpreted reservoir horizons and structural framework.

Inline 1413 ties to Tajjal-2 and confirms the framework from the previous line, this time through the central part of the block. The Upper Goru, Lower Goru, C and B markers are again traceable as coherent reflections, and their consistent two-way time separation from line to line means the interval thicknesses hold up here, in keeping with laterally continuous shelf sedimentation. The reflection package around the sands shows the same amplitude alternation of the interbedded sand-shale succession, and the continuity of the events fits the porous sands keeping their lateral extent between the central and southern wells.

Subtle changes in amplitude and reflection continuity along this line track changes in the internal properties of the sands, and locally enhanced or subdued responses are worth flagging as possible improved porosity or a change in fluid fill. Because the section ties to Tajjal-2, the seismic character here can be checked straight against that well's petrophysical evaluation, tightening the link between reflection response and reservoir quality. Inline 1413 carries the target horizons into the center of the survey and adds an independent, well-controlled tie point to the regional correlation of the Lower Goru sands.

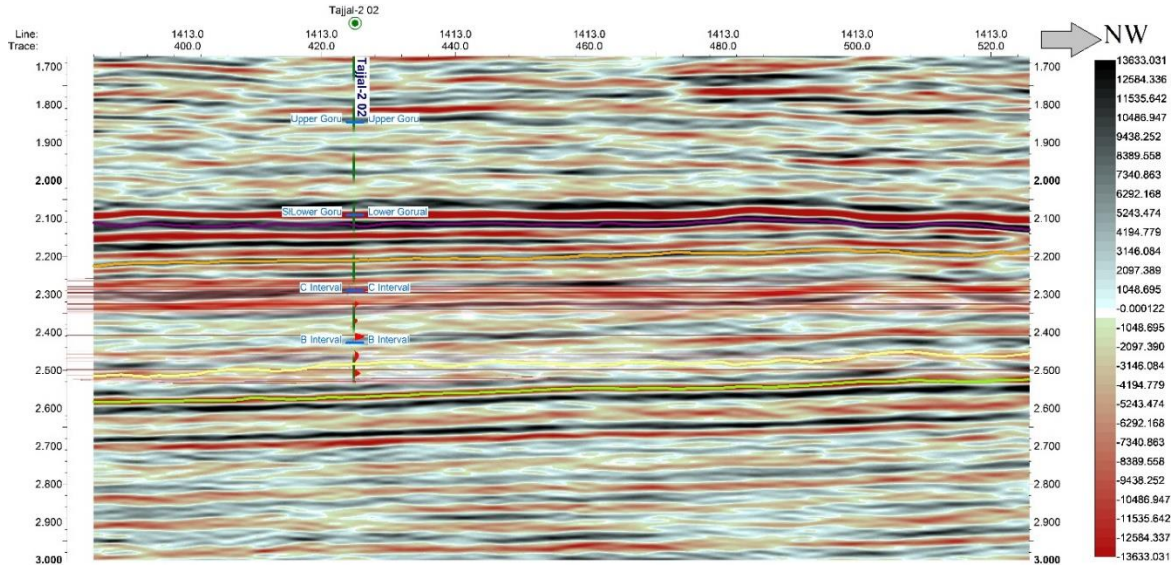


Figure 4. 9 Seismic inline 1413 showing the interpreted reservoir horizons and their lateral continuity.

Inline 1455 runs through Tajjal-1 and gives the fullest view of the reservoir succession, showing the Upper Goru, the shale interval, and the C, B and A sand intervals as clearly resolved, well-tied events. The horizons run continuously with a gentle structural configuration, and the well markers line up precisely with distinct seismic loops, which confirms the Tajjal-1 tie from the synthetic seismogram. The shale interval is a prominent, high-continuity marker separating the section above from the reservoir sands below, and the C, B and A intervals stack as a series of reflections whose amplitude records the vertical distribution of sand and shale.

The individual sand intervals resolve cleanly here, and that carries a practical point: the seismic has enough vertical resolution to separate the main reservoir units, which any meaningful inversion needs. Lateral changes in the strength and continuity of the sand reflections point to heterogeneity within the reservoir and flag where porosity may be better developed. Since Tajjal-1 sits at the northern end of the survey, this line lets the northern reservoir character be set against the central and southern expressions on the earlier inlines, closing the north-to-south picture. Inline 1455 is the reference stratigraphic section for the study, and the inversion results are read back against its tie framework.

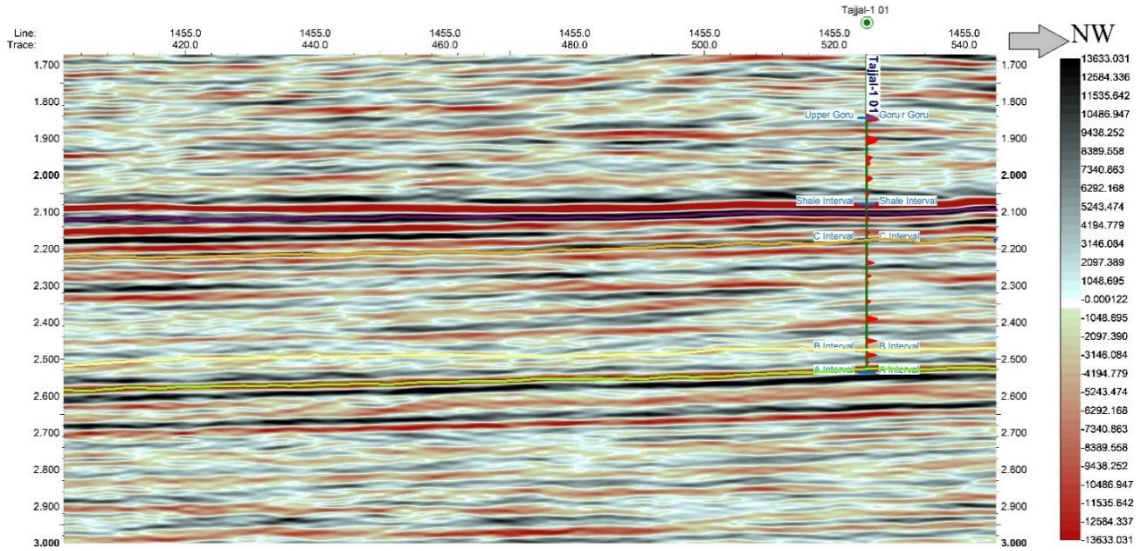


Figure 4. 10 Seismic inline 1455 through Tajjal-01 showing the interpreted reservoir intervals.

Crossline 420 cuts the reservoir succession at right angles to the inlines and tests lateral continuity in the perpendicular direction. The Upper Goru, Lower Goru, C and B markers stay traceable across the section, and their coherent geometry in this orientation shows the reservoir intervals carry across depositional strike as well as along it, which fits a laterally extensive shelf sand system rather than isolated, narrow sand bodies. The high- and low-amplitude alternation within the interval matches what the inlines show, so the interbedded sand-shale architecture holds in both structural directions.

This crossline shows the horizons mapped from the inlines closing consistently in the orthogonal direction, which is what reliable time and depth maps and an internally consistent inversion volume need. Local amplitude variations again mark zones of possible reservoir-quality change, and the sand reflections carrying through supports connected porous fairways rather than disconnected lenses. Crossline 420 confirms the inline interpretation by validating horizon continuity in two dimensions and by reinforcing the depositional model behind the reservoir characterization.

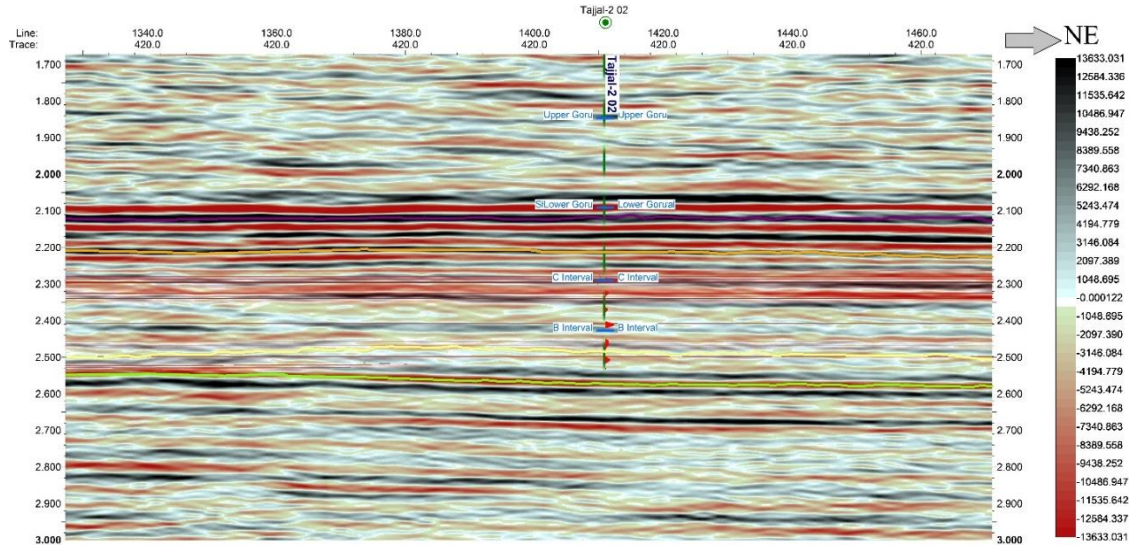


Figure 4. 11 Seismic crossline 420 showing the lateral continuity of the interpreted reservoir horizons.

Crossline 440 pushes the orthogonal control further across the survey with the same suite of interpreted horizons, testing the reservoir framework over more of the block. The reflection events keep good lateral continuity and the interval geometry stays coherent, so the stratigraphic architecture from the wells holds across this part of the volume. This crossline agrees with the adjacent sections, which means the horizon interpretation is internally consistent and the mapped surfaces tie correctly at every inline-crossline intersection, a basic requirement for accurate structural mapping.

The amplitude character of the sands on this line keeps showing the interbedded nature of the succession, and any local strengthening or weakening of the reflections reads as a lateral change in sand development or porosity. The reservoir reflections carrying through successive crosslines builds confidence that the porous sands are a laterally continuous target across the Gambat Block. Crossline 440 adds two-dimensional control that supports the time and depth surfaces and, in turn, the geometric framework for reading the inverted impedance volumes.

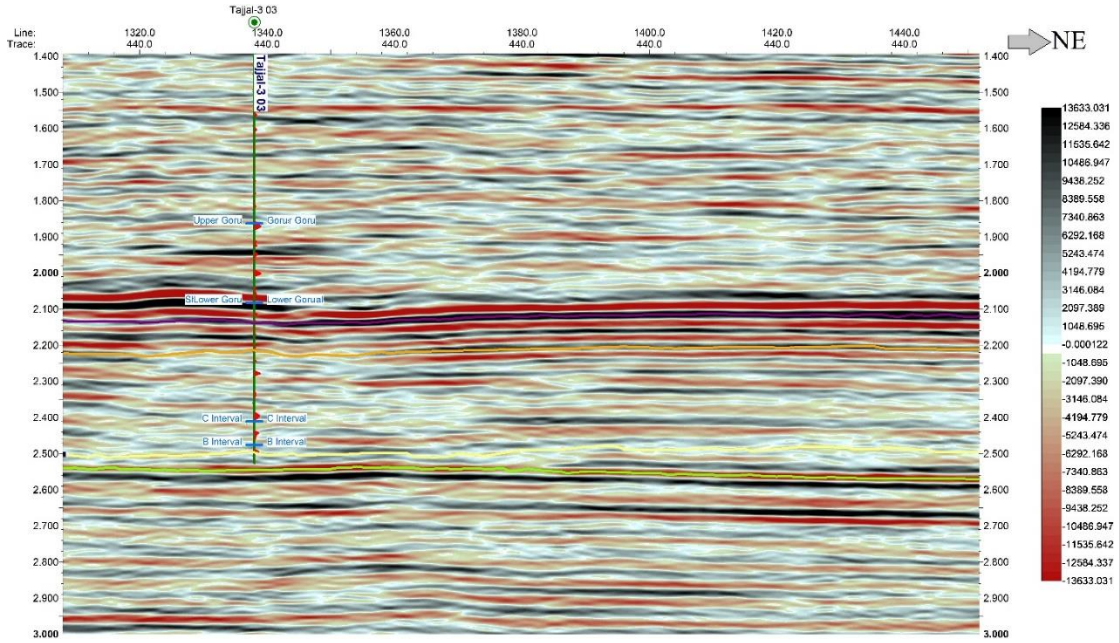


Figure 4. 12 Seismic crossline 440 showing the structural and stratigraphic continuity of the reservoir intervals.

Crossline 515 passes close to Tajjal-1 and adds an orthogonal tie alongside the inline 1455 interpretation in the north. The Upper Goru, shale interval, C, B and A markers stay traceable across the profile, and their alignment with the well shows the reservoir intervals keep their stratigraphic position in the crossline direction too. The reflection package reads cleanly: the shale interval is again a strong, continuous marker above the reservoir sands, and the stacked C, B and A reflections carry the amplitude variation of alternating sand and shale.

Anchored by Tajjal-1, this crossline lets the seismic character of the reservoir sands be checked against the well in the orthogonal orientation, a two-dimensional validation of the tie at the most fully logged control point in the survey. The sand reflections stay continuous across this line and the earlier crosslines, which confirms the reservoir target is laterally coherent throughout the block. Local amplitude and waveform variations flag candidate zones of better reservoir quality near Tajjal-1. Between them, the inline and crossline sections give a laterally continuous, well-calibrated horizon framework, show the reservoir sands persist in both structural directions, and pick out the amplitude variations the inversion is meant to turn into quantitative impedance and porosity.

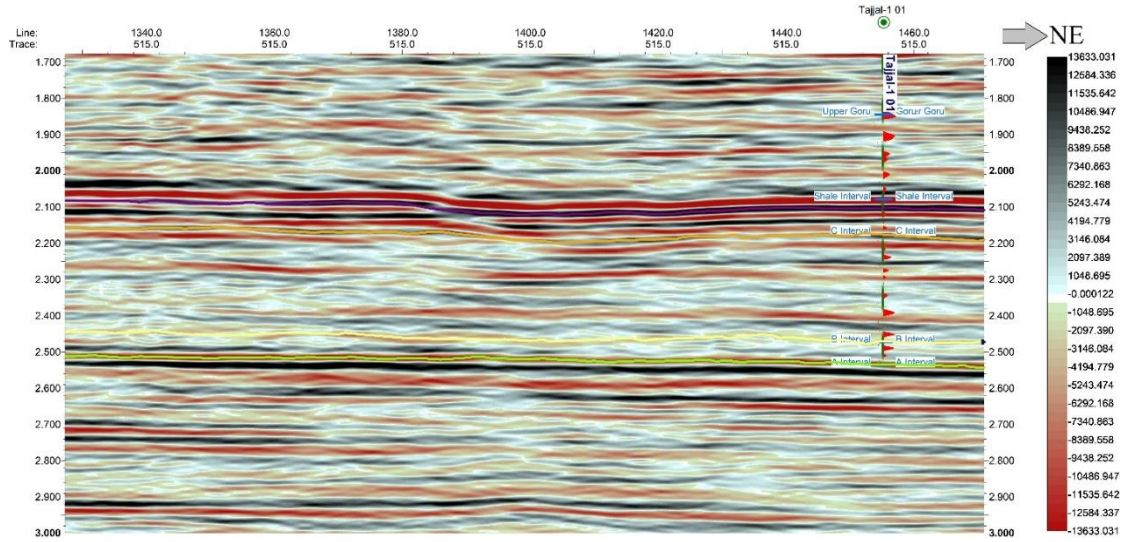


Figure 4. 13 Seismic crossline 515 showing the interpreted reservoir horizons near Tajjal-01

4.3.3 Time Maps

The two-way time structure map of the Lower Goru marker turns the horizon picked on the sections into a continuous surface and gives the first regional view of the structure at the top of the reservoir succession. It is contoured in two-way time, and the spread of contour values shows the shape of the surface: shallower times in the warmer colors are structurally high, deeper times in the cooler colors are the lows. The three wells plot on the surface, and their positions relative to the contours set the structural context of each borehole. Hydrocarbons collect at structural culminations, so where the wells sit relative to the time highs bears directly on prospectivity.

The smooth, continuous contour pattern fits the gently deformed, layer-cake character seen on the sections and shows the Lower Goru surface is not strongly faulted across most of the block, though local gradients mark the subtle relief that can steer hydrocarbon migration and entrapment. Since this surface caps the interval holding the porous sands, its geometry sets where those sands are structurally highest and where a buoyant hydrocarbon phase would tend to be trapped. Everything below it, the deeper C, B and A sand surfaces and, eventually, the depth maps, is referenced to this datum.

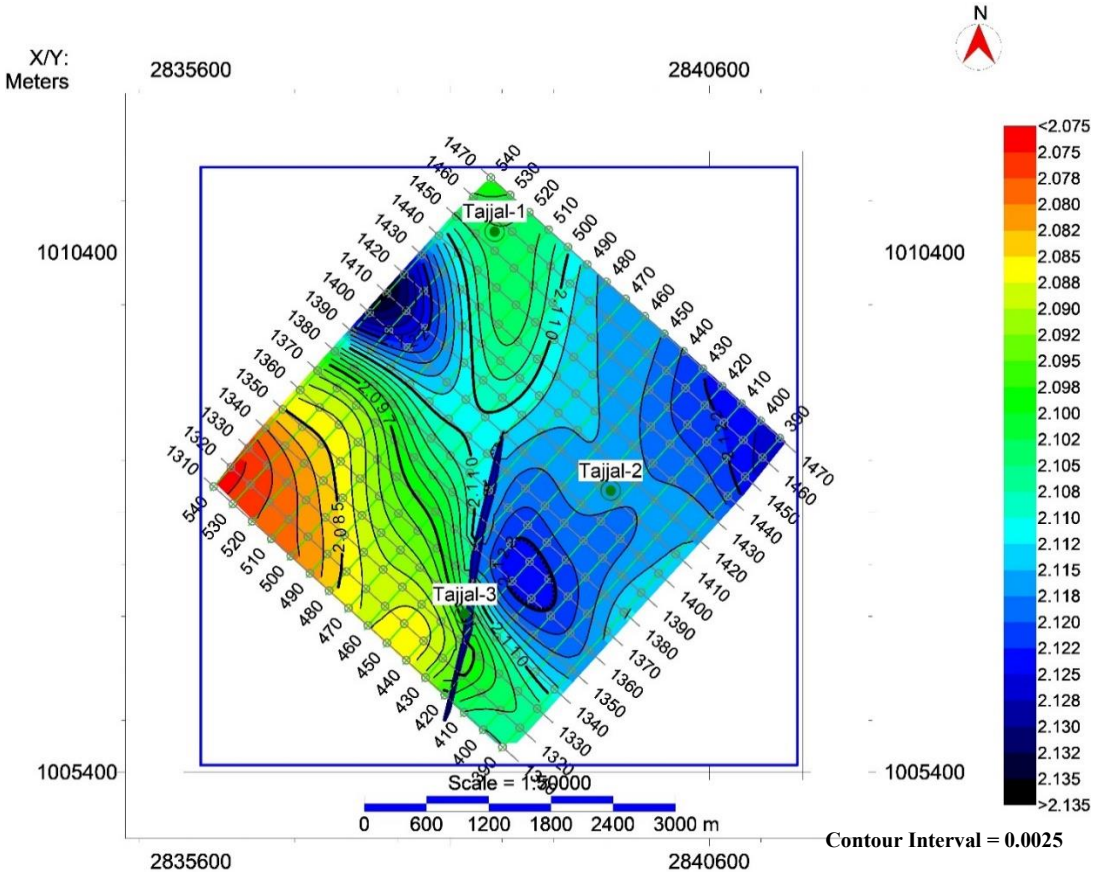


Figure 4. 14 Lower Guru Time Map two-way time map showing the structural configuration of the Lower Goru reservoir interval.

The two-way time map of the C interval sand shows the structure of the shallowest of the three principal reservoir sands and lets its geometry be set beside the overlying Lower Goru surface. The contour pattern broadly mirrors the Lower Goru marker, so the C sand follows the same regional framework and the section between them keeps a fairly constant thickness, in keeping with the continuous reflectors on the sections. The structurally high areas, at the shallower times, are the parts of the C sand most favorable for hydrocarbon accumulation; the deeper areas are the flanks and lows.

Where the three wells sit relative to these contours sets how the reservoir character at each borehole relates to the sand's structural position, and it controls the direction in which any hydrocarbon column would thin or thicken. The smooth contours reflect the lateral continuity of the C sand and support reading it as a coherent mappable unit rather than a broken-up body. With the top of the shallowest reservoir sand defined, the C interval impedance anomalies can later be judged against this surface to separate structurally controlled from stratigraphically controlled reservoir quality.

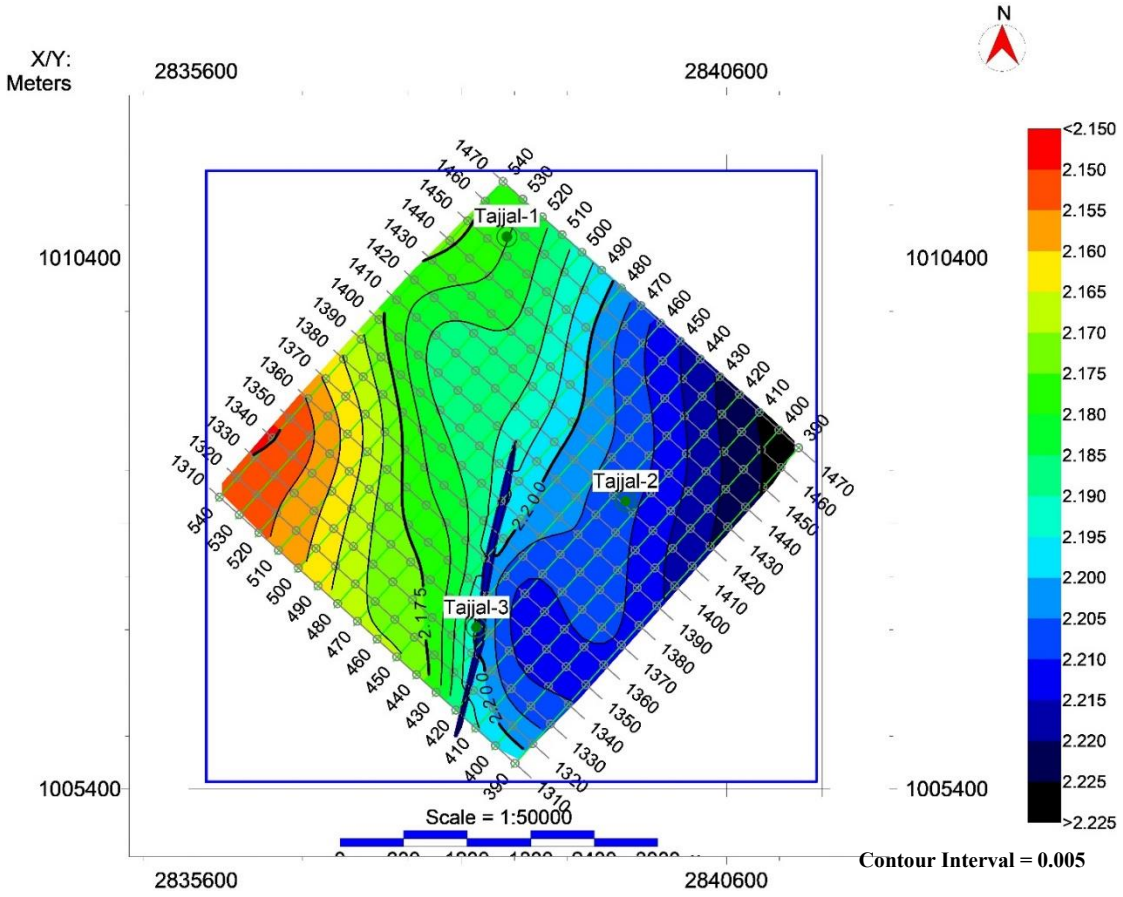


Figure 4. 15 C Interval Sand Time Map two-way time map showing the structural configuration of the C-sand interval.

The time structure map of the B interval sand describes the geometry of the study's main target, so its shape drives much of what follows. The contours trace a surface whose highs and lows come through in the two-way time variation, and its broad conformance with the shallower C sand and Lower Goru surfaces shows the B sand shares the same regional framework. Where the wells fall on this surface sets the structural setting in which the B sand was drilled and evaluated, and the B interval is the unit most closely tied to the petrophysical and inversion results.

The structurally high parts of the B sand, at the shallower times, are the areas of greatest interest for hydrocarbon entrapment, and where these highs sit relative to the wells decides whether the boreholes are well placed against the crest. The continuous, smooth contours reinforce the B sand as a laterally persistent reservoir, matching the coherent reflections on the sections. The B interval is the primary target for the porosity and impedance work that follows, and this surface is what the low-impedance porous sand fairways from the inversion are placed against, so they sit in their correct structural setting.

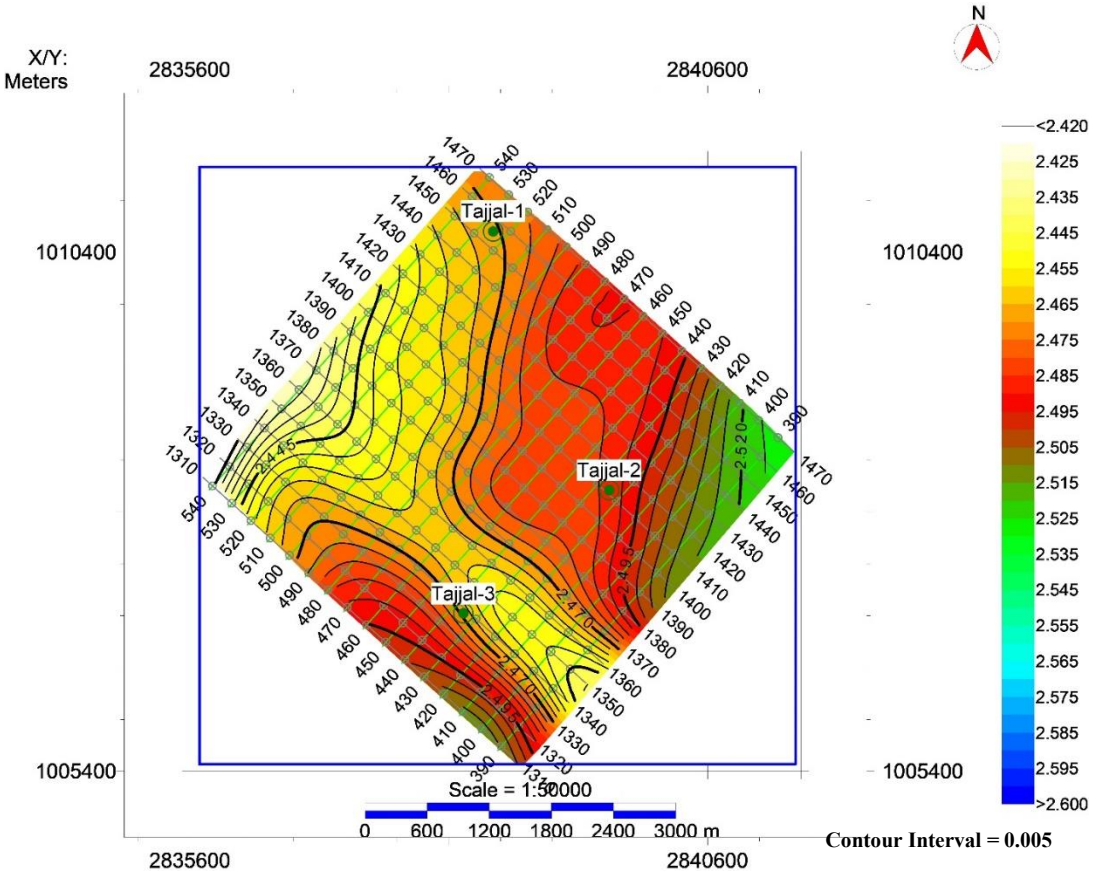


Figure 4. 16 B Interval Sand Time Map Two-way time map showing the structural configuration of the primary B-sand target.

The time structure map of the A interval defines the geometry of the deepest of the three reservoir sands and completes the vertical set of time surfaces through the Lower Goru package. The contours keep the regional structural grain of the shallower surfaces, and the broad conformance among the A, B and C surfaces shows the whole reservoir interval behaves as a structurally coherent package with only gradual thickness changes across the survey. The deeper two-way times of the A interval fit its position at the base of the succession.

The structural highs of the A sand, at the relatively shallower contour values, again mark the most prospective areas at this level, and where the wells sit relative to those highs sets the structural context for the deepest reservoir unit. The continuous contours support the A sand, like the sands above, being a laterally extensive reservoir rather than an isolated body. Between them, the Lower Goru, C, B and A time maps show a reservoir succession that is gently and coherently deformed, individual sands sharing a common structural framework, and wells that sample a consistent structural setting. These time surfaces are later converted to depth and used to constrain the inverted impedance volumes.

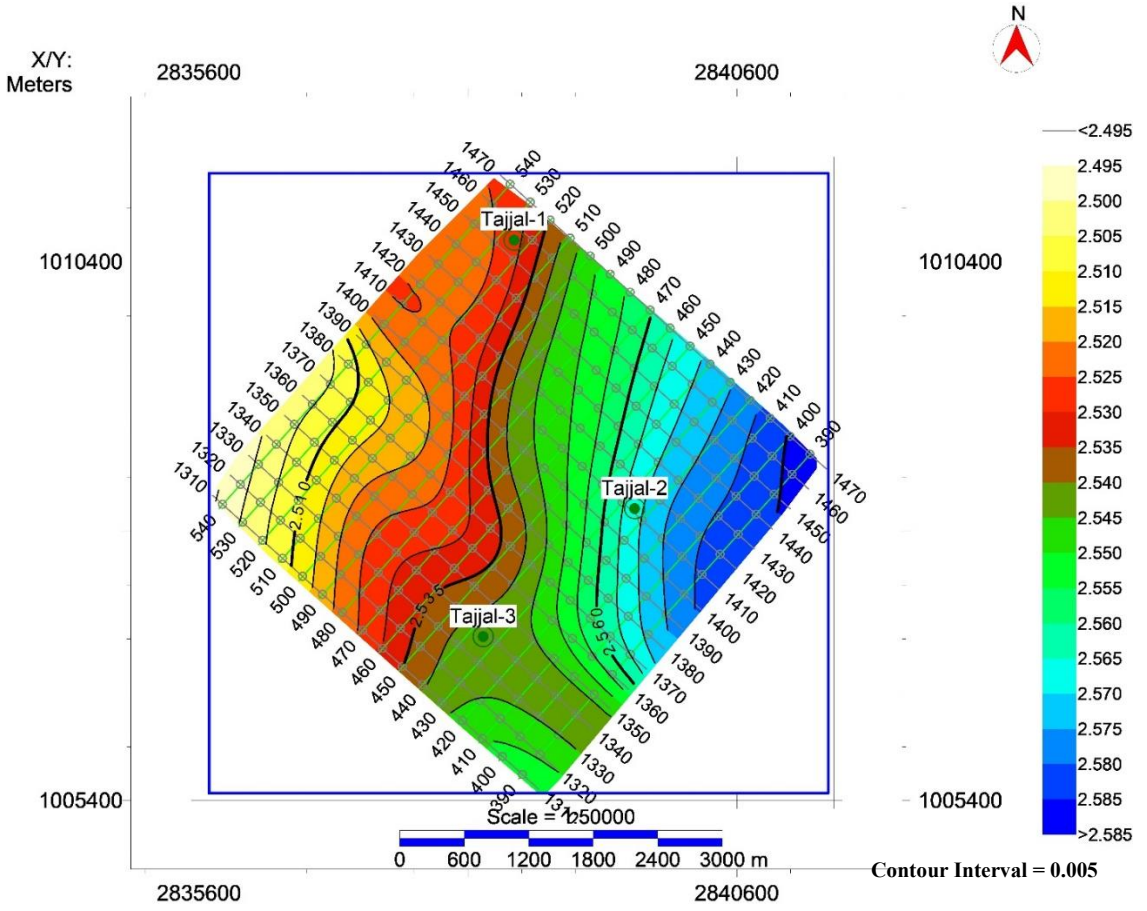


Figure 4. 17 A Interval Time Map Two-way time map showing the structural configuration of the A-sand interval.

4.3.4 Depth Maps

The depth structure map of the Lower Goru marker converts the two-way time surface to true vertical depth using well velocities, giving the first geologically calibrated view of the reservoir structure in a form usable for prospect evaluation and volumetrics. Going from time to depth removes the effect of lateral velocity variation and puts real numbers on the structural relief, the depth contours marking the elevated and depressed areas of the Lower Goru top. The depth surface and the time map share the same general form, so the velocity field introduces no severe distortion and the highs seen in time are real highs in depth.

Depth is where drilling targets, spill points and hydrocarbon column heights are ultimately set, so this map is what turns the seismic interpretation into an exploration decision. The wells against the depth contours give the true structural setting of each borehole and let the reservoir depth at any location be estimated with confidence. The gentle, continuous contours reflect the mild deformation of the Lower Goru surface and a

structurally simple trap geometry. This surface caps the reservoir succession, and the depths of the individual C, B and A sands are set against it.

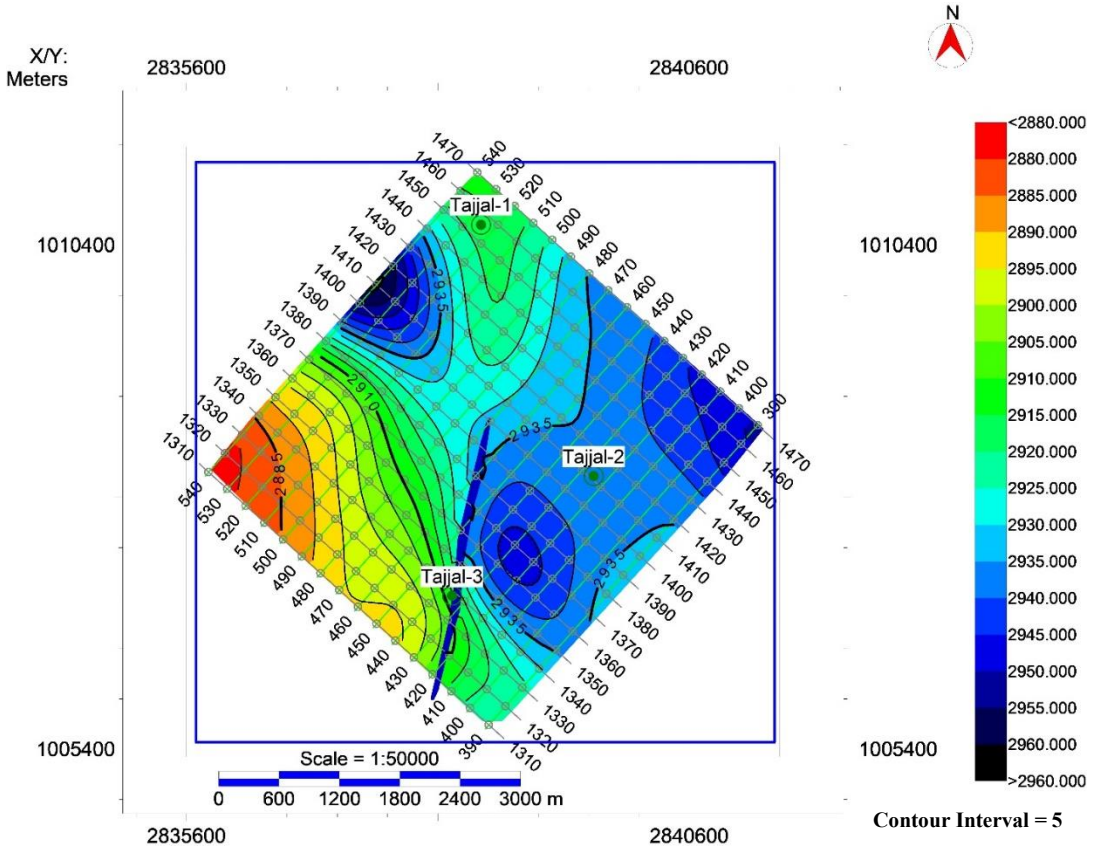


Figure 4. 18 Lower Guru Depth Map Depth map showing the structural configuration of the Lower Goru reservoir interval.

The depth map of the C interval sand puts the shallowest reservoir unit into true vertical depth and quantifies its burial and structural relief at its actual subsurface position. The depth contours track the overlying Lower Goru surface closely, which confirms the interval thickness is broadly maintained and that the C sand shares the same framework in depth as in time. The shallowest areas of the C sand are the crestal positions most favorable for hydrocarbon accumulation, and the depth values let the elevation of these culminations be set directly beside the wells.

Putting the C sand in depth lets the reservoir be judged in absolute terms, so the structural relief and the size of any trapped hydrocarbon column can be worked out quantitatively. The continuous depth contours reinforce the C sand as a laterally coherent reservoir, and its conformance with the deeper sands supports a consistent, structurally controlled geometry. This surface gives the calibrated structural context the C interval needs once the inversion-derived porosity and impedance are tied back to the real reservoir geometry.

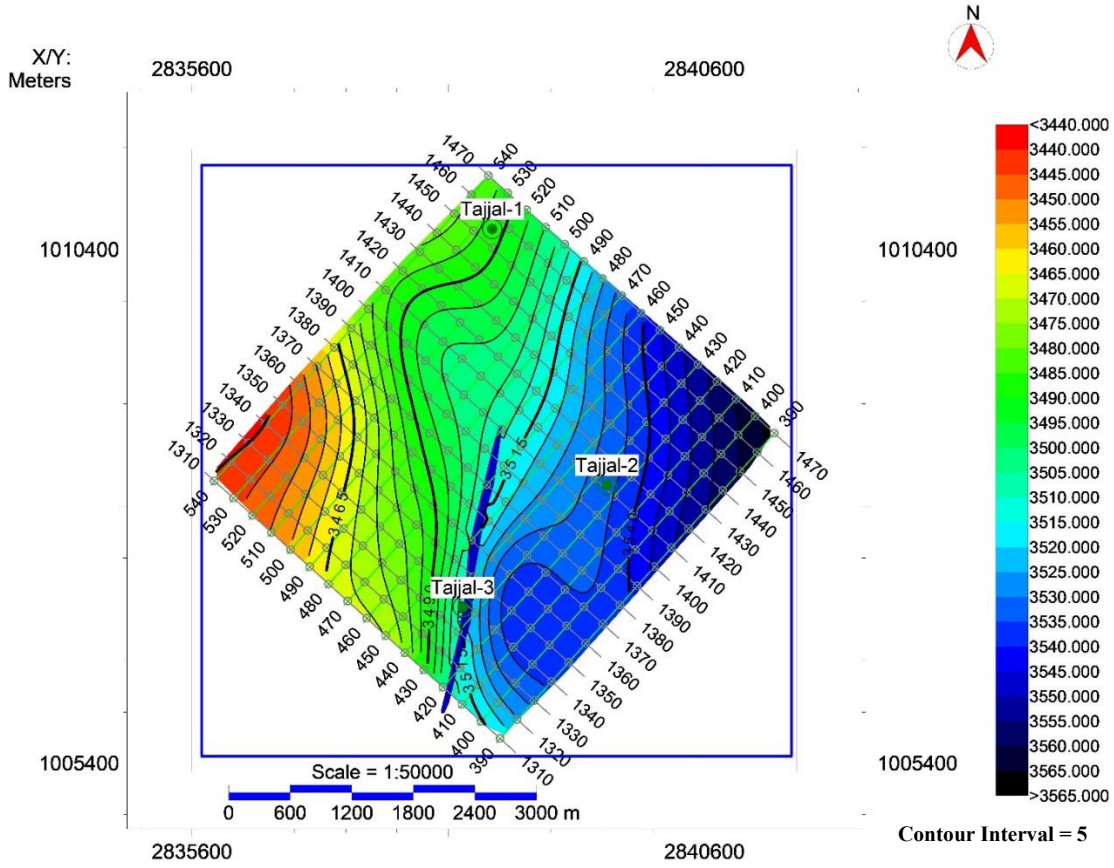


Figure 4. 19 C Interval Sand Depth Map Depth map showing the structural configuration of the C-sand interval.

The depth structure map of the B interval sand carries the most weight of the four, since the B sand is the principal target and true vertical depth gives the definitive structural picture, the characterization is measured against. The depth contours pick out the structural highs and lows of the B sand, and their conformance with the shallower surfaces confirms the sand sits coherently within the framework. The crestal areas, at the shallowest depths, are the most prospective for hydrocarbon entrapment, and the depth values put numbers on the relief available to hold a column.

Where the wells fall on these depth contours shows whether the boreholes sample the structurally best parts of the B reservoir, and they are the reference points where the depth-converted structure ties to hard data. The B interval carries the fullest petrophysical and inversion work, so this depth map is what pulls those results into a single reservoir model and positions the low-impedance porous sand fairways from the inversion in the true structural geometry. The continuous depth surface confirms the lateral persistence of the B sand and its standing as a laterally extensive, structurally simple target of primary importance in the Gambat Block.

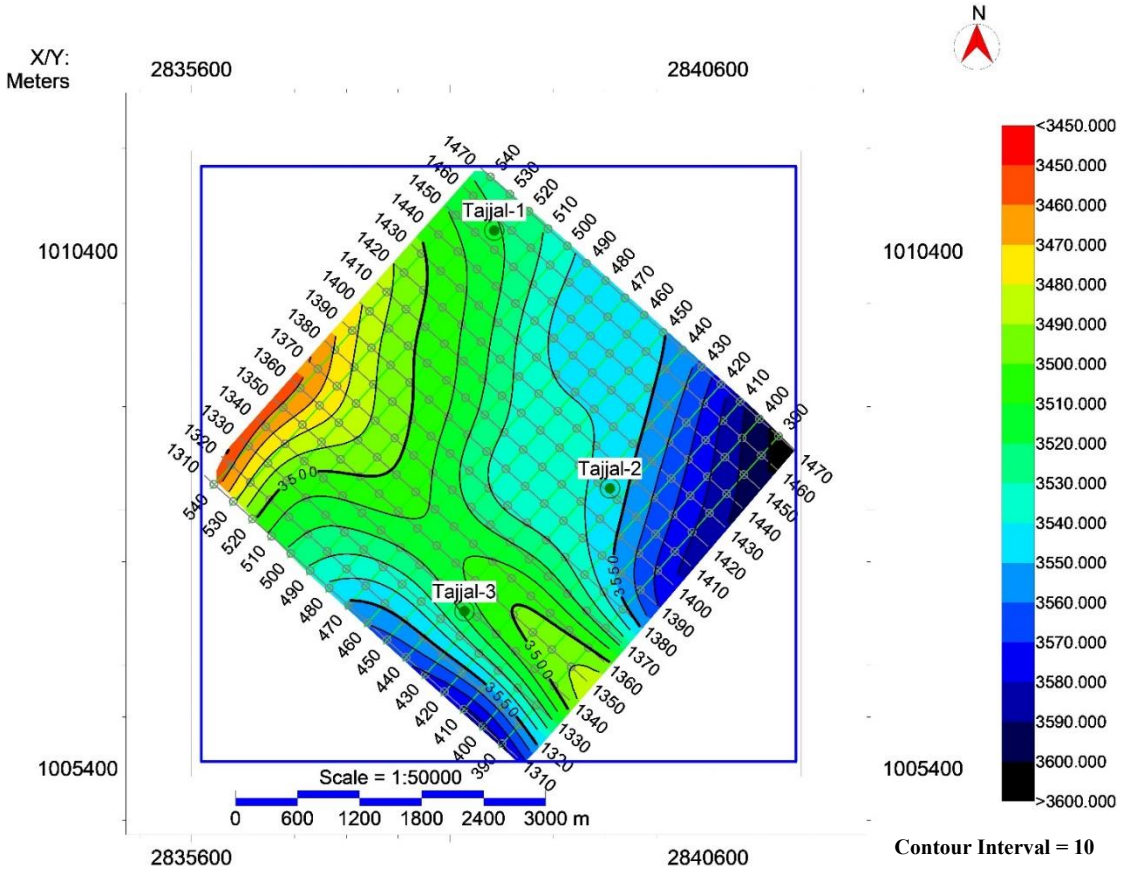


Figure 4. 20 B Interval Sand Depth Map Depth map showing the structural configuration of the primary B-sand target.

The depth map of the A interval sand finishes the depth-converted framework by fixing the true vertical depth of the deepest reservoir unit. The contours describe a surface that conforms to the regional grain of the overlying sands, and the consistent relationship among the A, B and C depth surfaces confirms the package behaves coherently through its whole vertical extent. The A interval's greater depths fit its basal position, and the shallowest parts of this surface again mark the area's most favorable for hydrocarbon accumulation at this level.

Where the wells sit against the A sand depth contours gives the true structural setting of the deepest reservoir and lets its burial depth be measured across the survey. The continuous contours support the A sand being laterally persistent, like the sands above it. Across all four surfaces, the Lower Goru, C, B and A depth maps show a reservoir succession that is gently deformed, structurally simple and laterally continuous, with individual sands sharing a common framework and wells sampling a representative structural setting. The rest of the chapter integrates the petrophysical evaluation and the inverted impedance results onto this depth framework

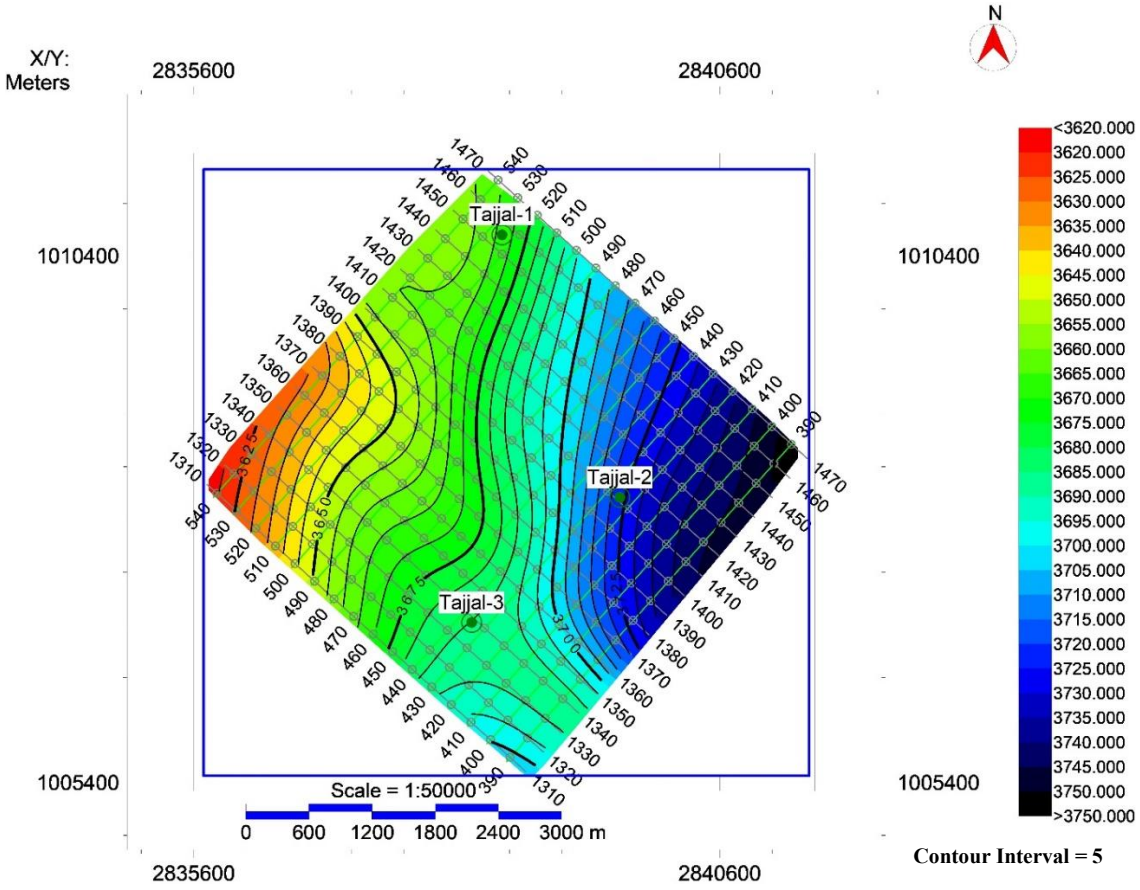


Figure 4. 21 A Interval Sand Depth Map Depth map showing the structural configuration of the A-sand interval.

4.4 Seismic Inversion

This figure places the inversion work within its conceptual hierarchy and sets out how the different classes of post-stack inversion applied later relate to each other. Post-stack seismic inversion converts the interface-based reflectivity of the seismic into a layer-based acoustic impedance. That helps because impedance is an intrinsic rock property tied to lithology, porosity and fluid content, whereas reflectivity only expresses the contrasts at boundaries. Stripping the wavelet and converting to impedance sharpens the reservoir units, cuts the tuning and interference effects that muddy amplitude interpretation, and gives a volume that can be read quantitatively for porous sand.

The scheme separates broadband, model-based approaches from band-limited or sparse-spike ones. Each rebuilds impedance under different assumptions, with different sensitivities to the input data and the low-frequency background. Running more than one method here is deliberate: when independent algorithms agree, the resulting impedance anomalies are more likely real subsurface features than artefacts of a single assumption. That is why impedance is the property of choice for the porous Lower Goru sands, and the wavelet

extraction, the low-frequency modelling, and the sparse-spike and model-based results follow from it.

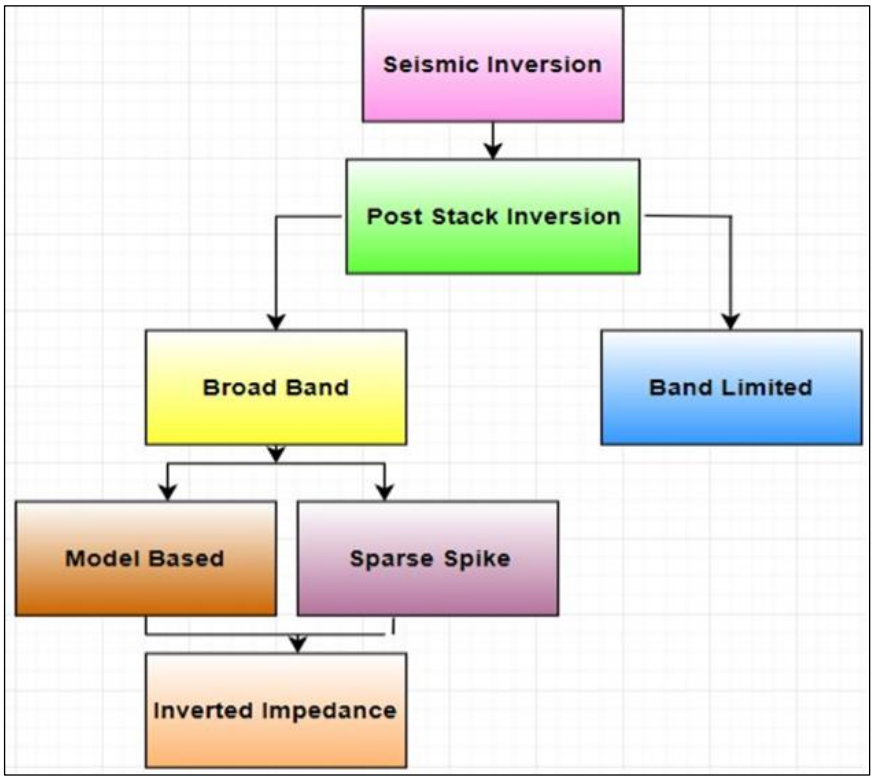


Figure 4. 22 Post stack inversion method for seismic impedance estimation

4.4.1 Wavelet Extraction

The extracted statistical wavelet feeds the inversion at its core, carrying the amplitude and phase the seismic imposes on the underlying reflectivity; getting it right is what lets the inversion recover true impedance rather than a wavelet-distorted version. The figure shows the wavelet in time and frequency: the time response has a well-defined, broadly symmetrical central peak with subordinate side lobes, the amplitude spectrum gives the frequency range in the data, and the phase spectrum shows the phase across that band. You want a compact, near-symmetrical, roughly zero-phase wavelet, because it maximizes vertical resolution and keeps reflection events correctly positioned against the impedance boundaries they represent.

The bandwidth in the amplitude spectrum sets the vertical resolution of the inversion and so the thinnest units it can resolve, while the phase stability controls how faithfully the inverted impedance reproduces the layering. Because the wavelet comes from the seismic data together with the well control in the synthetic tie, it represents the effective source signature at reservoir level and gives the deconvolution operator the inversion uses to remove the wavelet. Its reliability therefore drives the accuracy of the impedance volumes, and its

clean character supports the inversion faithfully representing the impedance structure of the porous Lower Goru sands.

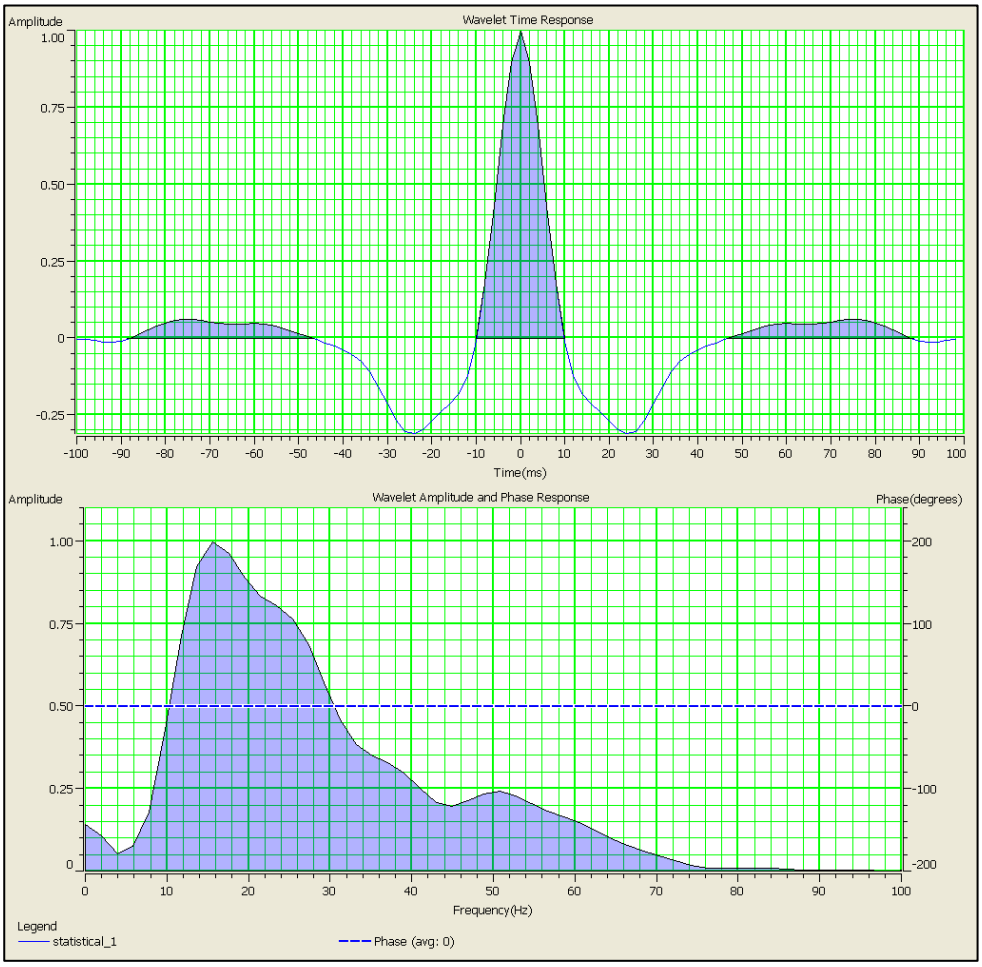


Figure 4. 23 Extracted seismic statistical wavelet for seismic inversion analysis

4.4.2 Low-Frequency Model

The low-frequency model fills in the part of the impedance spectrum the band-limited seismic cannot recover, and without it the impedance volume would be relative rather than absolute and geologically meaningful. Seismic data lack the low frequencies, below the bottom of the recorded band, that carry the background impedance trend; missing them, the inversion can only rebuild the relative variations sitting on an unknown background. The model here is built by interpolating the well impedance along the interpreted horizons, so the low-frequency background respects both the hard well data and the seismic structural framework.

How good that background is decides how accurate the absolute impedance can be, and therefore how well porous low-impedance sands can be told from the surrounding higher-impedance shales. Guided by the interpreted horizons, the model keeps the background impedance varying in a geologically reasonable way and carries the well-derived

trends into the inter-well space consistently with the structure. The seismic-derived impedance variations are added to this base during inversion, so its blend of well and horizon information is a key control on the reliability of the impedance volumes used to map the porous sands.

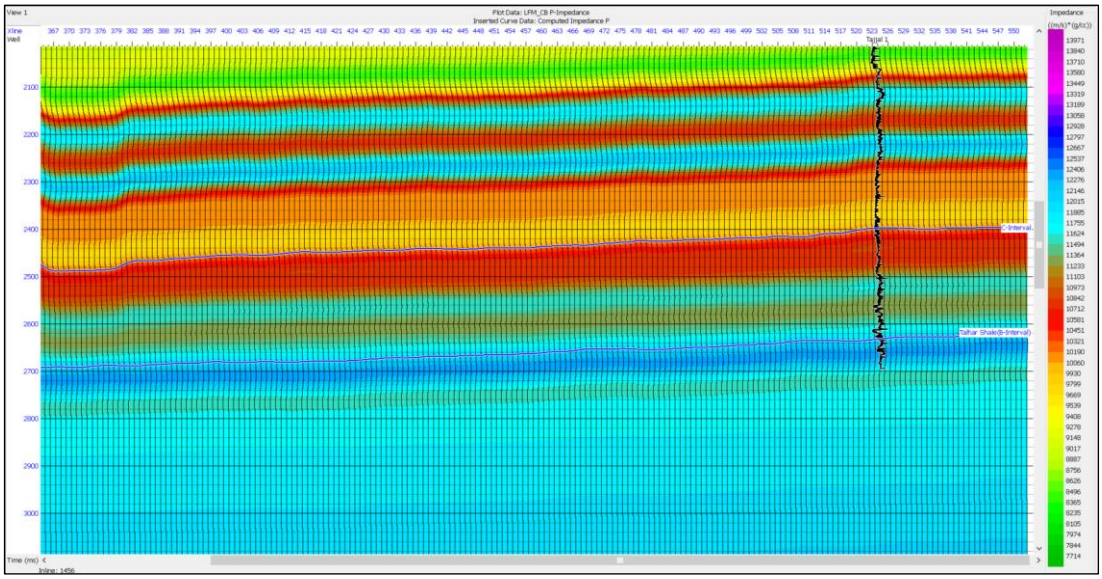


Figure 4. 24 Showing Low frequency model used for seismic model-based inversion algorithm

4.4.3 Flow Chart for the Model-Based Inversion Technique

The model-based flow chart lays out the alternative inversion strategy and where its logic parts from the sparse-spike approach; comparing the two is what underpins the reliability of the characterization. In the model-based scheme, an initial impedance model built from the well data and interpreted horizons is convolved with the wavelet to make a synthetic section, then compared with the observed seismic; the model is perturbed and the process repeated until the synthetic matches acceptably, at which point the final model is accepted. This forward-modelling and updating keeps the inverted impedance geologically plausible and consistent with the low-frequency background at every iteration.

The model-based approach's main strength is a full-bandwidth, geologically constrained impedance volume in which the absolute values are well controlled by the initial model, which makes it good for quantitative property estimation. Because it leans on that starting model, the well-and-horizon-based impedance has to be sound, and the workflow is set up so the data refine the model rather than override it. The model-based and sparse-spike methods rebuild impedance under different assumptions, so where they agree, the porous sand anomalies can be taken as robust. That is the case for running both, and the model-based results follow.

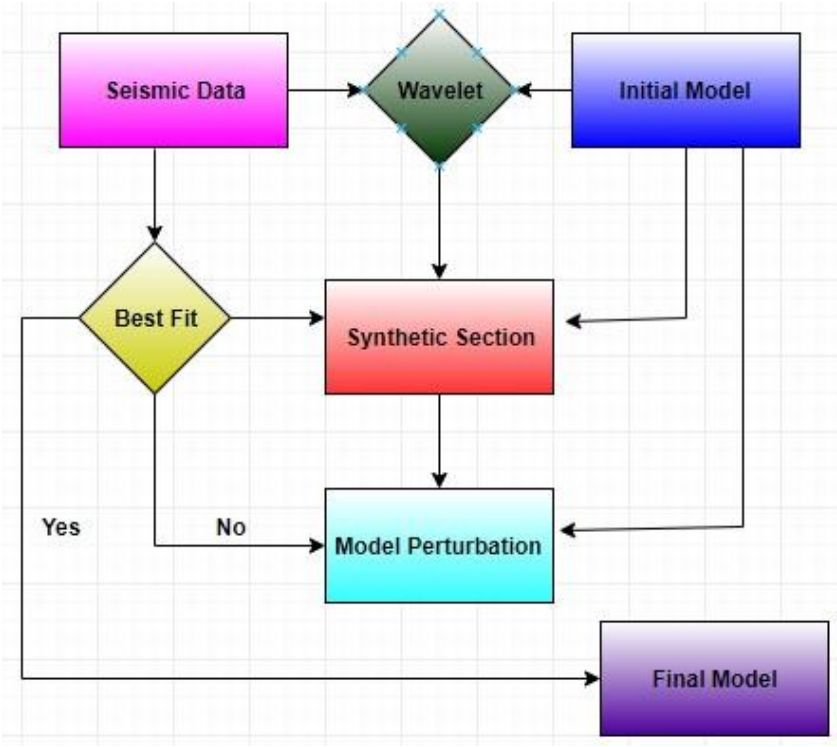


Figure 4. 25 Flow chart for the model-based inversion technique

4.4.4 Inversion Analysis Results of Model-Based Inversion

This panel validates the model-based inversion at the well by comparing the inverted impedance with the impedance measured at the borehole and with the low-frequency model; the three curves together show both the accuracy and the internal consistency of the method. The inverted impedance, in red, follows the log-derived impedance, in blue, closely through the reservoir interval, so the algorithm recovered the impedance structure faithfully, while the low-impedance model, in black, is the background trend the inversion sharpens with the seismic detail. The close agreement between inverted and measured impedance confirms the initial model, the wavelet and the seismic are mutually consistent and that the inversion is correctly calibrated at the control point.

The relationship between the inverted impedance and the low-frequency model shows how the inversion adds the mid- and high-frequency detail from the seismic to the low-frequency background from the model, giving a full-bandwidth impedance that resolves the individual units. Reproducing the impedance lows tied to the porous sands is the point that counts, since it shows the model-based volume, like the sparse-spike volume, can map the sands away from the well. That validates the model-based section, and with the matching sparse-spike analysis it shows both methods are well calibrated, so their agreement can be used to confirm the porous sand anomalies.

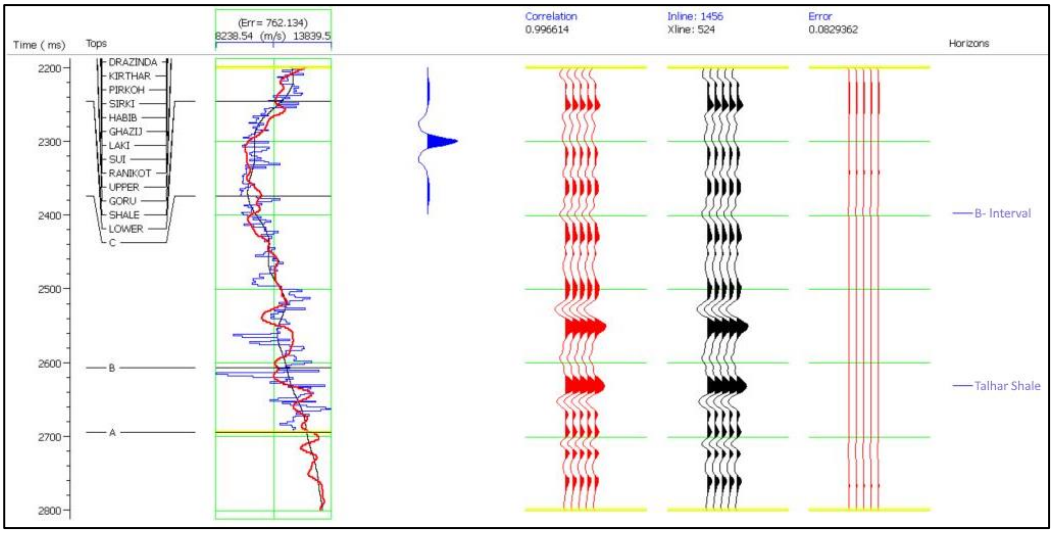


Figure 4. 26 Inversion analysis results of model-based inversion with inverted impedance (red), log impedance (blue), low impedance model (black)

4.4.5 The Inverted Impedance of Model-Based Inversion

The model-based impedance section maps the spatial distribution of acoustic impedance from the model-based inversion, and set against the sparse-spike section it gives a second, independent image of the porous sands to test how robust the interpretation is. The porous Lower Goru sands read as laterally coherent low-impedance zones inside the higher-impedance shale background, and the full-bandwidth, geologically constrained result is a smoothly varying but well-resolved image with absolute values reliably controlled by the initial model. The low-impedance fairways trace along the section and sit where the sparse-spike inversion put them, a strong sign the anomalies are real reservoir features.

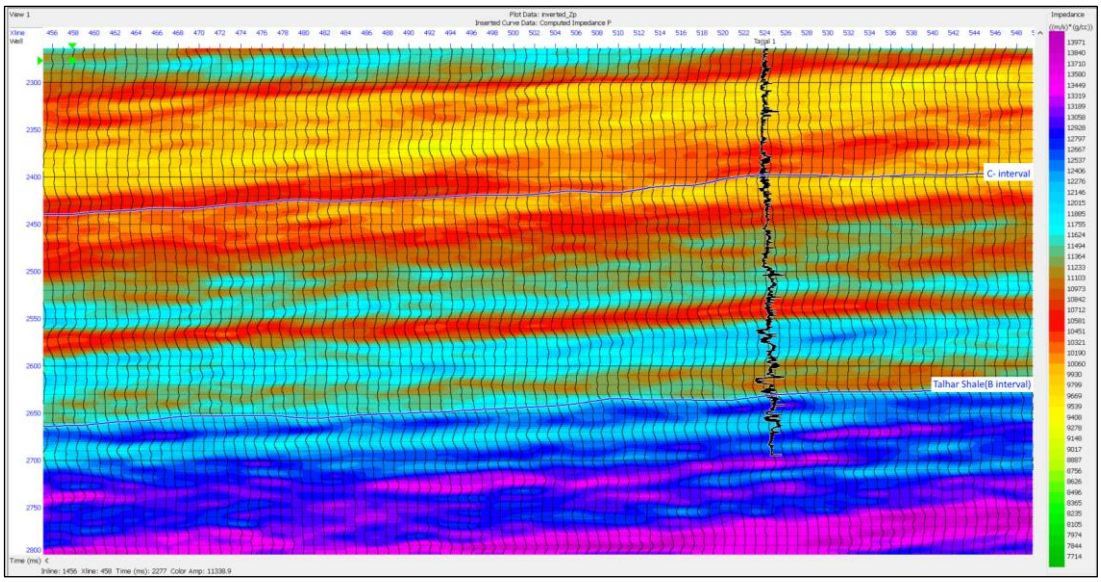


Figure 4. 27 The inverted impedance of model-based inversion algorithm

4.4.6 Horizon Map of the Top C and B Intervals Resolved by Three Post-Stack Inversion Techniques

The horizon-based impedance maps of the top C and B intervals pull the inverted impedance along the specific reservoir surfaces, giving the most direct, targeted view of porous sand distribution within the two principal units, resolved consistently by the three post-stack inversion techniques. Draping the impedance onto the interpreted horizons removes the effect of structural relief and shows the intrinsic reservoir property variation across each sand, so the low-impedance areas read directly as the best-developed porous sand. The C and B maps show the areal patterns of low impedance that define the fairways at each level, and these patterns matching across the three methods confirms the mapped distributions are robust.

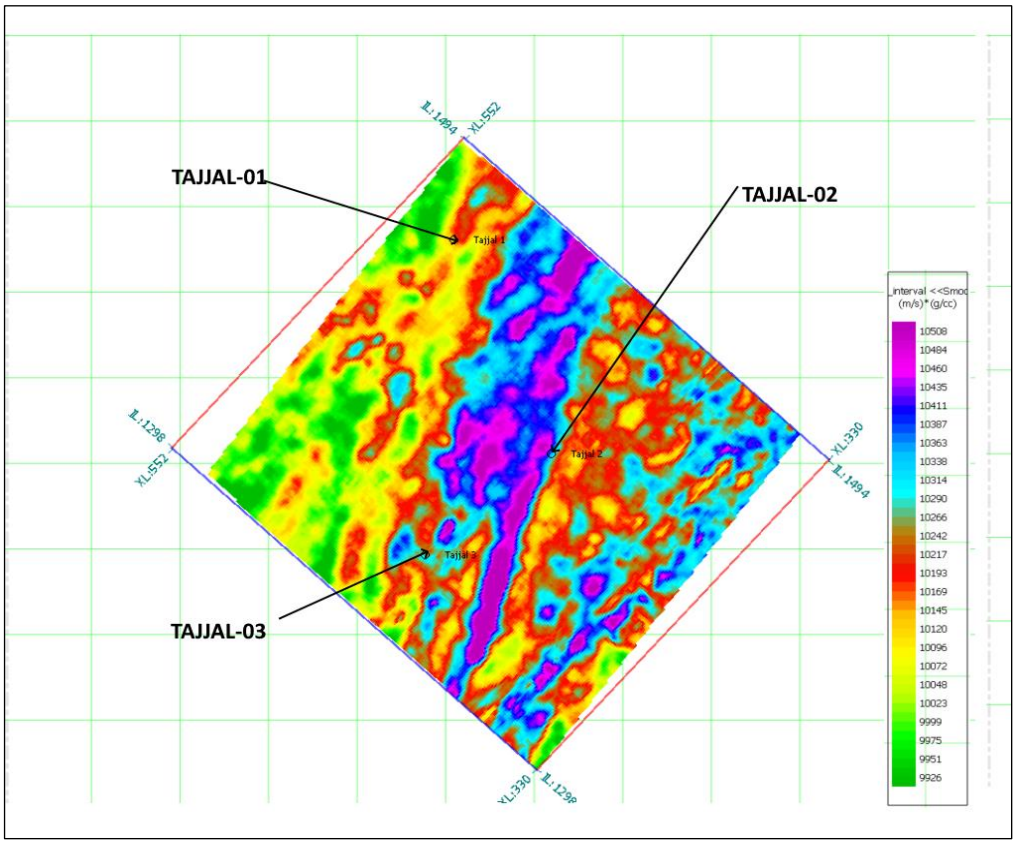


Figure 4. 28 Horizon map of the top C interval resolved by three post stack inversion techniques

Setting the C and B maps side by side shows how reservoir development varies vertically, whether the porous fairways shift or persist between the two levels, which informs the stacking and connectivity of the units. Where the low-impedance areas sit relative to the wells ties the mapped reservoir quality back to the calibrated petrophysical evaluations, so

the inversion predicts reservoir character correctly at the control points and extends that prediction between wells. The B interval is the primary target, so its horizon impedance map carries the most weight, outlining the areas of highest potential in the key unit. These horizon maps bring the structural and inversion results together into a focused picture of porous sand distribution, the final product of the post-stack inversion workflow and the answer to the study's central objective.

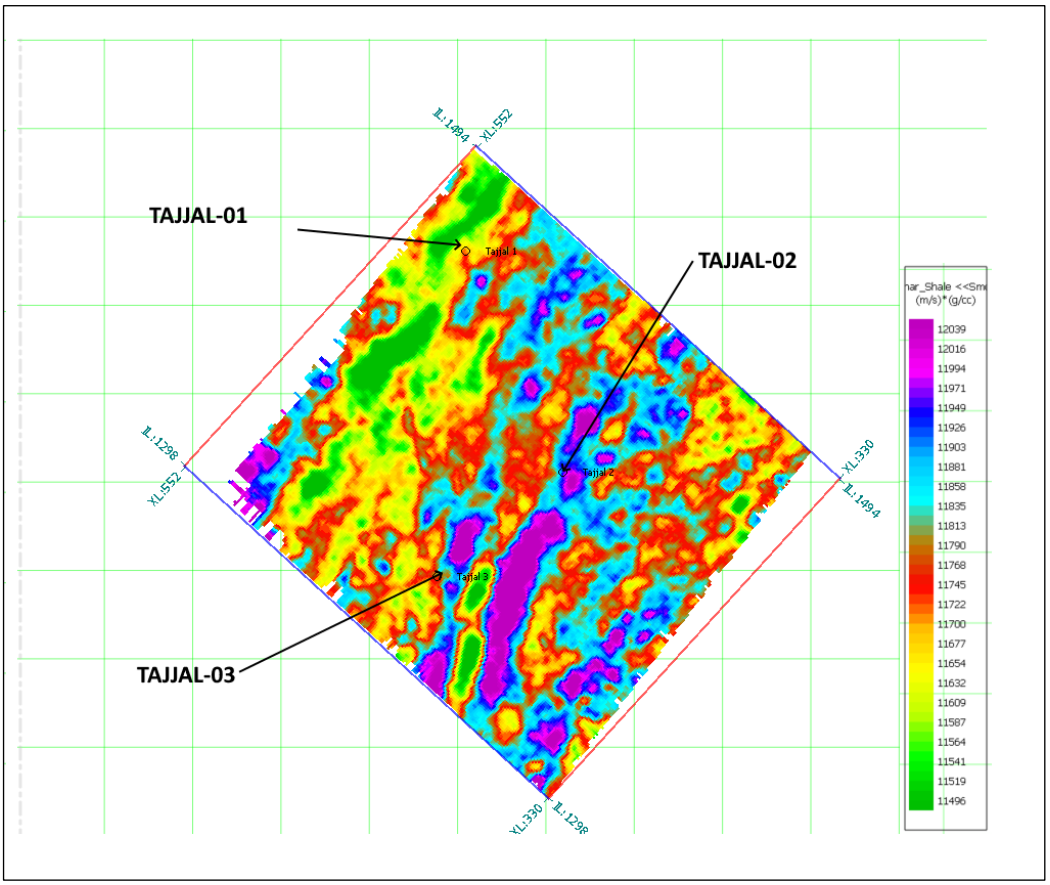


Figure 4. 29 Horizon map of the top B interval resolved by three post stack inversion techniques

4.5 AVO Modelling and Rock Physics

4.5.1 Workflow for Gassmann Substitution, AVO Modelling and Rock Physics Analysis

This workflow lays out the sequence of the amplitude-versus-offset and rock physics work, taking the characterization from acoustic impedance into the elastic and fluid domain. It runs from the well-to-seismic tie and log conditioning, through the petrophysical logs and Gassmann fluid substitution, to angle gathers for both the water-bearing and gas-bearing cases, the extended elastic impedance analysis for the fluid and lithology angles, and finally the cross plots of the rock properties. Together the steps give a physically consistent way to

predict how the reservoir's seismic amplitude response changes with offset and with fluid fill, which acoustic impedance alone cannot show.

Gassmann fluid substitution does the central work here, letting the elastic properties be modelled under different fluid saturations and isolating the diagnostic effect of gas on the seismic response. The angle gathers and extended elastic impedance analysis build on that substitution to find the projections that best separate fluids and lithologies, and the closing cross plots test how well the derived attributes discriminate. This workflow complements the impedance inversion with an independent, physics-based route to detecting porous gas-bearing sands, and it sets the context for the fluid substitution, AVO and rock physics figures that follow.

4.5.2 Synthetic Seismogram of Tajjal-01

The Tajjal-01 synthetic seismogram modelling underlies the AVO analysis, generating the offset-dependent seismic response of the reservoir from the elastic logs and linking the well properties to the amplitude behavior that would show up on pre-stack data. The display shows the modelled gather with the elastic property inputs and the resulting amplitude across the range of incidence angles, so the change in reflection amplitude with offset at the reservoir boundary can be read directly. This modelling is needed because the AVO signature is set by the contrast in P-wave velocity, S-wave velocity and density between the sand and the encasing shale, and the synthetic gather makes that signature explicit for the in-situ case at the well.

Giving the modelled offset response at a calibrated well location, this synthetic seismogram is the reference the effect of fluid substitution is checked against, since comparing the in-situ response with the response after substituting a different fluid brings out the amplitude changes diagnostic of fluid type. The change in reflection amplitude with offset at reservoir level, shown here, characterizes the AVO class of the Lower Goru sand at Tajjal-01 and gives the physical footing for the fluid-substitution and AVO results that follow. The AVO synthetic adds the offset dimension to the acoustic impedance analysis, and that dimension is what carries the fluid discrimination central to this part of the study.

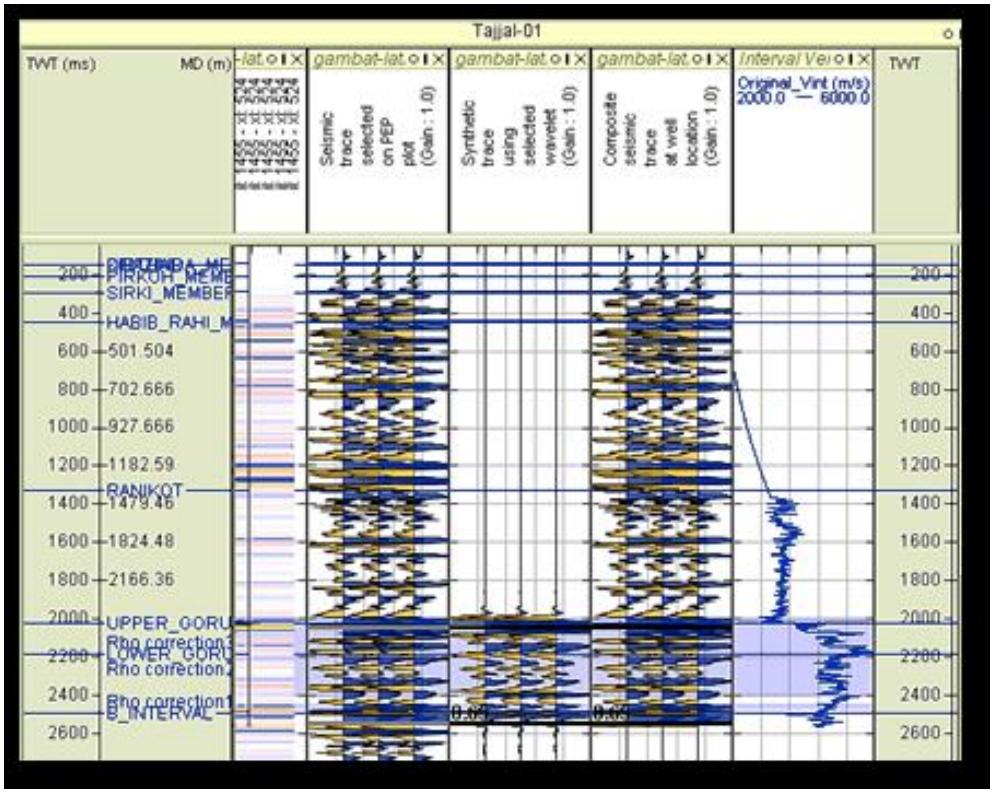


Figure 4. 30 Synthetic Seismogram of Tajjal-01

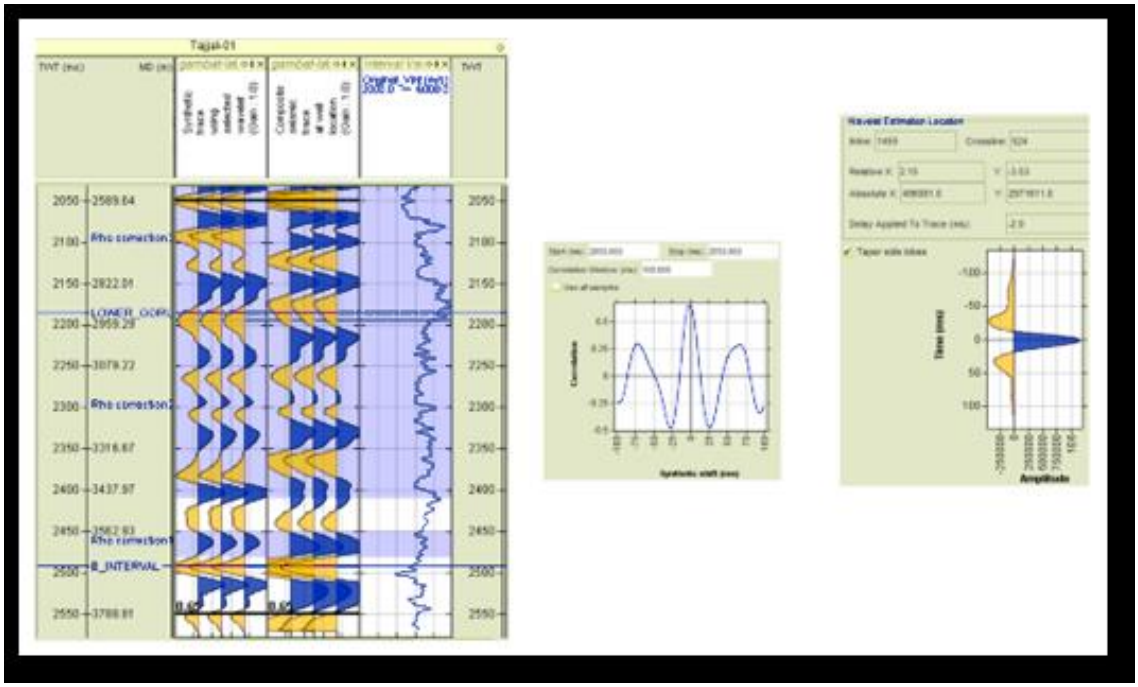


Figure 4. 31 Synthetic Seismogram of Tajjal-01 (continued)

4.5.3 Base Map with Seismic Line Displaying Synthetic Seismogram

This base map with the seismic line and synthetic seismogram gives the spatial context for the AVO and rock physics modelling, locating the analyzed line and the modelled

well response within the survey and tying the offset-dependent analysis to a specific position in the reservoir. Showing the synthetic along the seismic line lets the modelled response be compared directly with the real seismic character at the same location, so the elastic model used for the AVO analysis represents the actual seismic expression of the reservoir. The well, the line and the survey geometry together fix exactly where the fluid-substitution and AVO results apply and how they relate to the mapped fairways.

This figure ties the well-based elastic modelling to the seismic data, keeping the AVO interpretation anchored to a real seismic response rather than developed in isolation. That the synthetic matches the seismic along the line validates the elastic model at reservoir level and reinforces the fluid-discrimination analysis that depends on it. This calibration in space and character sets the fluid substitution and AVO modelling within the survey's structural and stratigraphic framework and connects the elastic analysis back to the reservoir geometry from the impedance inversion.

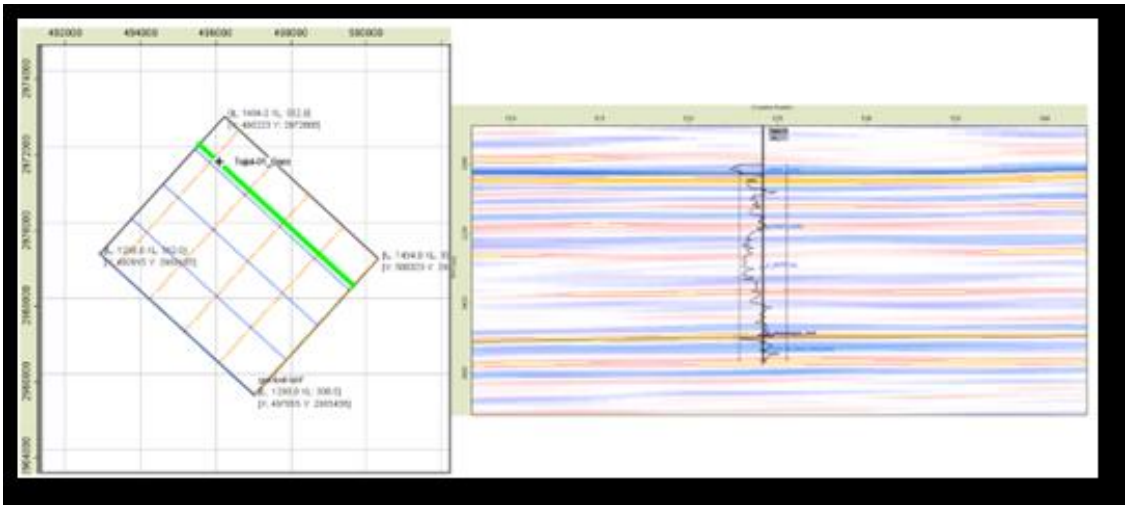


Figure 4. 32 Base map with Seismic line displaying synthetic seismogram

4.5.4 The Sand Intervals of Lower Goru Formation B Interval Under Study and the Seismic Event

This figure narrows the analysis to the B interval of the Lower Goru Formation, the primary target, by tying the sand units logged in the well to the corresponding seismic event and fixing the exact stratigraphic level for the fluid substitution and AVO modelling. Pinning down the seismic event tied to the B sand keeps the amplitude and offset analysis at the right reservoir horizon and lets the modelled response be matched cleanly to the observed reflection. The logged sand and the seismic event lining up confirms the B interval gives a recognizable seismic response and can be studied directly on the data.

Isolating the B interval and its seismic expression concentrates the rock physics and AVO analysis on the unit that carries the exploration interest, and it sets the reference reflection for the fluid-substitution modelling that follows. Identifying the sand and its event links the petrophysical description, the impedance inversion result and the AVO analysis at a single, well-defined level, keeping the different strands of the characterization coherent. Focusing on the B interval keeps the modelling of fluid effects and offset behavior directly relevant to characterizing the porous reservoir sand.

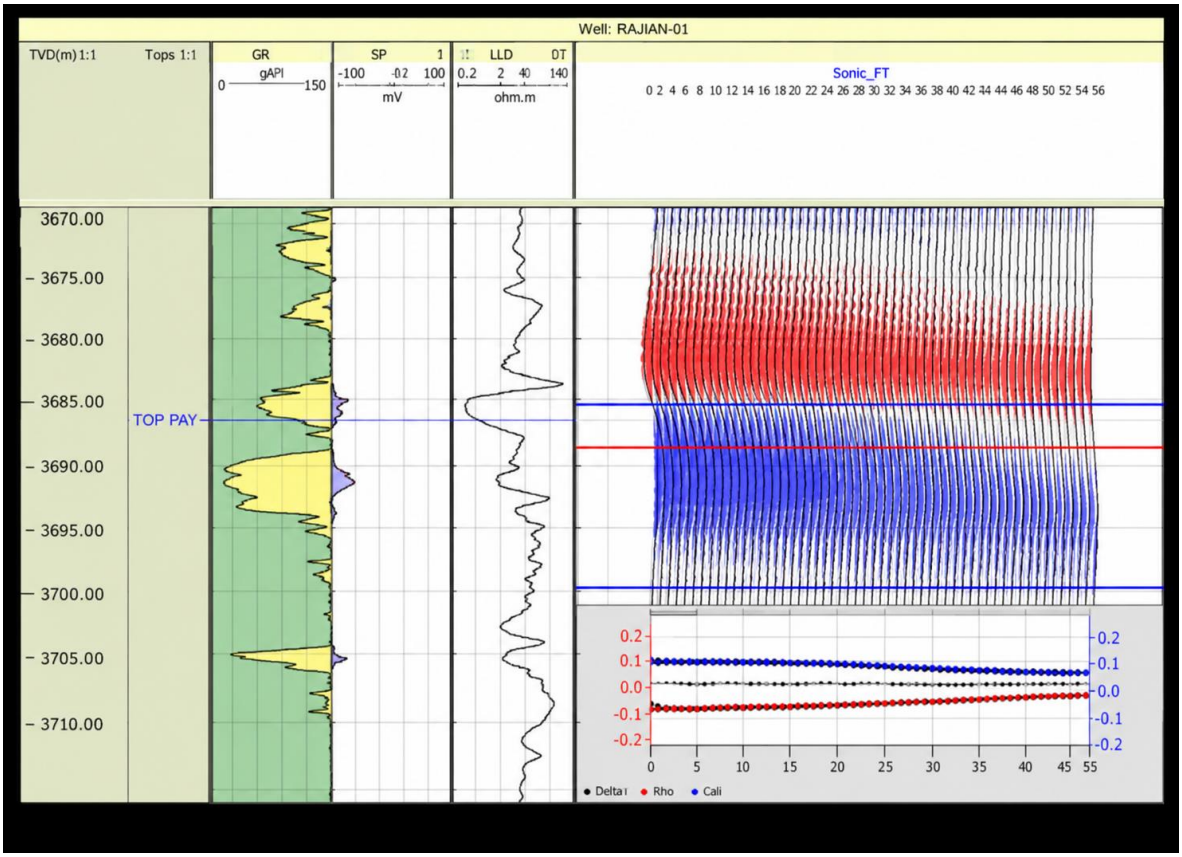


Figure 4. 33 The sand intervals of Lower Goru Formation B interval under study and the seismic event

4.5.5 Fluid Substitution

The fluid substitution figure is the core rock physics experiment of the study: Gassmann theory computes the elastic response of the reservoir under a different pore fluid, isolating the effect of fluid fill on the seismic properties from the rock frame and porosity. Swapping the in-situ fluid for a different saturation and recomputing P-wave velocity, density and the derived elastic attributes shows how the reservoir response changes between the water-bearing and gas-bearing states, and that comparison is the physical basis for seismic fluid discrimination. The substitution produces a measurable change in the elastic

properties of the sand, which confirms the reservoir is fluid-sensitive and that its seismic response carries information about the pore fluid.

The direction and size of the changes from fluid substitution are diagnostic of the reservoir type. Introducing gas into a porous sand cuts its P-wave velocity and density, which lowers its acoustic impedance and changes its offset behavior; that is the low-impedance signature the inversion picks up, and it points ahead to the AVO response. Because the substitution runs in a controlled rock physics framework on the calibrated well properties, the modelled fluid effect is physically consistent and a reliable prediction of how gas saturation shows in the seismic. The analysis pins the causal chain from gas saturation to reduced impedance to the AVO response, and it supports reading the low-impedance inversion anomalies as porous, gas-bearing sands.

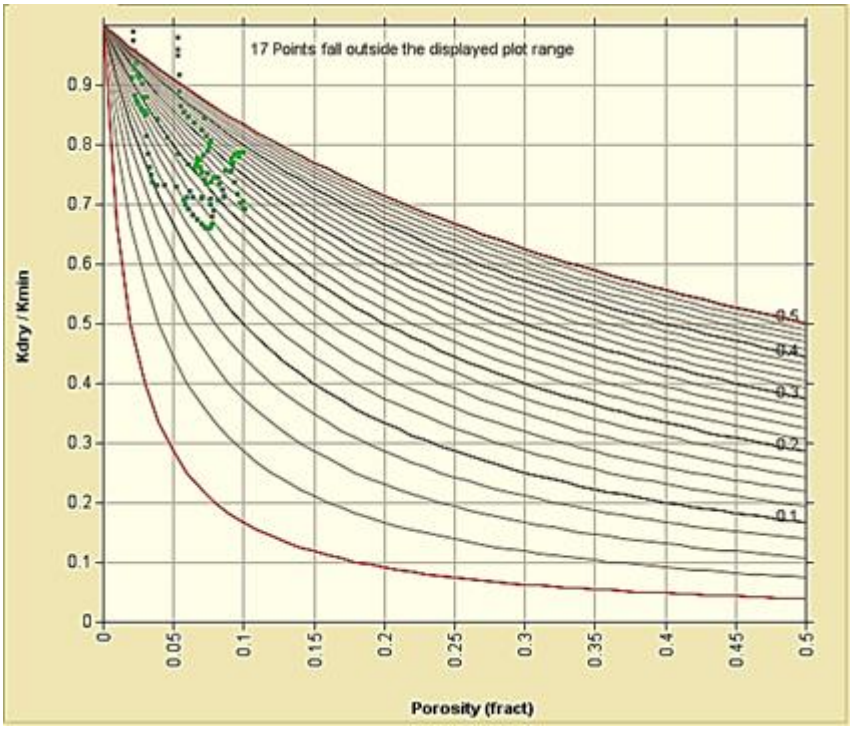


Figure 4. 34 Fluid substitution

4.5.6 AVO Classes on the Basis of AVO Response

This figure sets out the established classification of amplitude-versus-offset responses, the interpretive frame for the modelled AVO behavior of the Lower Goru reservoir, since the AVO classes describe how reflection amplitude varies with offset for different combinations of sand impedance and encasing lithology. The classification separates sands whose impedance is greater than, similar to, or lower than the surrounding media, and it names the associated amplitude behaviors, dimming, phase reversal and brightening with offset, along with the near-zero impedance contrast class in which a weak

zero-offset reflection grows in magnitude with offset. These categories give the diagnostic vocabulary needed to classify the reservoir response and tie it to the rock and fluid properties behind it.

This scheme earns its place here by letting the Lower Goru sand be assigned to a particular AVO class, which captures its expected seismic behavior and ties that behavior to porous, gas-bearing sandstone, an independent, amplitude-based check on the reservoir interpretation from impedance. The framework sets the criteria the modelled and observed AVO responses are compared against, ahead of the specific classification of the Lower Goru sand in the following figures. Placing the reservoir response in a recognized scheme connects the rock physics and fluid-substitution results to a standard model and strengthens the physical basis for the fluid and lithology discrimination that follows.

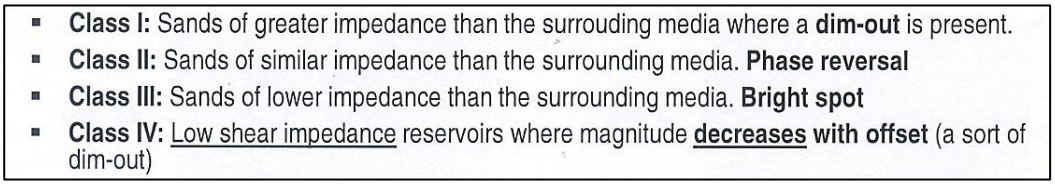


Figure 4. 35 AVO classes on the basis of AVO response (Ostrander, 1984)

4.5.7 AVO Classes (Rutherford and Williams)

This figure takes the amplitude-versus-offset classification further with the widely used scheme that relates the intercept and gradient behavior of gas sands to their impedance contrast with the encasing shales, refining the frame for interpreting the Lower Goru response. The scheme separates gas sands by whether the sand has higher, comparable or lower impedance than the surrounding media, and it links each class to a characteristic combination of zero-offset reflection amplitude and rate of change of amplitude with offset. Formalizing these relationships gives a quantitative basis for diagnosing the reservoir response and inferring the sand-shale impedance relationship from the observed AVO behavior.

This scheme ties AVO behavior directly to reservoir properties: the class the Lower Goru sand belongs to reflects both its impedance contrast and its fluid content, and so constrains the interpretation. Establishing the class clarifies how gas saturation and the low impedance of the porous sand show up in the offset domain and confirms the amplitude response is consistent with the low-impedance inversion signature. The modelled fluid-substitution and AVO results are assessed against this refined framework, and it leads into identifying the reservoir response as a specific AVO class in the analyses that follow.

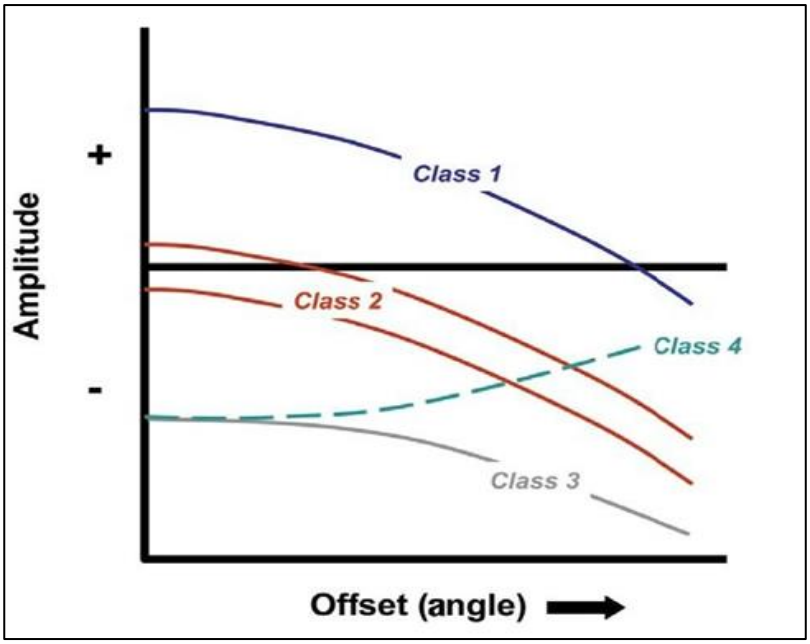


Figure 4. 36AVO classes (Rutherford and Williams, 1989)

4.5.8 Fluid Substitution and AVO Analysis

This figure brings the fluid substitution and AVO analyses together to show how changing the pore fluid alters the offset-dependent seismic response, giving the direct evidence linking gas saturation to a diagnostic amplitude signature. Comparing the modelled angle gathers and amplitude-versus-offset behavior for the water-bearing and gas-bearing cases shows that introducing gas changes both the reflection amplitude and its variation with offset in a way consistent with the recognized AVO classes, so the reservoir response is fluid-dependent and pre-stack amplitude can discriminate gas from water. The contrast between the two fluid cases isolates the seismic expression of gas and validates the physical basis for AVO-based fluid detection in the Lower Goru sand.

The combined analysis unites the rock physics prediction with the seismic amplitude response, showing that the impedance reduction from gas, established in the fluid-substitution modelling, comes with the offset behavior the AVO classification predicts. That the impedance effect and the amplitude effect agree reinforces reading the porous sands as gas-bearing and gives an independent confirmation of the reservoir characterization from the inversion. Showing the diagnostic amplitude response of the gas-saturated reservoir, this figure fixes the AVO signature of the Lower Goru sand and leads into the detailed look at its intercept and gradient behavior next.

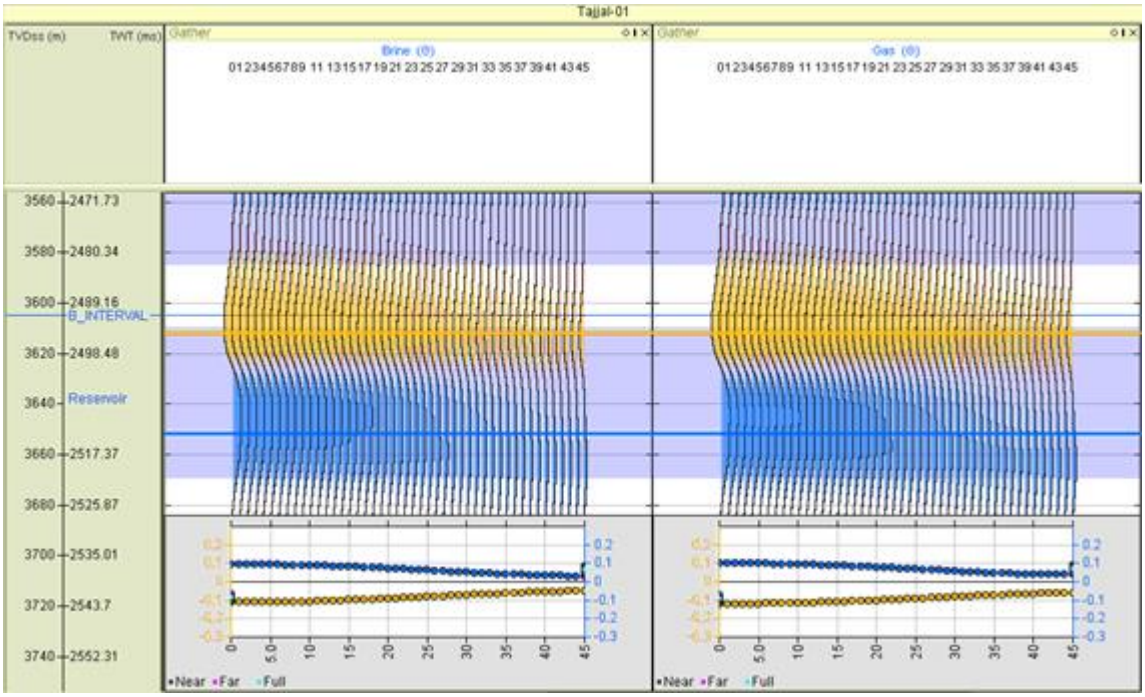


Figure 4. 37 Fluid substitution and AVO analysis

4.5.9 AVO Class 2 Intercept and Gradient Response

This figure examines the intercept and gradient behavior of the reservoir response and identifies it as the AVO class 2 signature, characteristic of porous gas sands whose acoustic impedance is close to that of the encasing shales, as happens in moderately compacted and consolidated sands. Class 2 has a reflection coefficient close to zero at normal incidence together with a negative gradient, so the reflection becomes increasingly negative and its magnitude grows with offset, and this happens specifically where the impedance contrast across the sand-shale interface is small while the Poisson's ratio contrast introduced by gas remains large. Identifying the Lower Goru reservoir as class 2 squares the observed amplitude behavior with the modest impedance contrast between the porous sand and its encasing lithology and confirms the reservoir is a gas-bearing sand whose seismic expression is carried mainly by the far offsets.

The class 2 character has a real consequence for interpretation: the weak zero-offset reflection can cause the reservoir to be missed on stacked and near-offset data, where no bright spot appears, so the diagnostic amplitude emerges only once the far offsets are examined and getting the class right keeps the response from being overlooked. The intercept and gradient analysis also confirm the AVO signature is consistent with the acoustic impedance from the inversion, a coherent, physically based picture in which the fluid substitution, the impedance response and the offset behavior all point the same way. Fixing the AVO class of the Lower Goru reservoir, this figure completes the amplitude-based fluid

and lithology discrimination and reinforces the identification of the porous gas sands that are the study's target.

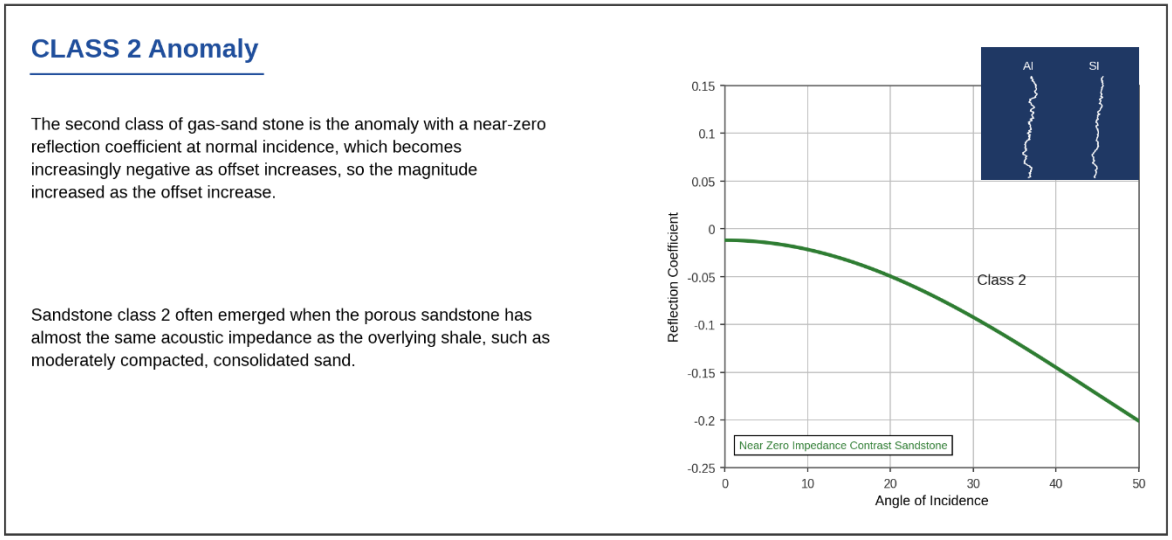


Figure 4. 38 AVO class 2 intercept and gradient response

4.6 Rock Physics

4.6.1 Cross Plot for Vp versus Vs

The cross plot of P-wave velocity against S-wave velocity is a fundamental rock physics discriminator, useful here because the relationship between the two velocities responds to both lithology and fluid content and so gives an independent way to separate the reservoir sands from the shales and to pick out fluid effects. The data are color-coded for brine-bearing sand, gas-bearing sand and shale, and the populations fall on distinct trends, the sands and shales following separate Vp-Vs relationships that reflect their different mineralogy and texture. The sand and shale trends separating confirms the reservoir's elastic properties differ systematically from the encasing lithology, the physical prerequisite for both impedance-based and AVO-based discrimination.

The feature that carries the fluid information is the shift of the gas sand points away from the brine sand points, because gas cuts the P-wave velocity more than the S-wave velocity and so lowers the Vp-Vs ratio, separating the gas-bearing sand from its water-bearing equivalent. This independently confirms the fluid effect modelled in the Gassmann substitution and gives direct evidence the reservoir sands are gas-sensitive, backing the low-impedance and class 2 AVO interpretations. Showing that sands, shales and fluid types fall in distinct regions of the Vp-Vs domain, this cross plot gives the rock physics basis for separating reservoir from non-reservoir and gas from brine, ahead of the further cross plots that test additional attribute combinations.

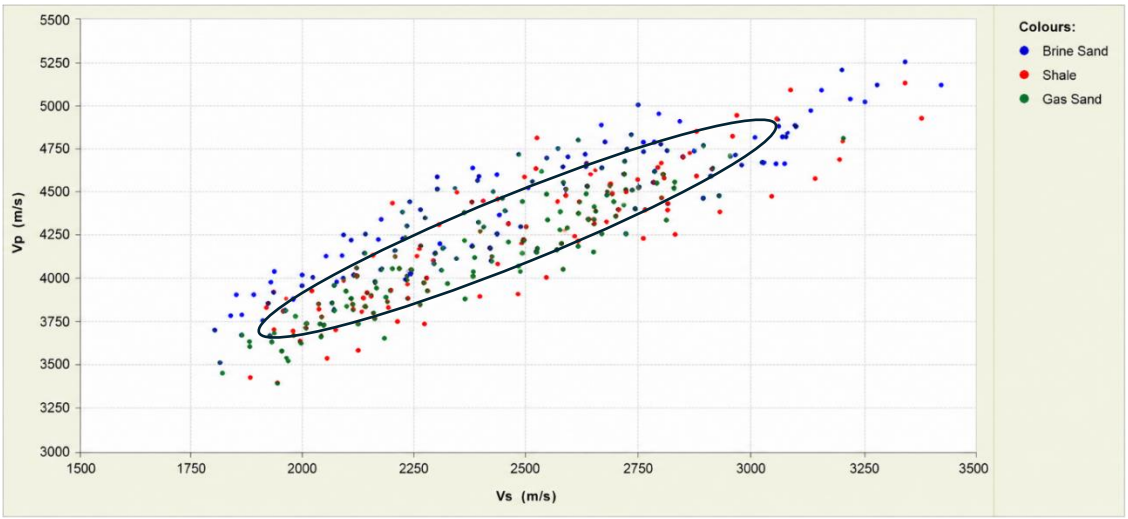


Figure 4. 39 Cross plot for Vp vs Vs

4.6.2 Cross Plot for AI versus Poisson's Ratio

The cross plot of acoustic impedance against Poisson's ratio pairs a property sensitive mainly to lithology and porosity with one strongly sensitive to fluid content, a two-dimensional discriminator that separates the reservoir sands, the shales and the fluid types better than either dimension alone. The brine sand, gas sand and shale populations are color-coded and fall in different regions, with the gas sands showing both lower acoustic impedance and lower Poisson's ratio than the brine sands and shales. The separation works because it uses two independent aspects of the elastic response, which makes porous gas sands more reliable to identify.

The drop in Poisson's ratio for the gas sands is the sharpest fluid signal in the plot, since Poisson's ratio is very sensitive to gas and falls steeply when gas replaces water in the pore space, driving the gas sands into the low-impedance, low-Poisson's-ratio corner. This confirms the fluid discrimination from the earlier analyses and shows acoustic impedance paired with Poisson's ratio works as a seismic fluid and lithology indicator for the Lower Goru reservoir. The porous gas sands separating clearly in the acoustic impedance-Poisson's ratio domain reinforces the physical basis for the inversion and AVO interpretations and motivates the extended elastic impedance analysis for the optimal fluid-lithology projection.

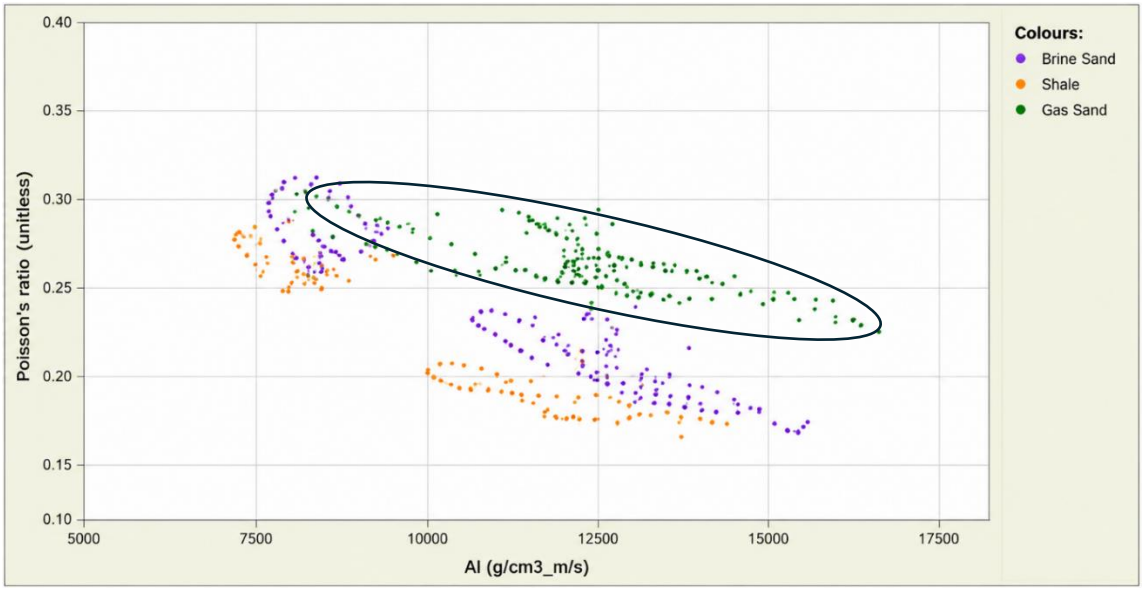


Figure 4. 40 Cross plot for AI vs Poisson ratio

4.6.3 Cross Plot for Lambda-Rho versus Mu-Rho

The lambda-rho against mu-rho cross plot pulls apart the two Lamé parameters that acoustic impedance rolls together, and that split is what makes it a sharper discriminator than impedance on its own. Lambda-rho, the product of incompressibility and density, responds strongly to whatever fills the pore space, while mu-rho, the product of rigidity and density, depends on the rock frame and is almost blind to the pore fluid. Both axes are in GPa·g/cm³, with lambda-rho running from about 23 to 64 and mu-rho from about 20 to 73. The samples split into two branches, a lower one for the tighter, lower-porosity intervals and an upper one for the better developed sands, and the three populations keep the same ordering in each. The gas sands hold the low lambda-rho side of the plot, the brine sands lie to their right, and the shales carry the highest lambda-rho values.

The direction of the separation says more than its size. At comparable mu-rho the gas and brine points are pulled apart almost entirely along the horizontal axis, the gas sands sitting several GPa·g/cm³ to the left of their brine-saturated equivalents while their mu-rho values stay close to them. This is what Gassmann's relations predict: replacing brine with gas lowers the saturated bulk modulus and therefore lambda, but leaves the shear modulus untouched, so mu-rho moves only through the small reduction in bulk density. The pattern confirms that the fluid substitution behaved physically, and it shows the division of labor between the two attributes, lambda-rho as the fluid indicator and mu-rho as the lithology indicator. Because the gas sands hold a region of this space that neither the brine sands nor the shales reach, the pair discriminates porous gas-bearing sand more cleanly than acoustic

impedance alone. That supports the low-impedance anomalies mapped by the model-based and sparse-spike inversions and matches the class 2 AVO response modelled at Tajjal-01.

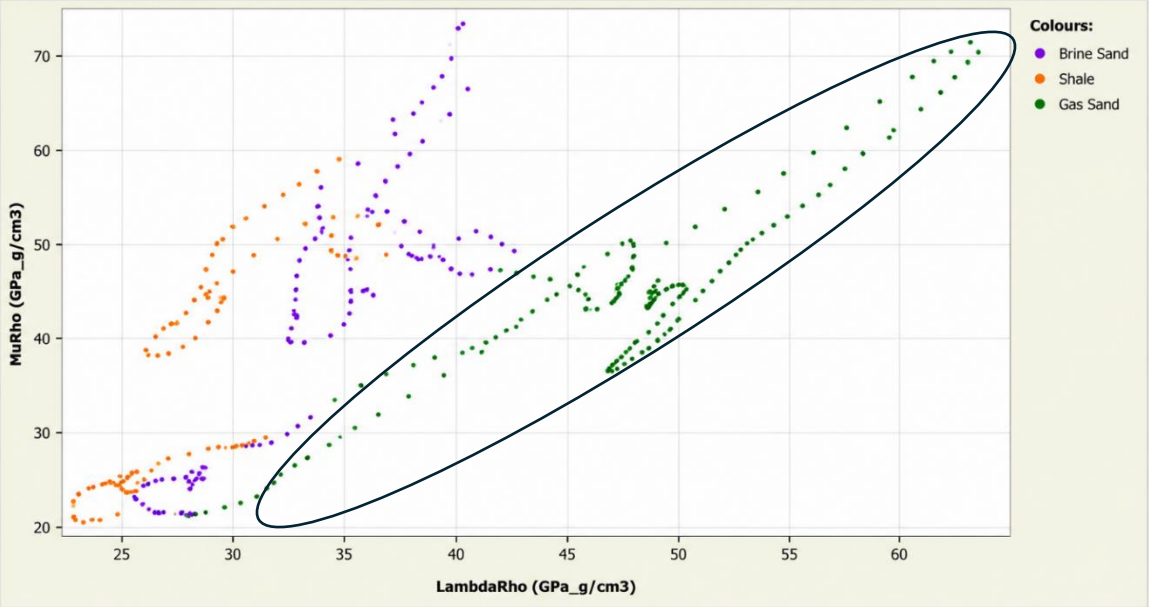


Figure 4. 41 Cross plot for Lambda Rho vs Mu Rho

4.6.4 Chi 32 Angle Best Separates Both the 02 Fluids as well as the 02 Lithologies

This figure presents the extended elastic impedance analysis and settles on the chi angle of thirty-two degrees as the projection that best separates the two fluids and the two lithologies, the end point of the search for the optimal seismic attribute for reservoir and fluid discrimination. Extended elastic impedance generalizes acoustic impedance by projecting the elastic properties onto an axis set by a rotation angle chi, and sweeping that angle tunes the attribute to maximize the contrast between the target populations. A chi angle of thirty-two degrees separating the brine sand, gas sand and shale best defines the specific projection that most effectively isolates the porous gas sands from the water-bearing sands and the shales.

This optimal angle is useful because the corresponding extended elastic impedance attribute can be computed from seismic data and used to map the fluid and lithology distribution across the survey with more discriminating power than acoustic impedance alone. As the note indicates, the projection gives the best separation of the gas sand points for both sand intervals, which confirms the attribute works for the principal targets and not just one unit. The extended elastic impedance projection that best discriminates fluid and lithology gives the most sensitive rock-physics-based indicator of porous gas sand in the study, and it feeds directly into the final cross plot, which combines this attribute with a further fluid-sensitive parameter.

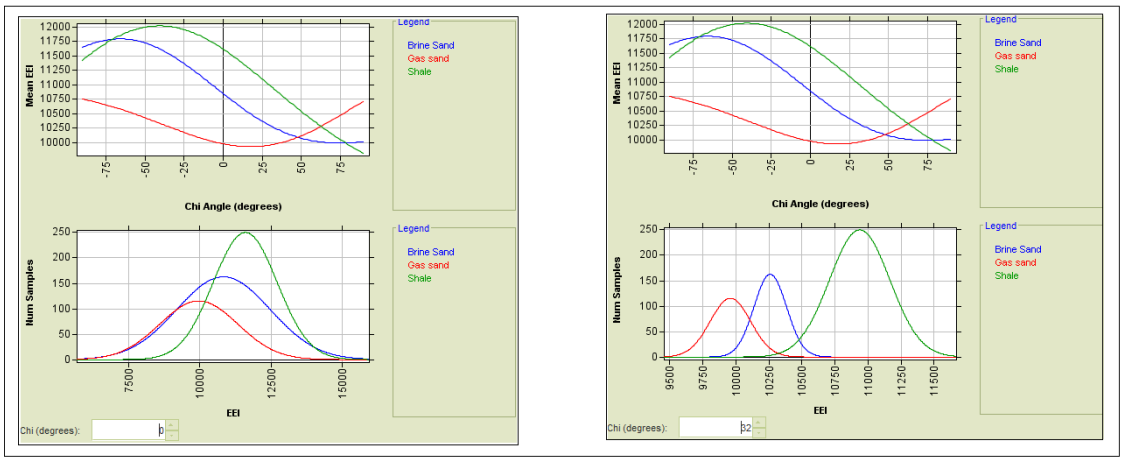


Figure 4. 42 EEI Analysis

4.6.5 Cross Plot for Lambda-Rho versus EEI at Chi 32

The final cross plot of lambda-rho against the extended elastic impedance at the optimal chi angle of thirty-two degrees combines two of the most fluid- and lithology-sensitive attributes in the study, the most refined discrimination of the porous gas sands and the close of the rock physics analysis. Lambda-rho, the product of the Lamé incompressibility parameter and density, is strongly sensitive to pore fluid and falls in the presence of gas, while the extended elastic impedance at chi thirty-two degrees best separates the fluids and lithologies, so the pair uses complementary sensitivities. The brine sand, gas sand and shale populations are color-coded and fall in clearly separated regions, the gas sands pushed toward the low lambda-rho and diagnostic extended elastic impedance values that mark porous, gas-bearing reservoir.

The clear separation of the gas sands in this combined attribute space is the most effective fluid and lithology discrimination in the analysis and shows that lambda-rho combined with the optimally projected extended elastic impedance is a robust seismic indicator of the porous reservoir sands. It pulls together the evidence from across the chapter, the low acoustic impedance from the inversion, the class 2 AVO response, the reduced Poisson's ratio and Vp-Vs ratio, and the optimal extended elastic impedance projection, into a single, physically consistent picture of the reservoir as porous gas-bearing sandstone. With the gas sands definitively separated in this refined domain, the final cross plot completes the reservoir characterization and gives the quantitative evidence behind the conclusions drawn from the post-stack seismic inversion and rock physics analysis of the Lower Goru sands in the Gambat Block

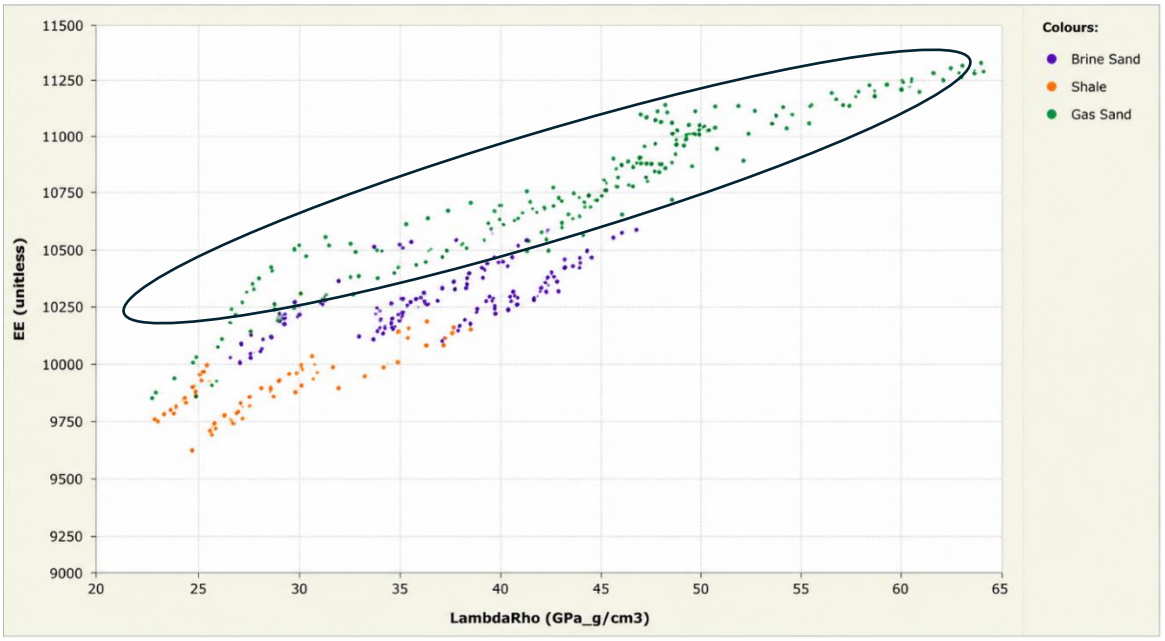


Figure 4. 43 Cross plot for Lambda Rho vs EEI at chi 32

.

CONCLUSIONS

The integrated petrophysical, seismic, post-stack inversion, AVO, and rock-physics analyses provided a consistent characterization of the Lower Goru reservoir in the Gambat Block, with the B-sand as the primary target.

1. Petrophysical Analysis: The Tajjal-1, Tajjal-2, and Tajjal-3 wells show favorable reservoir characteristics in the target B-sand, including low shale volume, effective porosity, elevated resistivity, and relatively low water saturation. Density-neutron and M-N cross plots further support the interpreted lithology and reservoir-fluid response.

2. Seismic Interpretation: Interpretation of the 3D seismic data established the structural and stratigraphic framework of the Lower Goru reservoir succession. The interpreted horizons show lateral continuity, while the mapped fault and structural configuration provide the framework for evaluating the B-sand reservoir and its trapping geometry.

3. Post-stack seismic inversion: model-based inversion successfully transformed the seismic response into acoustic-impedance volumes and identified low-impedance zones associated with the porous reservoir. The B-sand horizon map provides the principal indication of its lateral reservoir distribution beyond the well locations.

4. AVO and Rock physics: AVO analysis and Gassmann fluid substitution indicate a Class 2 AVO response for the target B-sand. The Vp–Vs, AI–Poisson's ratio, $\lambda\rho$–$\mu\rho$, and EEI analyses provide supporting evidence for distinguishing the interpreted gas-bearing reservoir response from brine-bearing and non-reservoir intervals. EEI at $\chi = 32°$ provided the strongest discrimination among the tested elastic attributes.

5. Integrated interpretation: The integration of petrophysical results, seismic interpretation, acoustic-impedance inversion, AVO, and rock physics reduces the ambiguity associated with using any single method. The combined results support the interpretation of the Lower Goru B-sand as the primary porous, gas-bearing reservoir target and provide a basis for assessing its distribution and quality between the Tajjal wells.

REFERENCES

Afzal, J., Kuffner, T., Rahman, A., & Ibrahim, M. (2005). *Seismic and well-log-based sequence stratigraphy of the Early Cretaceous, Lower Goru "C" sand of the Gambat sub-basin, Lower Indus Platform, Pakistan* [Paper presentation]. Pakistan Petroleum Convention, Islamabad, Pakistan.

Ahmad, N., Fink, P., Sturrock, S., Mahmud, T., & Ibrahim, M. (2004). *Sequence stratigraphy as a predictive tool in the Lower Goru fairway, Lower and Middle Indus Platform, Pakistan* [Paper presentation]. PAPG Annual Technical Conference, Islamabad, Pakistan.

Aki, K., & Richards, P. G. (1980). *Quantitative seismology: Theory and methods*. W. H. Freeman.

Alam, S. (2002). *Reservoir characterization and resource estimation of the Gambat Field, Lower Indus Basin, Pakistan* [Internal technical report]. OMV Pakistan Exploration.

Archie, G. E. (1942). The electrical resistivity log as an aid in determining some reservoir characteristics. *Transactions of the AIME, 146*(1), 54–62. https://doi.org/10.2118/942054-G

Asquith, G., & Krygowski, D. (2004). *Basic well log analysis* (2nd ed.). American Association of Petroleum Geologists.

Avseth, P., Mukerji, T., & Mavko, G. (2005). *Quantitative seismic interpretation: Applying rock physics tools to reduce interpretation risk*. Cambridge University Press.

Avseth, P., Mukerji, T., Mavko, G., & Dvorkin, J. (2010). Rock-physics diagnostics of depositional texture, diagenetic alterations, and reservoir heterogeneity in high-porosity siliciclastic sediments and rocks: A review of selected models and suggested work flows. *Geophysics, 75*(5), 75A31–75A47. https://doi.org/10.1190/1.3483770

Berger, A., Gier, S., & Krois, P. (2009). Porosity-preserving chlorite cements in shallow-marine volcaniclastic sandstones: Evidence from Cretaceous sandstones of the Sawan gas field, Pakistan. *AAPG Bulletin, 93*(5), 595–615. https://doi.org/10.1306/01300908096

Biot, M. A. (1956). Theory of propagation of elastic waves in a fluid-saturated porous solid: I. Low-frequency range. *The Journal of the Acoustical Society of America, 28*(2), 168–178. https://doi.org/10.1121/1.1908239

Castagna, J. P., & Backus, M. M. (Eds.). (1993). *Offset-dependent reflectivity: Theory and practice of AVO analysis*. Society of Exploration Geophysicists.

Castagna, J. P., Batzle, M. L., & Eastwood, R. L. (1985). Relationships between compressional-wave and shear-wave velocities in clastic silicate rocks. *Geophysics, 50*(4), 571–581. https://doi.org/10.1190/1.1441933

Castagna, J. P., & Swan, H. W. (1997). Principles of AVO cross plotting. *The Leading Edge, 16*(4), 337–344. https://doi.org/10.1190/1.1437626

Chopra, S., & Marfurt, K. J. (2007). *Seismic attributes for prospect identification and reservoir characterization*. Society of Exploration Geophysicists. https://doi.org/10.1190/1.9781560801900

Doll, H. G. (1948). The SP log: Theoretical analysis and principles of interpretation. *Transactions of the AIME, 179*(1), 146–185. https://doi.org/10.2118/948146-G

Dvorkin, J., & Nur, A. (1996). Elasticity of high-porosity sandstones: Theory for two North Sea data sets. *Geophysics, 61*(5), 1363–1370. https://doi.org/10.1190/1.1444059

Ellis, D. V., & Singer, J. M. (2007). *Well logging for earth scientists* (2nd ed.). Springer. https://doi.org/10.1007/978-1-4020-4602-5

Gassmann, F. (1951). Über die Elastizität poröser Medien. *Vierteljahrsschrift der Naturforschenden Gesellschaft in Zürich, 96*, 1–23.

Goodway, B., Chen, T., & Downton, J. (1997). Improved AVO fluid detection and lithology discrimination using Lamé petrophysical parameters. *SEG Technical Program Expanded Abstracts, 1997*, 183–186. https://doi.org/10.1190/1.1885795

Hampson, D., & Russell, B. (1991). AVO inversion: Theory and practice. *The Leading Edge, 10*(6), 39–42. https://doi.org/10.1190/1.1436821

Han, D., Nur, A., & Morgan, D. (1986). Effects of porosity and clay content on wave velocities in sandstones. *Geophysics, 51*(11), 2093–2107. https://doi.org/10.1190/1.1442062

Jadoon, I. A. K., Lawrence, R. D., & Lillie, R. J. (1994). Seismic data, geometry, evolution, and shortening in the active Sulaiman fold-and-thrust belt of Pakistan, southwest of the Himalayas. *AAPG Bulletin, 78*(5), 758–774.

Kadri, I. B. (1995). *Petroleum geology of Pakistan*. Pakistan Petroleum Limited.

Kazmi, A. H., & Jan, M. Q. (1997). *Geology and tectonics of Pakistan*. Graphic Publishers.

Larionov, V. V. (1969). *Borehole radiometry*. Nedra.

Mavko, G., Mukerji, T., & Dvorkin, J. (2009). *The rock physics handbook: Tools for seismic analysis of porous media* (2nd ed.). Cambridge University Press. https://doi.org/10.1017/CBO9780511626753

Munir, K., Iqbal, M., Farid, A., & Bhatti, A. S. (2011). Sequence stratigraphy of the Sembar Formation and the Lower Goru Member: Implications for reservoir characterization, Indus Basin, Pakistan. *Journal of Petroleum Geology, 34*(4), 395–412.

Nur, A., Mavko, G., Dvorkin, J., & Galmudi, D. (1998). Critical porosity: A key to relating physical properties to porosity in rocks. *The Leading Edge, 17*(3), 357–362. https://doi.org/10.1190/1.1437977

Odegaard, E., & Avseth, P. (2004). Well log and seismic data analysis using rock physics templates. *First Break, 22*(10), 37–43. https://doi.org/10.3997/1365-2397.2004017

Ostrander, W. J. (1984). Plane-wave reflection coefficients for gas sands at nonnormal angles of incidence. *Geophysics, 49*(10), 1637–1648. https://doi.org/10.1190/1.1441571

Pendrel, J. (2001). Seismic inversion: Still the best tool for reservoir characterization. *CSEG Recorder, 26*(1), 5–14.

Pickett, G. R. (1966). A review of current techniques for determination of water saturation from logs. *Journal of Petroleum Technology, 18*(11), 1425–1433. https://doi.org/10.2118/1446-PA

Poupon, A., & Leveaux, J. (1971). Evaluation of water saturation in shaly formations. *Transactions of the SPWLA Annual Logging Symposium, 12*, Paper O.

Raymer, L. L., Hunt, E. R., & Gardner, J. S. (1980). *An improved sonic transit time-to-porosity transform* [Paper presentation]. SPWLA 21st Annual Logging Symposium, Lafayette, LA, United States.

Rider, M., & Kennedy, M. (2011). *The geological interpretation of well logs* (3rd ed.). Rider-French Consulting.

Russell, B., & Hampson, D. (1991). Comparison of post stack seismic inversion methods. *SEG Technical Program Expanded Abstracts, 1991*, 876–878. https://doi.org/10.1190/1.1888870

Rutherford, S. R., & Williams, R. H. (1989). Amplitude-versus-offset variations in gas sands. *Geophysics, 54*(6), 680–688. https://doi.org/10.1190/1.1442696

Schlumberger. (1989). *Log interpretation principles/applications*. Schlumberger Educational Services.

Sheriff, R. E., & Geldart, L. P. (1995). *Exploration seismology* (2nd ed.). Cambridge University Press. https://doi.org/10.1017/CBO9781139168359

Shuey, R. T. (1985). A simplification of the Zoeppritz equations. *Geophysics, 50*(4), 609–614. https://doi.org/10.1190/1.1441936

Smith, T. M., Sondergeld, C. H., & Rai, C. S. (2003). Gassmann fluid substitutions: A tutorial. *Geophysics, 68*(2), 430–440. https://doi.org/10.1190/1.1567211

Taner, M. T., Koehler, F., & Sheriff, R. E. (1979). Complex seismic trace analysis. *Geophysics, 44*(6), 1041–1063. https://doi.org/10.1190/1.1440994

Tiab, D., & Donaldson, E. C. (2015). *Petrophysics: Theory and practice of measuring reservoir rock and fluid transport properties* (4th ed.). Gulf Professional Publishing.

Toqeer, M., Ali, A., Alves, T. M., Khan, A., Zubair, & Hussain, M. (2021). Application of model based post-stack inversion in the characterization of reservoir sands containing porous, tight and mixed facies: A case study from the Central Indus Basin, Pakistan. *Journal of Earth System Science, 130*(1), Article 43. https://doi.org/10.1007/s12040-020-01543-5

Wandrey, C. J., Law, B. E., & Shah, H. A. (2004). *Sembar Goru/Ghazij composite total petroleum system, Indus and Sulaiman-Kirthar geologic provinces, Pakistan and India* (U.S. Geological Survey Bulletin 2208-B). U.S. Geological Survey.

Whitcombe, D. N., Connolly, P. A., Reagan, R. L., & Redshaw, T. C. (2002). Extended elastic impedance for fluid and lithology prediction. *Geophysics, 67*(1), 63–67. https://doi.org/10.1190/1.1451337

White, R., & Simm, R. (2003). Tutorial: Good practice in well ties. *First Break, 21*(10), 75–83. https://doi.org/10.3997/1365-2397.2003022

Wyllie, M. R. J., Gregory, A. R., & Gardner, L. W. (1956). Elastic wave velocities in heterogeneous and porous media. *Geophysics, 21*(1), 41–70. https://doi.org/10.1190/1.1438217

Yasin, Q., Sohail, G. M., Ding, Y., Ismail, A., & Du, Q. (2020). Estimation of petrophysical parameters from seismic inversion by combining particle swarm optimization and multilayer linear calculator. *Natural Resources Research, 29*(6), 3291–3317. https://doi.org/10.1007/s11053-020-09641-3

Yilmaz, Ö. (2001). *Seismic data analysis: Processing, inversion, and interpretation of seismic data* (2nd ed.). Society of Exploration Geophysicists. https://doi.org/10.1190/1.9781560801580

Zaigham, N. A., & Mallick, K. A. (2000). Prospect of hydrocarbon associated with fossil-rift structures of the southern Indus Basin, Pakistan. *AAPG Bulletin, 84*(11), 1833–1848.

Zoeppritz, K. (1919). Über Erdbebenwellen VII B: Über Reflexion und Durchgang seismischer Wellen durch Unstetigkeitsflächen. *Nachrichten von der Königlichen*

Gesellschaft der Wissenschaften zu Göttingen, Mathematisch-Physikalische Klasse, 1919, 66–84.

APPLICATION OF POST-STACK SEISMIC INVERSION FOR THE CHARACTERIZATION OF POROUS RESERVOIR SAND, GAMBAT BLOCK, CENTRAL INDUS BASIN, PAKISTAN

by Mohsin Raza

Submission date: 25-Jul-2026 11:20PM (UTC-0700)
Submission ID: 2995867888
File name: RESERVOIR_SAND,_GAMBAT_BLOCK,_CENTRAL_INDUS_BASIN_PAKISTAN.docx (68.09K)
Word count: 20274
Character count: 119393

APPLICATION OF POST-STACK SEISMIC INVERSION FOR THE CHARACTERIZATION OF POROUS RESERVOIR SAND, GAMBAT BLOCK, CENTRAL INDUS BASIN, PAKISTAN

ORIGINALITY REPORT

8%	2%	7%	1%
SIMILARITY INDEX	INTERNET SOURCES	PUBLICATIONS	STUDENT PAPERS

MATCH ALL SOURCES (ONLY SELECTED SOURCE PRINTED)

1%

★ Sanjeev Rajput, Ravi Kant Pathak. "Seismic Exploration to Reservoir Excellence", Springer Science and Business Media LLC, 2025

Publication

Exclude quotes	Off	Exclude matches	Off
Exclude bibliography	Off		